THE UNIVERSITY OF QUEENSLAND

AUSTRALIA

Numerical and Experimental Investigations of Thermo-hydrodynamic Characteristics of Ice Slurry in Helical Heat Exchangers

Amin Kamyar

B.Sc., M.Eng. Mechanical Engineering

A thesis submitted for the degree of Doctor of Philosophy at

The University of Queensland in 2019

School of Mechanical and Mining Engineering

Abstract

Mining industry has experienced a dramatic change over the past 20 years in terms of methods, equipment as well as human resource policies. These changes have had impacts on the design of mine ventilation systems. Despite all the advantages of surface Bulk Air Cooling (BAC) systems, implementing an underground solution for thermal pollution especially for ultra-deep mines becomes essential. In addition, with the increase in the mining depth and the pumping distance the operational cost of underground BAC also rises. The location and working fluid becomes important as the depth of working areas increases. The performance of the heat exchanger is a critical factor as it affects the energy consumption and thermal conditions of the underground environment. Ice slurry has been recently proposed as a new potential coolant for deep underground cooling as it is prone to no or slight increase in temperature when pumped to working areas. To investigate the feasibility of such systems for mine cooling, characterizing the heat exchanger behaviour operating with ice slurry is crucial. This study will explore the thermal and hydraulic performance of ice slurry used as coolant in a coil heat exchanger. Finite volume approach in Computational Fluid Dynamics (CFD) along with experiments will be implemented to characterize the heat transfer and flow within the heat exchanger.

In the first part of the research, a detailed numerical investigation of the thermo-hydrodynamic performance of a helical coil heat exchanger operated with a laminar and non-Newtonian flow of ethyl-alcohol ice slurry subject to phase change is presented. The Bingham plastic model is used to reflect the non-Newtonian behaviour of ice slurry. The phase change of ice slurry is modelled using the enthalpy-porosity method. The pressure drop and heat transfer of ice slurry in a double-turn helical coil are determined in terms of ice mass fraction and *Dean* number.

The second part of the research numerically examines the flow characteristics of monopropylene glycol ice slurry through a horizontal U-bend. An Eulerian two-phase model is used to investigate the effect of inlet flow velocity, particle diameter and ice volume fraction on the particle distribution and pressure drop throughout the U-bend. The flow is considered isothermal so the heat transfer and melting of solid particles are not taken into account.

In the final stage of the study, the aim is to experimentally investigate the flow characteristics of an ice slurry through horizontal and vertical U-bends. The effects of flow rate (inlet velocity), ice volume fraction and pipe diameter on the pressure drop and loss coefficients of the U-bend for horizontal and vertical orientations are investigated. To get a clear picture the ice slurry structure, the flow is also visualized in both straight and bend sections.

Declaration by author

This thesis is composed of my original work, and contains no material previously published or written by another person except where due reference has been made in the text. I have clearly stated the contribution by others to jointly-authored works that I have included in my thesis.

I have clearly stated the contribution of others to my thesis as a whole, including statistical assistance, survey design, data analysis, significant technical procedures, professional editorial advice, financial support and any other original research work used or reported in my thesis. The content of my thesis is the result of work I have carried out since the commencement of my higher degree by research candidature and does not include a substantial part of work that has been submitted to qualify for the award of any other degree or diploma in any university or other tertiary institution. I have clearly stated which parts of my thesis, if any, have been submitted to qualify for another award.

I acknowledge that an electronic copy of my thesis must be lodged with the University Library and, subject to the policy and procedures of The University of Queensland, the thesis be made available for research and study in accordance with the Copyright Act 1968 unless a period of embargo has been approved by the Dean of the Graduate School.

I acknowledge that copyright of all material contained in my thesis resides with the copyright holder(s) of that material. Where appropriate I have obtained copyright permission from the copyright holder to reproduce material in this thesis and have sought permission from co-authors for any jointly authored works included in the thesis.

Amin Kamyar

January 2019

Publications included in this thesis

- **Amin Kamyar**, Saiied M Aminossadati, Christopher R Leonardi. *Thermo-hydrodynamics of a helical coil heat exchanger operated with a phase-change ice slurry as a refrigerant*. Heat Transfer Engineering. https://doi.org/10.1080/01457632.2018.1428989

Submitted manuscripts included in this thesis

- **Amin Kamyar**, Saiied M Aminossadati, Christopher R Leonardi, Agus P Sasmito, Sebastien Poncet. *Flow characterization of monopropylene glycol ice slurry through a horizontal U-bend: Part I: A numerical approach*. International Journal of Refrigeration. (**Under review**)

- **Amin Kamyar**, Saiied M Aminossadati, Christopher R Leonardi, Sebastian Gund, Michael Kauffeld. *Flow characterization of monopropylene glycol ice slurry through U-bends: Part II: An experimental approach*. International Journal of Refrigeration. (**Under review**)

Other publications during candidature

Conference abstracts:

- **Amin Kamyar**, Saiied M Aminossadati, Christopher R Leonardi. *Thermal and hydraulic performance of a heat exchanger operated with ice slurry as refrigerant*. Proceedings of the 7th IAHR International Conference on Cooling Tower and Heat Exchangers, Gold Coast, Australia, September 2015.

- **Amin Kamyar**, Saiied M Aminossadati, Christopher R Leonardi, Agus P Sasmito. *Current developments and challenges of underground mine ventilation and cooling methods*. Proceedings of the 16th Coal Operators' Conference, Mining Engineering, University of Wollongong, 10-12 February 2016, 249-262.

Industrial magazine articles:

- **Amin Kamyar**, Saiied M Aminossadati, Christopher R Leonardi. *Potential strategies towards energy-efficient mine ventilation and cooling systems*. Australian Resources and Investment, 2017. **11**(6): p. 49-50.

Contributions by others to the thesis

No contributions by others

Statement of parts of the thesis submitted to qualify for the award of another degree

No works submitted towards another degree have been included in this thesis

Research Involving Human or Animal Subjects

No animal or human subjects were involved in this research

Acknowledgements

I would like to express deep gratitude to my principal supervisor Associate Professor Saiied Aminossadati for his constant guidance and kindness. He has opened my eyes to new stages of opportunity and strength with his inspiring mentorship.

I would also like to extend my appreciation to my Co-supervisor Dr Christopher Leonardi for his invaluable advisory and contribution during my PhD journey.

I am grateful to The University of Queensland for providing me with the financial support through the Australian Government Research Training Program (RTP) Scholarship. The donors of the Walter and Eliza Hall travelling scholarship which provided the opportunity to expedite the completion of the thesis are also acknowledged.

In 2018, I had the opportunity to visit the Karlsruhe University of Applied Sciences, Germany for two months. I benefited from hands-on experience with ice slurry and other refrigeration technologies. My appreciation goes to Professor Michael Kauffeld for having me and accepting me as a member of his Ice Slurry team. Thanks are also extended to Mr Sebastian Gund and Mr Kushal Sharma for their valuable contribution during establishment of the ice slurry test rig.

I wish to thank my officemates Jon McCullough and Travis Mitchel for all the unforgettable chats, laughs and time we shared together during these four years of PhD life.

Finally, I tend to take this opportunity to appreciate the indispensable and perpetual support from my father, mother and sister whose words have always instilled motivation into my life. Without their unconditional love and care, I would not have made it this far.

Financial support

This research was supported by an Australian Government Research Training Program Scholarship.

The research was also supported by the Graduate School International Travel Award (GSITA) provided by the UQ Graduate School.

The donors of the Walter and Eliza Hall travelling scholarship which provided the possibility of conducting the experiments for this study are also acknowledged.

Keywords

ice slurry, pressure drop, heat transfer, non-Newtonian fluid, computational fluid dynamics, helical coil, U-bend

Australian and New Zealand Standard Research Classifications (ANZSRC)

ANZSRC code: 090913, Mechanical Engineering, 70%

ANZSRC code: 060999, Mining Engineering, 30%

Fields of Research (FoR) Classification

FoR code: 0913, Mechanical Engineering, 70%

FoR code: 0999, Mining Engineering, 30%

Table of Contents

List of Figures

List of Tables

Nomenclature

A_{mush}	mushy zone constant
b	coil pitch, m
Be	*Bejan* number
c_p	specific heat, J/K
C_D	drag force coefficient
C_L	lift force coefficient
C_{TD}	turbulent dispersion force coefficient
$C_{1\varepsilon}$	constant in Eq. (5.21)
$C_{2\varepsilon}$	constant in Eq. (5.21)
C_μ	constant in Eq. (5.25)
D	pipe diameter, m
D_T	thermal diffusivity, m^2/s
De	*Dean* number
d_i	tube inner diameter, m
E_{gen}	total entropy generation per unit length, W/m K
E_{gen}^*	entropy generation number
E_p^*	entropy generation due to fluid friction
E_T^*	entropy generation due to heat transfer
F	thermophysical property of the water-ethanol solution in Eq. (4.7)
f	friction factor
d_s	ice particle diameter, m
e_{ss}	particle-particle restitution coefficient
e_{sw}	particle-wall restitution coefficient

F_D drag force, N

F_L lift force, N

F_{TD} turbulent dispersion force, N

g gravity acceleration, m/s^2

G production of turbulence kinetic energy

g_0 radial distribution function

H_{is} mass enthalpy of the ice slurry, J/kg

H_l latent heat of the ice slurry, J/kg

h_{ref} reference enthalpy, J/kg

h heat transfer coefficient, W/m^2 K

I unit vector

K consistency coefficient

k_c thermal conductivity, W/m K

k turbulence kinetic energy, m^2/s^2

k_{θ_s} diffusion coefficient

L, l length, m

$\dot{m}$ mass flow rate, kg/s

Nu_m average *Nusselt* number

n flow index

Pe *Peclet* number

q' heat transfer rate per unit length, W/m

q'' wall heat flux, W/m^2

r radius of the tube, m

R radius of the coil, m

P pressure, Pa

Re	Reynolds number
Re_c	critical *Reynolds* number
S	source term (Eq. (4.3) and Eq. (4.6))
T	temperature, K
T_f	bulk temperature, K
T_{ref}	reference temperature, K
T_{wall}	wall temperature, K
U	bulk velocity, m/s
v_p	velocity of the solid phase, m/s
u	axial velocity, m/s
v	velocity vector, m/s
x, y, z	cartesian coordinates, m
X	parameter in the polynomial equation (Eq. (4.7))
X_m	constant in the polynomial equation (Eq. (4.7))
Y	parameter in the polynomial equation (Eq. (4.7))
Y_m	constant in the polynomial equation (Eq. (4.7))

Greek Letters

α_l	liquid mass fraction
$\alpha_{s,m}$	ice mass fraction
α_s	ice volume fraction
ω	liquid phase mass fraction in Eq. (4.4) and Eq. (4.5)
ε	ratio of yield stress to wall shear stress

ε_t	turbulent dissipation rate, m^2/s^3
θ	axial angle measured along the axis of the helical coil, degrees
β	axial angle measured along the axis of the bend, degrees
β_{sl}	ratio of characteristic relaxation times
δ	momentum exchange coefficient
ϕ_w	specularity coefficient
γ_s	bulk viscosity, Pa.s
η	constant in Eq. (5.12)
φ_{ls}	liquid-solid energy exchange coefficient
λ_{θ_s}	collisional dissipation of energy, kg/m s^3
μ	viscosity, Pa s
μ_p	plastic viscosity, Pa s
μ_t	turbulent viscosity, Pa s
θ_s	granular temperature
ρ	density, kg/m^3
σ	dispersion Prandtl number
τ	shear stress, Pa
ζ	bend loss coefficient

Subscripts

B	*Bingham* model
in	inlet
is	ice slurry
l	liquid

liquidus	liquid phase condition
M, m	mixture
max	maximum
P	*Power-law* model
s	solid
sl	solid-liquid interaction
ls	liquid-solid interaction
ss	particle-particle interaction
solidus	solid phase condition
sw	solid-wall interaction
u=0	static ice slurry
w	wall

Chapter 1 Introduction

1.1 Background

Australian mines are directed toward deeper underground operations as exploration tools discover orebodies located at great depths. Deeper working environments imply the need for a feasible means of combating the thermal pollution. Workers subjected to heat stress experience serious hazards in terms of health, safety, productivity and morale. In general, there are two common strategies for underground cooling; one is the use of mine ventilation and cooling effect of the airflow; and use of refrigeration to provide working areas with low-temperature environments. Despite the recent developments in mine air-conditioning, many Australian miners still suffer from thermal discomfort while on duty. Thus, higher cooling capacities at deeper levels becomes the major concern of mining companies which imposes higher initial and operational costs. The rise in energy costs on the other side, has made the companies to seek for energy management strategies that rectify the inefficiencies of current refrigeration systems or reduce the excessive power consumptions.

Ice slurry refers to a pumpable suspension comprising an anti-freeze depressant such as alcohol and solid ice particles in micron size. Mining industry is one of the pioneers to introduce the idea of using ice slurries for underground cooling due to the higher cooling capacity of ice slurries compared to chilled water. As opposed to chilled water that gains heat while travelling through long pipes and experiences temperature increase, ice slurry maintain its temperature by exploiting the phase change of ice particles to absorb the heat. To determine optimal operating conditions, it is most important to understand then identify the conditions offering the best compromise between high heat transfer and low pressure drop.

1.2 Statement of the problem

With the increase in depth of mines, current refrigeration methods can no longer address the heat problem. Sending chilled air or water to deep areas is not efficient as the fluid absorbs heat and gets warm as it reaches the working areas. Ice cooling becomes one of the option for heat management in ultra-deep mines. However, due to the complex nature of ice slurry, there are contradictory reports on the hydrodynamic and thermal behaviour of these mixtures from previous experiments. The required pumping power is a major concern as the mixture must be transported to ultra-deep working areas. When reached at the heat exchanger to cool the critical areas, the heat transfer performance becomes substantial to trade off the energy consumption for pumping.

Transport of ice slurry requires accurate design of pumping systems as insufficient flow rates can cause stationary bed flow regimes inside pipe lines. This flaws the functionality of refrigeration systems using ice slurries. Various parameters affect the thermo-fluidic characteristics and flow regimes of ice slurries such as ice volume fraction, flow velocity, diameter of ice particles, pipe diameter, and additive solution. Curved geometries influence the transition of ice slurry flow regimes (heterogeneous to stationary bed) as the particle distribution is disturbed by the centrifugal forces and consequently secondary flow. The majority of the existing studies have focused on characterising the ice slurry flow in straight pipes. Effect of aforementioned parameters on the performance of ice slurry flows in coils and bends is still lacking for a better design of ice slurry cooling system.

1.3 Aim and Objectives

The aim of this project is to investigate the thermal and hydrodynamic characteristics of ice slurry flows in curved geometries including helical coil heat exchangers and bends. This aim will be achieved through the following objectives:

- Develop a model that is able to simulate the homogenous ice slurry flow in a helical coil exchanger considering the phase change and non-Newtonian rheological model;
- Investigate the effect of various parameters on pressure drop, heat transfer and flow pattern of ice slurry in a helical coil heat exchanger;
- Evaluate the optimum thermodynamic performance of the ice slurry-operated heat exchanger via entropy generation analysis;
- Study the flow structure of ice slurries in straight and bend pipes through flow visualisation;
- Investigate the flow characteristics, pressure drop and loss coefficients of ice slurry flow through a horizontal U-bend via multiphase numerical simulation, and;
- Assess the pressure drop and loss coefficients of ice slurry flow through horizontal and vertical U-bends.

1.4 Scope

This thesis focuses on investigating the thermal and hydrodynamic characteristics of ice slurry refrigerant in heat exchangers, in particular that with helical coil geometry, with the aid of more realistic models compared to previous studies. This study focuses on both single-phase and two-phase modelling of ice slurry flows.

In the first part of the research, a detailed numerical investigation of the thermo-hydrodynamic performance of a helical coil heat exchanger operated with a laminar and non-Newtonian flow of ethyl-alcohol ice slurry subject to phase change is presented. The Bingham plastic model is used to reflect the non-Newtonian behaviour of ice slurry. The phase change of ice slurry is modelled using the enthalpy-porosity method. The pressure drop and heat transfer of ice slurry in a double-turn helical coil are determined in terms of ice mass fraction and *Dean* number. In addition, the entropy generation analysis is introduced to evaluate the overall performance of the heat exchanger, taking into account the opposing effects of heat transfer and pressure drop. The optimum performance conditions of the ice slurry-operated heat exchanger is identified and discussed as well.

The second part of the research numerically examines the flow characteristics of monopropylene glycol ice slurry through a horizontal U-bend. An Eulerian two-phase model is used to investigate the effect of inlet flow velocity, particle diameter and ice volume fraction on the particle distribution and pressure drop throughout the U-bend. The flow is considered isothermal so the heat transfer and melting of solid particles are not taken into account. Shape of particles are considered spherical with constant diameter in each simulation. Pressure loss coefficients of the bend is also evaluated for different ice volume fractions and flow rates.

In the final stage of the study, the aim is to experimentally investigate the flow characteristics of an ice slurry through horizontal and vertical U-bends. The effects of flow rate (inlet velocity), ice volume fraction and pipe diameter on the pressure drop and loss coefficients of the U-bend for horizontal and vertical orientations are investigated. To get a clear picture the ice slurry structure, the flow is also visualised in both straight and bend sections.

1.5 Methodology

1.5.1 Numerical simulations

For the first two stages of the research, Computational Fluid Dynamics (CFD) is used with the aid of ANSYS FLUENT package.

For the first part, governing equations (continuity, momentum and energy) are discretised and solved for the helical coil heat exchanger based on finite volume method. The phase change of the ice slurry is implemented via enthalpy-porosity method. In order to introduce the non-Newtonian rheology of the ice slurry, User Defined Functions (UDF) are built and compiled in C language and then run by the solver.

For the second part, Eulerian multiphase model is used to solve the governing equations (continuity, momentum and turbulence) for solid and liquid phases separately which are treated as interpenetrative continua with interphase momentum exchange.

The following steps are taken when developing and solving the numerical models:

- Generate the geometry using ANSYS DesignModeler;
- Create an appropriate mesh for the geometry using ANSYS Meshing;
- Define the appropriate boundary conditions for the inlet, outlet and the wall;
- Read and compile the UDFs in ANSYS FLUENT;
- Initialize and run the simulation using ANSYS FLUENT;
- Post-process the solution and analyse the results.

1.5.2 Experimental study

The experiments were done using ice slurry production system owned by the Institut für Kälte, Klima und Umwelttechnik, Hochschule Karlsruhe. This ice slurry production system consists of a refrigeration cycle and an ice slurry storage tank. The ice slurry generator continuously produces ice slurry, which is then pumped to and stored in a tank. The ice slurry is then pumped into a test loop made from transparent material. A Coriolis flowmeter measures the density and the volume flow rate of the incoming ice slurry flow. The differential pressure sensor measures the pressure difference between the inlet and outlet of the bend. The ice slurry flow is also visualised using a camera to analyse the flow behaviour.

1.6 Structure of the thesis

This thesis is comprised of seven chapters. In the first chapter, the aim, objectives and a summary of the research is presented. In the second chapter, an overview of the current mine cooling methods and challenges in this area are presented. In the third chapter, a critical review of the literature on thermal and hydrodynamic characteristics is presented and research gaps are indicated. Chapter four presents a detailed numerical model and simulation results for heat transfer, fluid dynamics and entropy generation of ethanol-based ice slurry flow in a double-turn helical coil heat exchanger. Chapter four's results has been published as a journal paper. Chapter five includes the results for the multiphase modelling of isothermal monopropylene-glycol ice slurry through a horizontal U-bend. The results also include the validation of the pressure drop against the conducted experiments in the following chapter. In chapter five, the experimental findings of flow visualisation and pressure drop measurements for monopropylene-glycol ice slurry in horizontal and vertical U-bends are presented. Finally, research findings, conclusions and recommendations for future work are summarised and presented in chapter seven. Figure 1.1 depicts an overview of the structure of the research conducted in this thesis.

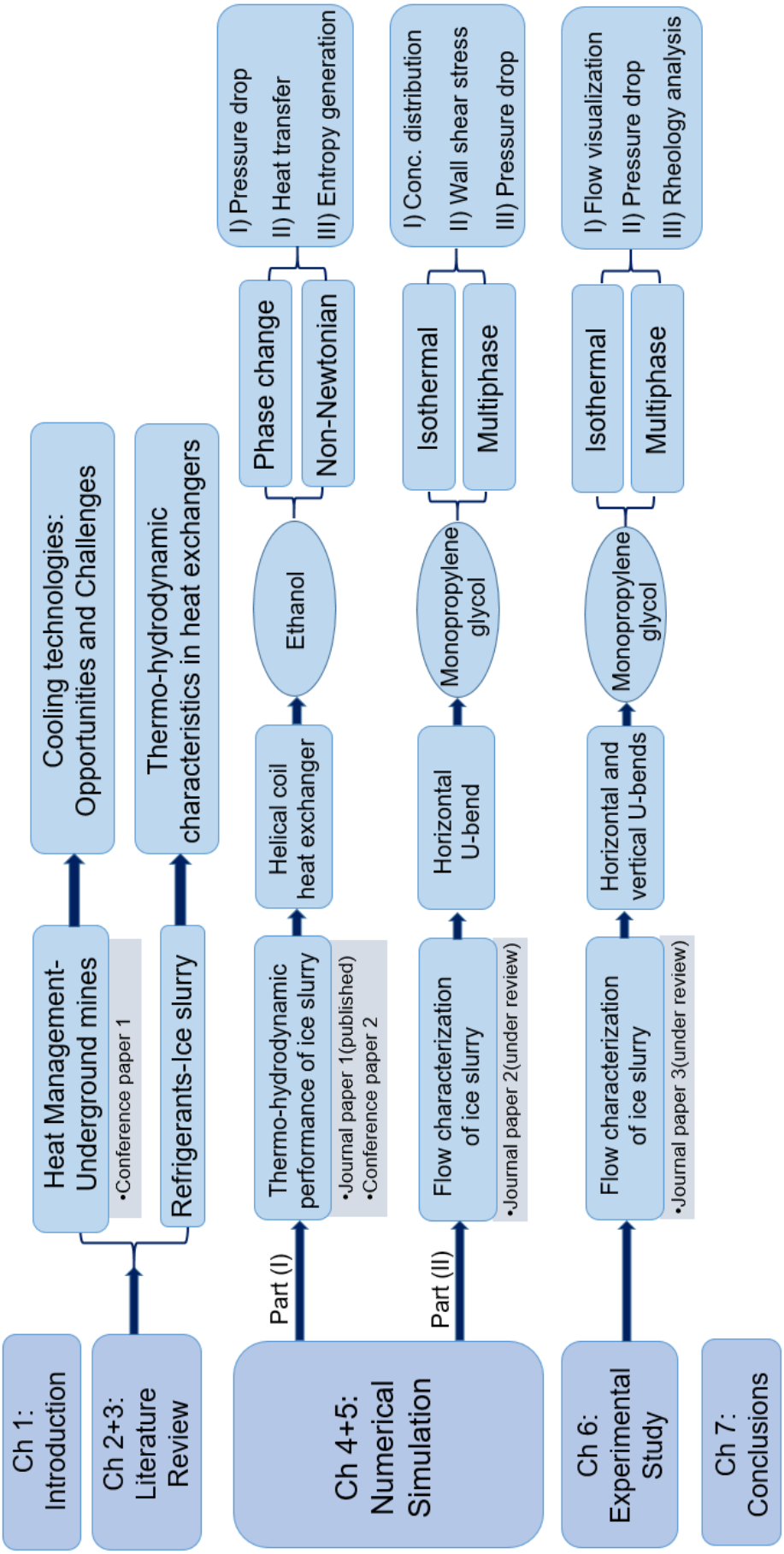

Figure 1.1. Overview of the research structure.

Some sections of the following chapter have been published as:

- **Amin Kamyar**, Saiied M Aminossadati, Christopher R Leonardi, Agus P Sasmito. *Current developments and challenges of underground mine ventilation and cooling methods*. Proceedings of the 16th Coal Operators' Conference, Mining Engineering, University of Wollongong, 10-12 February 2016, 249-262.

Candidate's Contribution to the authorship:

Authorship activities	Contribution
conception and design of the project	70%
analysis and interpretation of the research data	70%
drafting significant parts of the publication or critically reviewing	70%

Chapter 2 Mine cooling strategies and challenges

Design of mine ventilation systems has undergone many changes due to the dramatic developments experienced by the mining industry over the past 20 years. To provide the mining operations with a healthy working conditions at affordable costs, mine ventilation industry still requires further improvements despite the current ongoing feasible developments. Mine ventilation designers has also looked into measures that could optimise the energy consumption of mine cooling plants. The energy consumption by mine cooling plants should be reduced possibly without adversely affecting the safety and health of workers. This chapter presents an overview of the latest techniques used by the experts to address these issues. A revision of the novel ventilation strategies and mine refrigeration methods, and their ultimate effect on the workforce efficiency and mining costs would be identified. Finally, likely future developments in the area of mine cooling is outlined.

2.1 Introduction

Australian mines are directed toward deeper underground operations as exploration tools discover orebodies located at great depths. Deeper working environments imply the need for a feasible means of combating the thermal pollution. Workers subjected to heat stress experience serious hazards in terms of health, safety, productivity and morale [1]. In general, there are two common strategies for underground cooling; one is the use of mine ventilation and cooling effect of the airflow; and use of refrigeration to provide working areas with low-temperature environments. Despite the recent developments in mine air-conditioning, many Australian miners still suffer from thermal discomfort while on duty [2]. Thus, higher cooling capacities at deeper levels becomes the major concern of mining companies which imposes higher initial and operational costs. The rise in energy costs on the other side, has made the companies to seek for energy management strategies that rectify the inefficiencies of current refrigeration systems or reduce the excessive power consumptions. In order to achieve an energy efficient mine cooling system, determination of some factors are essential. These factors include optimum airflow and wet bulb temperature values, applying novel plant components, appropriate integration of components and on-demand plant operation [3]. Obviously, the implementation of energy efficiency projects must not counterbalance the comfortable working conditions for workers. To attain this goal, an exhaustive knowledge of the available technologies and their functionality for different conditions is vital. This chapter aims to give an overview of the latest mine cooling strategies being practiced in different mines. The characteristics of these technologies are presented in two categories of artificial (ventilation) and non-artificial (refrigeration) methods. In addition, the available optimization and energy efficiency technologies are outlined along with reported effects from the reviewed case studies. This study will hopefully

shed light on the current status of mine ventilation and refrigeration as well as potential energy management techniques for future Australian mining operations.

2.2 Sources of heat in mines

2.2.1 Natural sources of heat

This section deals with the heat transfer taking place as a result of natural sources such as the geometry of the mine excavation and the rock characteristics rather than the activities in the mine. The heat transfer phenomenon in the mine majorly takes place in the forms of conduction and convection depending on the medium. These mechanisms substantially lead to the increase of underground temperature and thus need to be recognized before trying to implement a cooling method.

2.2.1.1 *Heat flow from the rock into tunnel*

The amount of heat flow into the tunnelling in this case mainly depends on surface conditions and the nature of the atmosphere. Before heading into any quantitative consideration of the emanated heat from the strata, some practical qualitative observations are substantial to note. First of all, natural geothermal heat passing through the rock surface will increase the temperature of the airflow within the tunnel. By the increase in depth, this issue is further escalated as the surface of the wall approaches to that of the ventilation air while the temperature of the undistributed rock increases. As a result, the temperature difference which is the motive for the heat flowing into the underground is augmented with depth. Second issue is the humidity of the airflow. The increase in the dry bulb temperature is less notable if the airway is wet as a result of the evaporative cooling that may even reduce the temperature slightly. In this situation the overall effect is the increase in the heat content of the air-vapour mixture by the internal energy of the produced vapour. The different transient natures of the intake and return airways is another fact to take into account. While the intake air temperature changes in accordance with the climate, the temperatures of the main return arteries remain almost the same throughout the year. The main reason is the decrease in the mentioned temperature difference for the return airway as opposed to the changing temperature of cooled air entering the intake shaft. Nonetheless, the most remarkable rise in temperature takes place at the mineral winning areas. This is due to the give-up of heat from newly broken rock as well as the machinery on the working faces which will be discussed in the coming sections [4]. In addition to effective parameters such as temperature difference and thermal properties of the rock, the age of the tunnel also impacts the heat flow penetrating the airway and should be considered when calculating the heat load [5].

2.2.1.2 *Heat from coal transport*

Some parts of the heat is also released from the broken rock when being conveyed out of the mine as result of the close contact with the mine atmosphere. This issue is of importance particularly for coal mines as it accounts for a major heat source in coal operations.

2.2.1.3 *Auto-compression*

When a compressible fluid such as air moves towards the centre of the earth, it experiences a rise in temperature as a result of its potential energy into enthalpy and consequently the internal energy. This phenomenon is referred to as auto-compression which is not a "source" of heat in nature but adds to the required cooling capacity. The effect of humidity and change in the moisture constant should also be accounted when designing the required ventilation. Although this occurrence is more substantial for compressible fluids, it still affects the temperature of the water pumped into the mine. For every 1000m change in depth, auto-compression induces an increase of 9.66°C and 2.34°C in the temperatures of air and water, respectively. Despite this relatively small value for water, it can adversely influence the cooling capacity of the mine water pumped underground for cooling purposes. It is estimated that this change in the potential energy of water can be recovered up to 75% by driving a turbine as a means of conversion to mechanical work [6].

2.2.1.4 *Artificial sources of heat*

Some activities done underground cause the temperature of the working environment to rise. Since these activities are generally carried out by humans or the working equipment rather that natural phenomena, they are hereby referred to as "artificial" sources of heat. These mainly include mechanized equipment, human activity and explosives which are discussed in the following parts.

2.2.1.5 *Heat from machinery*

In the case of underground operations, the working of machinery comes with thermal pollution as with the consumption of electrical or chemical (diesel) forms of power some amount of heat is introduced into the working areas. For electrically driven equipment, the efficiency is a major indicator of the heat produced by the machinery. Greater efficiency implies that a smaller portion of the input power is converted to heat while the greater part of the power is changed into useful work done (to increase the potential energy against gravity). In addition, the efficiency of the equipment provides information on the distribution of the heat produced. The increase in efficiency has converse effects on the different locations of heat dissipation: lower temperature at the motor (gearhead) but greater temperature at the pick-point, conveyor rollers and along the length of the conveyor. When it comes to using diesel engines, the equipment may produce three time as much heat as electrically

driven types since the bulk of heat input (combustion) is dissipated into the environment. This remains almost true even for LHD trucks where work is done against gravity. Another worthwhile fact is that some portion of the produced heat by diesel engines is in the form of latent heat. This will add moisture to the ventilated atmosphere per each litre of fuel consumption [4, 7].

2.2.1.6 *Human activity*

Human body generates a certain amount of heat in accordance with the level of muscular activity. Other parameters such as physical health and fitness as well as mental state would vary the heat dissipation rate from the body. To get a grasp of this, metabolism can generate heat rates from 174W for a fairly light manual work up to 622W for a heavy duty activity. This mode of heat production is generally responsible for a minor portion of the required cooling in an underground environment, however it becomes notable in areas with labour-intensive activities are being carried out in a poorly ventilated region (e.g. heading).

2.2.1.7 *Heat from blasting*

A considerable amount of heat is released after underground blasting which depends on the type of explosives and usually ranging from 3700 to 5800 kJ/kg [8]. The generated heat emerges into two parts; one is the explosion fumes which accounts for a maximum heat load on the ventilation and the rest will be transferred to the broken rock. The amount of heat storage in the rock is ruled by the mining method. If the blasting is carried out within a region through which ventilation air passes such as an open stope or a longwall face with a high fragmentation, majority of the heat will be transferred out of the broken rock rapidly. On the contrary, in case of blasting takes place in a fairly closed region such as a sublevel or with a forced caving technique the transient release of heat from the broken rock will be rather slow.

Australian coal mines, especially in Queensland, are also prone to spontaneous combustion as the consequence of high strata temperature. Thus, the rise in the ambient and goaf air temperatures add to the possibility of spontaneous combustion which implies the significance of heat load calculation. For the case of longwall coal mines, a major part of the heat load stems from the working face, open goaf areas and panel/main road conveyor belt roads.

2.3 Mine cooling strategies

The ventilation code of practice is an approved guide to achieve the Australian standards of health and safety. This code applies to both coal and metalliferous mines and regulates all activities during the life of mine such as exploration, construction operation and final mine closure. The guide

presents rules of thumb for ventilations systems in terms of wind speed, location of elements. For instance, a minimum wind speed of 0.3 m/s in an airway is recommended for underground ventilation.

With the increase in the temperature of the underground working environment, the conditions approach an allowable upper limit called heat stress index. When the conditions surpass this index, operations must be curtailed unless a suitable mine cooling strategy is introduced. There are various heat stress indices used worldwide such as dry-bulb temperature and wet bulb temperature of which the latter is quite common since it is appropriate for humid environments as well. For instance in Australian mines, the rule of thumb is that with average temperatures exceeding 28°C wet-bulb (on the hottest days) or the temperature of any working area exceeding 32°C, an underground cooling method must be implemented. Wet bulb temperature has been widely used in South African mines as a thermal stress index as well. Beside wet bulb temperature, some other countries in Europe such as German coal mining industry sometimes use the concept of effective temperature [9]. In France, other indices namely the Belgian effective temperature and resultant temperature defined in terms of dry/wet bulb temperature and air velocity v are used.

Upon the definite need for a cooling strategy, the responsible parties should decide on the some basic aspects of the method to be implemented [2]:

- The location (surface/underground)
- Form of cooling (self-contained underground, underground air cooling by chilled water from surface, ice plants, surface bulk air cooling, etc)
- Required cooling capacity of each form of cooling
- Capital and operation cost of the method to be used

Each of the available methods has its own merits and demerits. The satisfactory function of the mine air-conditioning system provides the hot underground mines with the opportunity to exploit deeper reserves and to increase the production. Figure 2.1 shows the hierarchy used by Anglo American operations in terms of different cooling strategies for South African mines. With Australian mines being affected by similar conditions, the trend is to implement the experience obtained for the gold and platinum mines of South Africa. However, the dynamic nature of longwall mining (with frequent moving face) brings about the need for a hierarchy of various strategies for coal mining [10].

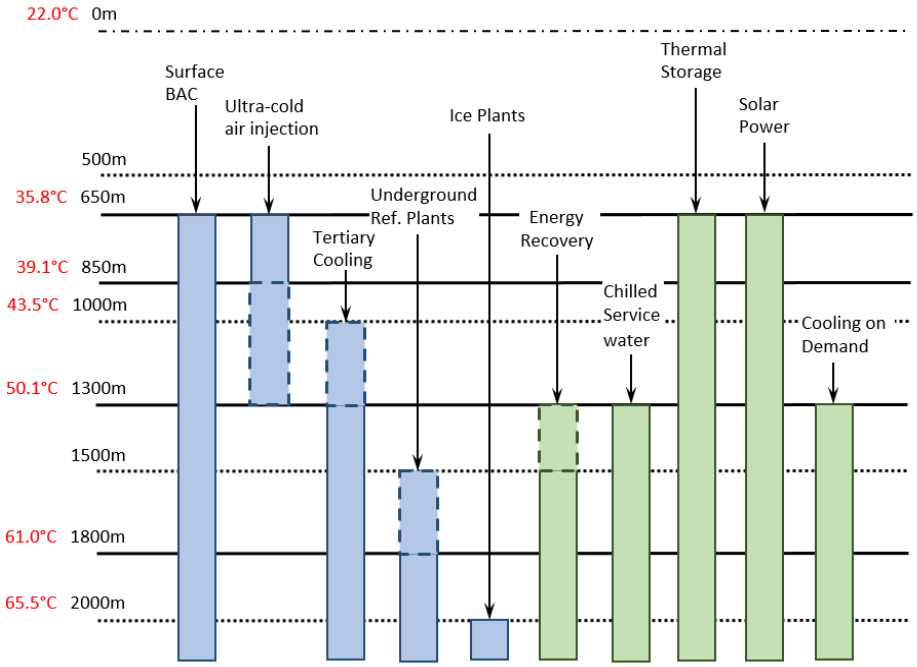

Figure 2.1. Hierarchy of implemented cooling strategies by Anglo American operations for South African mines [10].

2.3.1 Non-artificial cooling strategies

These types of underground temperature control methods do not entail refrigeration plants and mainly use ventilation cooling with the aid of a large fan over the intake shaft. The heat control mechanisms within the context of ventilation includes providing higher airflows either by increasing the primary airflow or introducing higher local airflows with the aid of air-movers or other auxiliary devices. There are also rules of thumb to determine the required airflow in underground tunnels. In the case of Australian mines which are highly mechanised with large orebodies, a value of 180 m^3/s per Mtpa is typical. Other values are also suggested for the air velocities in different airways: maximum velocities of 6 m/s for horizontal intake, 10-12 m/s for horizontal exhaust and 13-16m/s for vertical airways (this limit increases for deeper mines) [11]. Other methods in line with conventional ventilation are also available to work as heat management strategies. Fill mining method to reduce the heat emission in the mined-out areas by filling the area and closing it timely is one of the techniques. Other procedures involve controlling the heat stemming from the sources such as rock, machinery, ground-water and blasting. Some of these control measures can be expressed as: spraying the rock cliffs with insulation material; increasing wind speed; pre-cooling the coal seam; eliminating low-efficient machinery; localized ventilation in the electrical chamber; using auxiliary fans and relocating the current ones; separating the working hours from blasting periods [12]. Although the aforementioned strategies have certain advantages, they are not fully capable of tackling

the thermal pollution issue for ultra-deep mines and introduction of a refrigeration method becomes inevitable.

2.3.2 Artificial cooling strategies

Introduction of mechanical refrigeration systems dates back to the mid-1800s with applications in food and document preservation. The first 'apparatus for treating air' was patented by Willis Carrier in 1906 followed by the term "air conditioning" being coined by engineer Stuart Cramer for the first time later in the same year. The first centrifugal refrigeration machine for cooling larges spaces was patented by Carrier in 1921 [13]. The first use of artificial cooling for underground mines goes back to 1860s when heat control was done by transporting blocks of ice underground in ore cars. However, the earliest use of vapour compression refrigeration was in 1921 to cool an underground depth of about 2400m at the Morro Velho mine in Brazil [4]. In Australia, a 3 MW plant was installed at Mount Isa for the first time in 1960s that used chilled water to cool the deep environments with the aid of high-pressure coil heat exchanger. However, the first surface refrigeration system for an Australian coal mine was in the Bowen Basin at Central Colliery for a depth of 542m about two decades ago [10].

2.3.2.1 *Mine refrigeration plants: Surface Bulk Air Cooling (BAC)*

Currently this is the most commonly-used cooling technique in Australian coal mining (Figure 2.2). The largest surface BAC in Australia is operates at Mount Isa with a capacity of 36MWR [14]. The vapour compression cycle works on the basis of compressing the refrigerant vapour to a high pressure (and high temperature) before sending it to the condenser (a heat exchanger) where it reaches a liquid form. Condensation is done with the aid of cold water coming from cooling towers. High pressure liquid then flows into a receiver followed by an expansion valve. Upon passing through the valve, the liquid refrigerant experiences an abrupt drop in pressure (along with dramatic drop in temperature) and sudden expansion (flash off) resulting in the evaporation of the liquid. The low-pressure liquid then flows to the surge drum which separates the liquid and gas phases to ensure only vapour is sent to the compressor. The liquid refrigerant passes through the evaporator (another heat exchanger) where it absorbs the heat from air or water and boils. The vaporized refrigerant then enters the compressor and refrigeration cycle restarts [4]. Efficiency of each of these components affect the Coefficient of Performance (COP) of the refrigeration cycle.

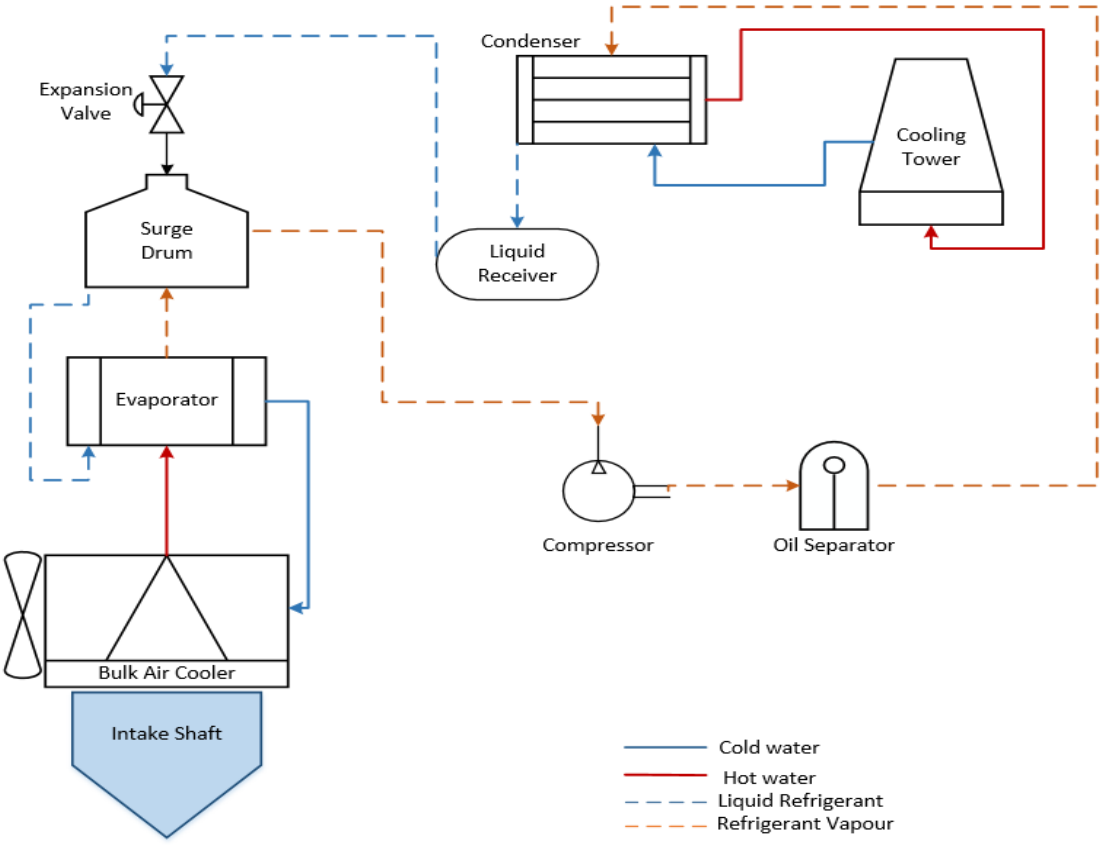

Figure 2.2. Schematic of a typical surface Bulk Air Cooling (BAC) refrigeration plant.

Brake [15] thoroughly indicated the key engineering considerations in the design of mine refrigeration plants. The author outlined that the major components as screw compressors, ammonia refrigerant, plate heat exchangers as evaporator/condenser as well as cooling towers require specific design criteria. Safety and environmental considerations are to be born in mind while selecting the refrigerant. While selecting heat exchangers, fouling minimization on both hot and cold sides is a substantial issue. Recently, Hooman et al. [16] presented an inclusive step-by-step guide for proper selection and design of mine BAC heat exchangers in terms of parameters such as size, location, inlet conditions, water loading, environmental conditions and surrounding activities. Special cases including the extremities of the plant operation or design requirements of remote mining locations should be also considered. Lack of unique design code for mine cooling plants, has prevented most plants from fully exploiting the refrigeration capacity [2]. The major challenge encountered when using this technique is the arrival of an acceptable cooled air at the coal face considering the long distance from the plant. Depending on the mine layout, the transit time of intake air changes according to the air velocity. For deeper mines, this means more opportunity for the air to pick up heat and other contaminants.

2.3.2.2 *Mine refrigeration plants: Underground cooling techniques*

Despite all the advantages of surface BAC, implementing an underground solution for thermal pollution especially for ultra-deep mines becomes essential. Here, the underground mines owning a depth of equal or greater than 2000 m are considered as “ultra-deep”. Underground refrigeration is usually maintained by: chilled water from surface, secondary cooling of air, recirculation in ventilation districts or tertiary (in-stope) cooling. For longwall and development, the trend is to locate a coil heat exchanger (BAC) in a mined loop. Chilled water is then pumped through the insulated steel pipes (installed boreholes) to the underground coil BAC. A great proportion of the intake air is directed to pass through the BAC chamber with the aid of air locks or auxiliary fans [10]. Figure 2.3 demonstrates the schematic of the overall design of such a system studied by O’Connor et al. [17] to evaluate the feasibility for a Bowen Basin mine. On the right hand side, location of the heat exchanger is shown relative to the longwall panel. Comparing the positional efficiency of the various methods (surface BAC without underground cooling; surface BAC with underground cooling and underground cooling only), the authors found that utilizing the underground heat exchanger alone is the best option.

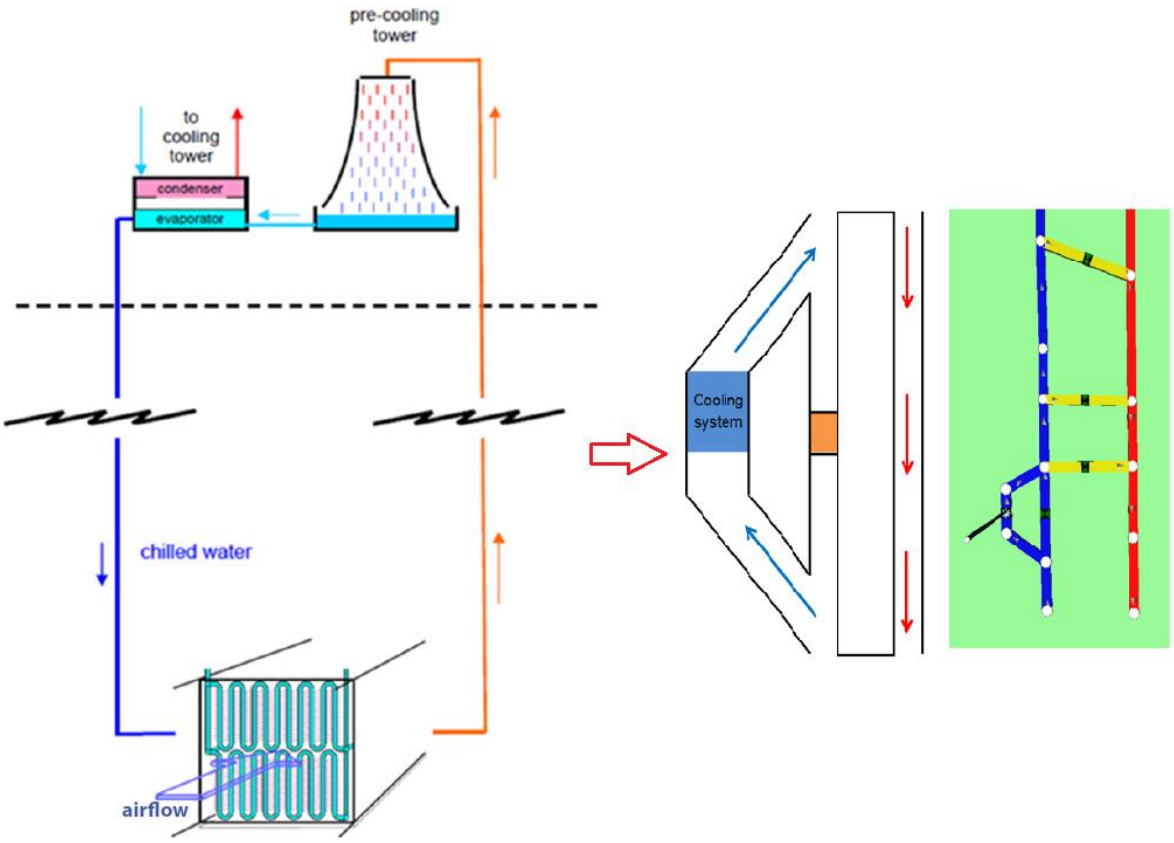

Figure 2.3. Schematic of an underground cooling system and location of the BAC for a Bowen Basin mine [17].

With the increase in the mining depth and the pumping distance, the operational cost of underground BAC also rises. Locating the refrigeration plant underground, is another method that shortens the distance in which chilled water (air) travels. An example of such systems is presented in Figure 2.4. This technique was studied by Ramsden et al. [18] and compared with surface cooling systems. The major limitation regarding the use of this type is the insufficient source of heat rejection which is the return air only. While surface plants reject the heat to the general ambient air, the limited hot air flow in the intake airways has adverse effects on the efficiency of underground plants. This is along with higher comparative costs due to the needs for high-pressure compressors, extra excavation and installation [19]. For coal mines, another challenge stems from the frequent movement of equipment with longwall as opposed to metal mining.

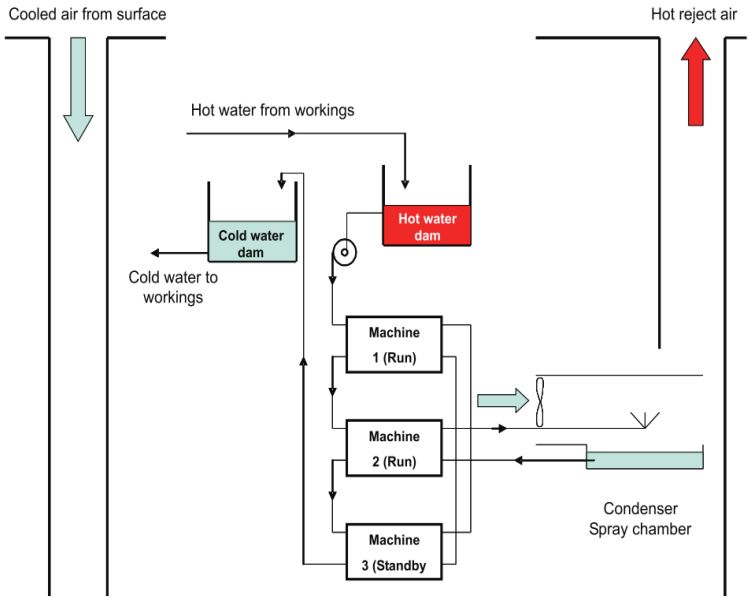

Figure 2.4. Schematic of underground refrigeration plant [18].

Thus, in some cases the underground refrigeration system consists of two components: the main refrigeration plant chamber and chillers as well as the movable component which comprise air coolers (coil heat exchangers) with water distribution network. Some other mines use a “hybrid” system which is a mixture of surface BAC and underground refrigeration with BAC located in critical locations. For instance, this system was planned for block cave operation copper mine in Arizona, USA including surface BAC with a capacity of 105.2MW and underground air coolers providing 38.5MW [20].

As the mine gets deeper, larger volumes of air is needed which imposes rises in both capital and operational costs. For a deep underground mine, it would cost around $30 million with an annual operating cost of $5 million to decrease the wet bulb temperature by almost 3ºC. This has been the case for South African gold mines with underground BAC. However, installation of underground

refrigeration plants, is limited as the heat should be dumped via exhausting the air through the long distance to the surface. Thermal storage systems has been suggested to be cost-competitive for Australia coal mines [10].

2.3.2.3 *Mobile localized (spot) cooling*

When the evaporator of the refrigeration unit is in the direct contact with the airflow at the place where cooling is required (i.e. face cooling). The absorbed heat in the condenser is also dumped directly to the return air. Benefits of this system is the immediate cooling at the spot and no loss in efficiency due to water reticulation. Spot coolers work on the same basis as domestic air-conditioning units except that the heat is rejected to the outside atmosphere [4]. District cooling has been implemented for in South African since 1950s with capacities ranging from 100 kWR to 500 kWR. The use of mobile spot coolers is a prevailing strategy for cooling German coal mine longwall faces as well. This technique a lot likely to be used in Australian mines with the increase is mining depths. However, the challenge is the necessity of an approval for the operation of such coolers in Australian mines [10].

Due to the large energy consumption of conventional vapour-compression cooling systems, some alternatives have been introduced for spot cooling in mining applications. One of these techniques is the use of vortex tubes. This device, invented by Ranque [21], works based on the fact that if the vortex motion of a fluid is confined in a cylindrical tube a significant temperature separation occurs causing one end of the tube to cool down and the other to warm up. This phenomenon takes place without the help of any moving parts. Despite the relative low refrigeration capacity of vortex tubes, they can be a potential candidate for underground district cooling for many reasons such as light weight, usable when electricity is not available, low initial cost, instantaneous operation and no need for expert operator [22]. Figure 2.5 delineates the overall system and detailed structure of a vortex tube. Upon the injection of the high pressure fluid, major part of the fluid rotates and moves forward along the periphery of the tube. However due to the nature of the fluid dynamics, the inner part of the flow returns toward the cold exit. As a result of a pressure gradient created by the forced vortex, a cold core is formed near the injection leading to temperature drops [23].

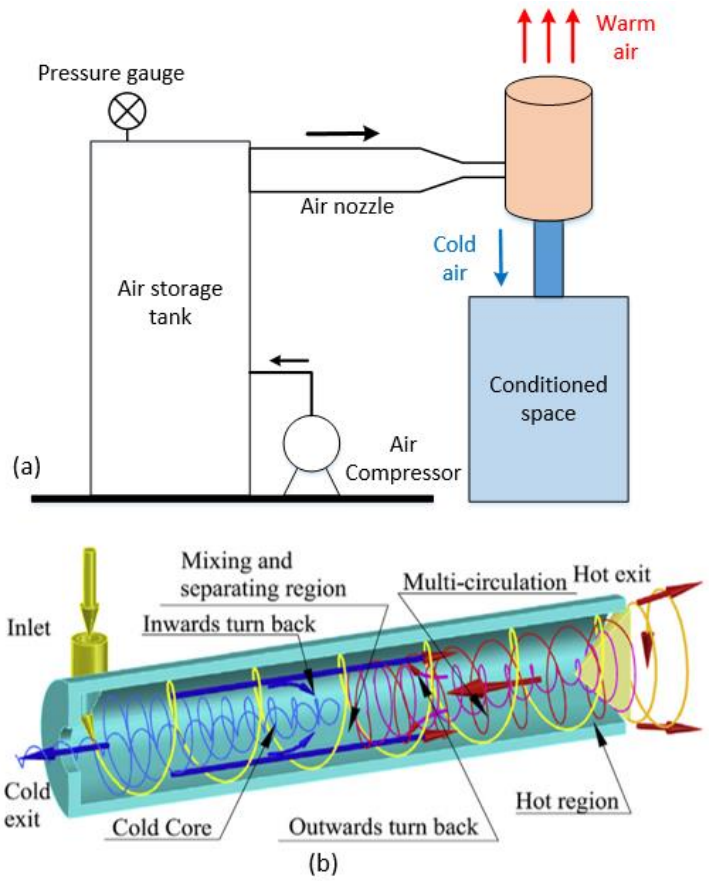

Figure 2.5. (a) A vortex tube refrigeration system [22] (b) flow structure inside a vortex tube [23]

Although the function of a vortex tube seems different from regular cooling systems, it can be analysed as classic thermodynamic cycle to shed light on the temperature, pressure and velocity profiles [24]. The feasibility of using vortex tube refrigeration was investigated by Jinggang et al. [25] for the first time. The authors indicated the beneficial application of this technique for underground cooling due to a number of reasons: making use of compressed gas underground, possibility of moving the system with the mining work face, no need for long pipping, major cost saving and overall reduction in greenhouse gas emissions. The work on this type of cooling strategy is still immature and should be extended for future potential mining applications.

Another novel proposal to provide district cooling in underground environments is the use of high-pressure water as driving fluid in an ejector refrigeration system [26]. Figure 2.6 illustrates the schematic of a water vapour refrigeration unit and its major components. The working principle of an ejector is based on gas (vapour) extraction from a space via discharging a motive fluid (water). The fluid exits as a jet through a nozzle acting as a vacuum pump that draws the gas (vapour) into the diffuser and mixing tube. Transfer of energy between the water jet and the low-energy vapour, leads to the mixing of fluids resulting in condensation of a great part of the vapour [27]. Upon cooling the water to a certain temperature, if the pressure is adjusted to a value lower than the saturation pressure

of that temperature water will start to boil. Due to the high enthalpy of vaporization of water, a small mass fraction (0.17%) should be evaporated in order to have a reduction of 1°C in temperature. Steam-jet ejectors can provide the low pressures required for this purpose. The ultimate result is the removal of heat from the evaporator section by the motive water jet.

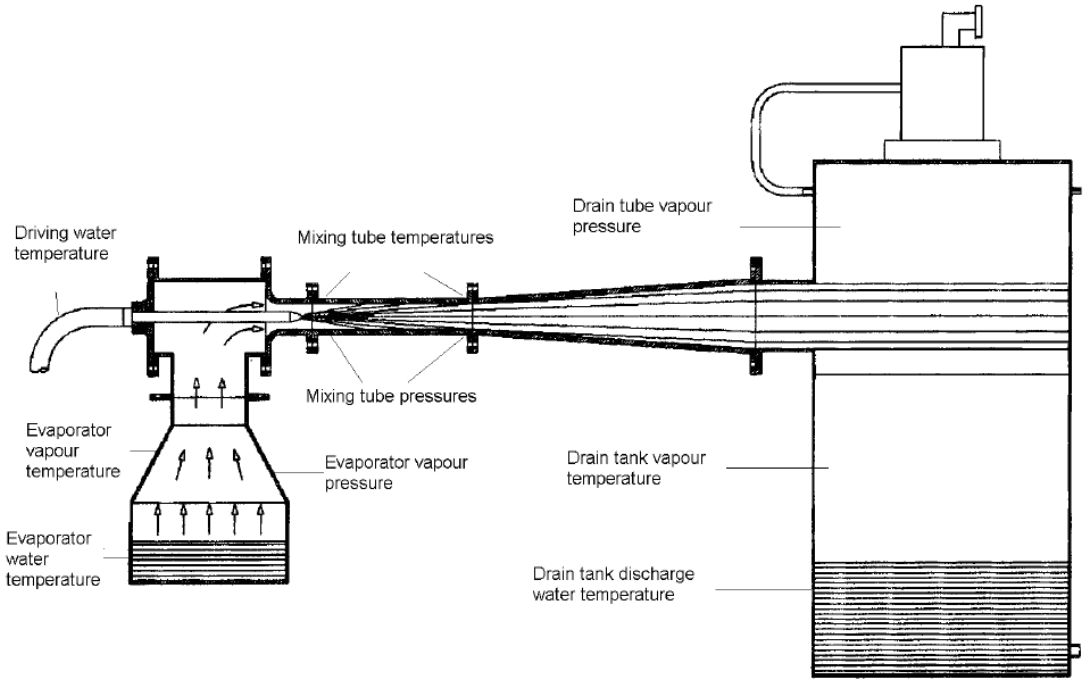

Figure 2.6. Schematic of an ejector for water vapour refrigeration [26].

Butterworth and Sheer [28] investigated the potential functionality of such systems for underground cooling using the available mine water. It was concluded that this technology can be implemented for backfill cooling. The backfill, which is used to fortify supports and enhance the ventilation control, usually imposes a heat load on the ventilation itself. Installing a cooling ejector system on the levels above the stopes, high-pressure water jet will reduce the temperature of the backfill efficiently. Layout of such this proposed technique is shown in Figure 2.7. Alternatively, the ejector can be integrated with an energy recovery device such as a Pelton turbine to make use of the hydraulic energy extracted from the diverted water.

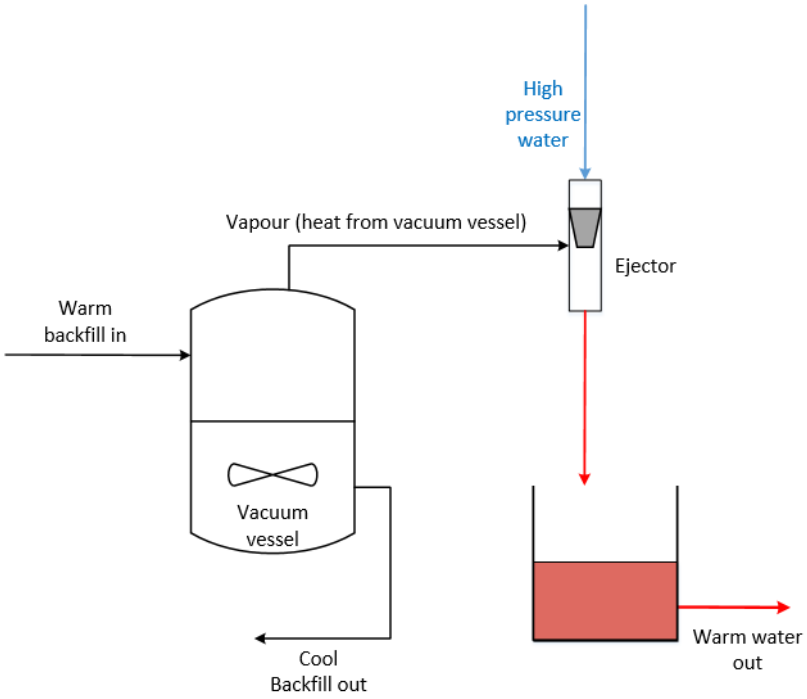

Figure 2.7. Backfill cooling system using water ejector.

2.3.2.4 *Ice cooling systems*

Use of ice from surface for underground cooling dates back to 1927 which was found to be inefficient and infeasible [29]. Later on, South African Mponeng mine tested the use of ice to provide cooling at a depth of 4km with rock temperatures reaching 55°C. Compared to chilled water, with a reduction of 70% in the mass flow rate the same cooling capacity can be provided using melting ice. The initial, operating and maintenance costs of ice producing power plants are high. For the case of South African mines, the advantages of running such systems outweigh the cost-imposed burdens when a pumping head of 2500m is reached. This can be the case for future Australian ultra-deep mines as well [10]. When water is pumped underground, its temperature goes up as a result of its potential energy being converted to heat. As indicated by Kidd [30], for the case of Vaal Reefs mine, an increase of about 2.4°C per 1000m of pipe run were measured. Whereas for ice slurry, the mixture temperature will remain almost constant due to melting of ice. In another study by [31] the application of ice slurry for underground cooling at the Western Deep Level Gold Mine, South Africa was described. An ice slurry plant comprising of four 3MW units were used to produce the ice slurry transported to depths of 4000m with the aid of gravity. Mackay et al. [32] carried out a comparative modelling to specify the break-even depth at which each refrigeration mode should be applied for Impala Platinum mine, South Africa. Figure 2.8 shows their comparison results regarding the required mass flow rate of cooling modes (chilled water vs. ice from surface) with the increase in depth. Despite the excessive growing trend of required flow rate of chilled water, the ice flow rate for the

same refrigeration capacity is still affordable at lower depths. The authors also indicated that in terms of cost analysis, after a depth of 2900m the results are in favour of ice cooling method. However, it was elaborated that for depth of 1900m till 2300m chilled water is still the most cost-effective and can be applied in a more feasible way when integrated with some technologies such as secondary cooling of intake air, proper pipe insulation, turbine energy recovery and high-pressure U-tube systems. It should be borne in mind that economics of ice slurry cooling systems are influenced by factors such as power tariffs, climate, geothermal gradient and heat from artificial sources [4]. This implies that a techno-economic analysis of ice plants before implementation on any mine site is beneficial.

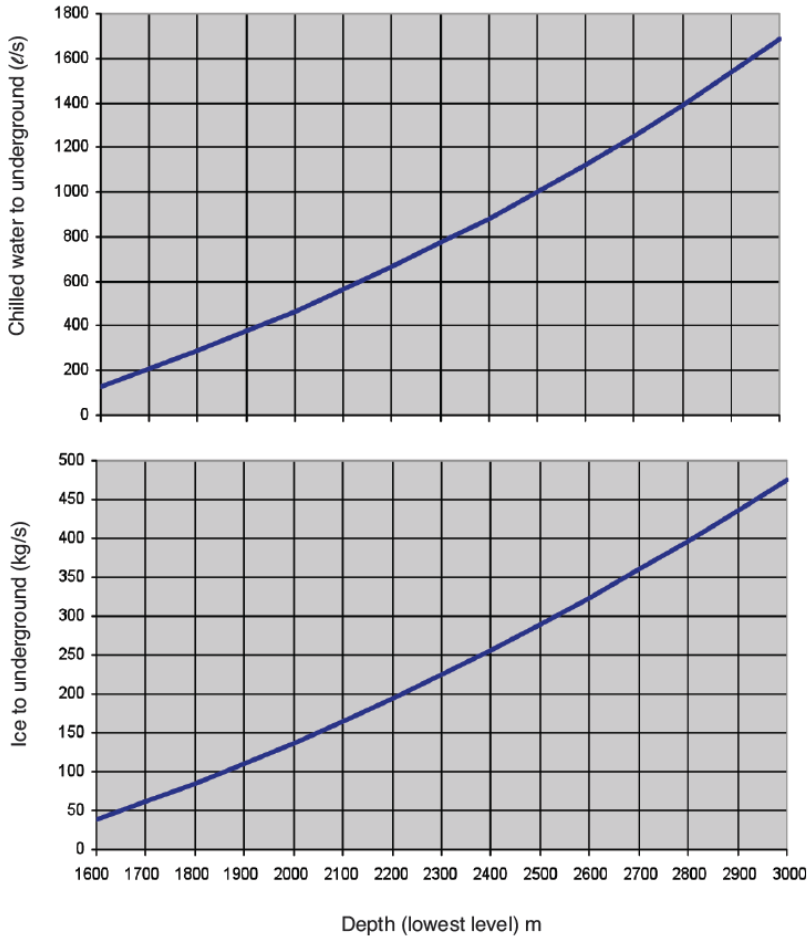

Figure 2.8. Required mass flow rate of cooling modes (chilled water vs. ice from surface) with the increase in depth [32].

It is noteworthy that ice can also be produced for other purposes than underground cooling, which is the thermal energy storage and load shifting capability. These systems are particularly worth implementing where power tariffs are levied such that substantial savings can be achieved by producing ice at night (off-peak periods) and using it during daytime at peak tariff. In terms of power cost saving, this technique might not be profitable for Australian mines due to fixed tariffs; however,

it could help to install a smaller refrigeration plant by load profiling where there are electricity constraints [19]. For this application, the refrigeration plant consists of two components: primary (base load) machine and thermal storage dam. Chilled water exits the former and then enters the latter which contains tube banks. Glycol passes through these tubes and causes a layer of ice to be formed during low-temperature periods throughout the day. The formed ice then adds to the cooling capacity by melting during hotter periods of operations [20]. Figure 2.9 shows the schematic of such a system.

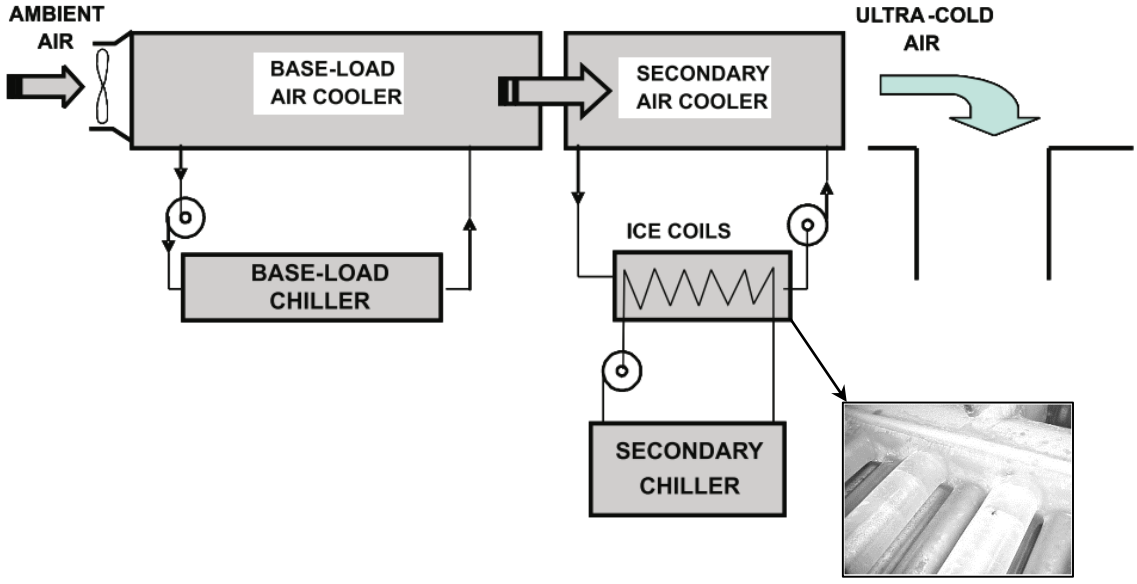

Figure 2.9. Schematic of refrigeration plant integrated with ice thermal storage [18].

2.4 Optimization and energy saving methods

A summary of available underground cooling strategies was presented in the previous section. However, these systems are sometimes the main electricity consumers bringing about significant operating costs. Thus, mining companies often seek for energy efficiency or optimization techniques to tackle this challenge. As mentioned before, the initial engineering considerations in design and selection of optimal refrigeration components is the primary step to prevent energy and cost over-expenditure. In this section, the energy efficiency improvement techniques that can be integrated with the designed/implemented cooling plants will be discussed.

With the advent of computer technologies, it is now possible to implement an accurate monitoring and control techniques to observe the conditions of air temperature and velocity, contaminants and water flow. Real-time Energy Management System (REMS) is currently drawing more attention as a tool providing an optimized schedule for refrigerating the hot underground areas

[33]. The purpose is to reduce the energy consumption of mine cooling with the aid of technologies such as Variable Speed Drives (VSD), control valves and other Demand-Side Management (DSM) methods. Pelzer et al. [34] implemented this strategy for three South African mines to monitor and optimize the inlet chiller temperature. They reported a value of 32,416 MWh reduction in electricity consumption due to the increase in COP of the plant. The application of the same monitoring system was also reported by Vosloo et al. [35] for water reticulation system of Kopanang gold mine in South Africa. The authors claimed that a 2% reduction in overall power consumption corresponding to an annual cost saving of US$636,400. In another study by du Plessis et al. [36] the outcome of implementing various energy saving strategies for Kusalethu mine in South Africa was reported. The applied strategies included evaporator and condenser flow control using VSD, BAC water flow control using valves and retrofitting of old pre-cooling towers. The implementation of these strategies were found to result in a saving of about 31% in the total plant power consumption while keeping the refrigeration and ventilation requirements met and the COP of the cooling system enhanced overall (See Figure 2.10). As one of the techniques, the effect of VSDs was investigated by du Plessis et al. [37] for 20 South African mine cooling systems. The feasibility of installing VSDs for chiller compressor motor, and all pump and fan motors were estimated. It was concluded that a power savings of about 168,633 and 144,721 MWh/year is achievable by installing VSDs on chiller compressor motors and all pump motors, respectively. Mare et al. [38] also explored the effect of energy saving strategies by varying the flow according to the demand for two mine case studies. VSDs were installed on the evaporator, condenser and BAC pump motors. For evaporator, the strategy helped to monitor and control the dam level while for the condenser it provided a fixed temperature difference within the condenser vessel (See Figure 2.11). Reduction of full-load conditions for the BAC and a fixed constant wet bulb temperature (8°C) was also attained. Beside these merits, major barriers of using VSDs are mainly indicated as technical (non-linear loads), economic (high price) and awareness (personnel scepticism about achievable energy saving) issues. By addressing these issues, implementation of VSDs for Australian mine cooling system might be more common in future.

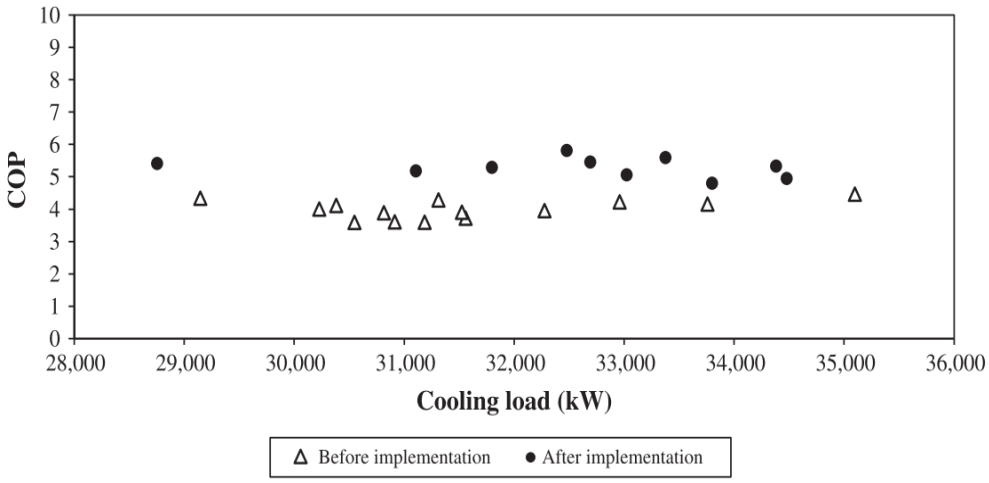

Figure 2.10. COP of the cooling system before and after implementing the energy saving strategies by [36].

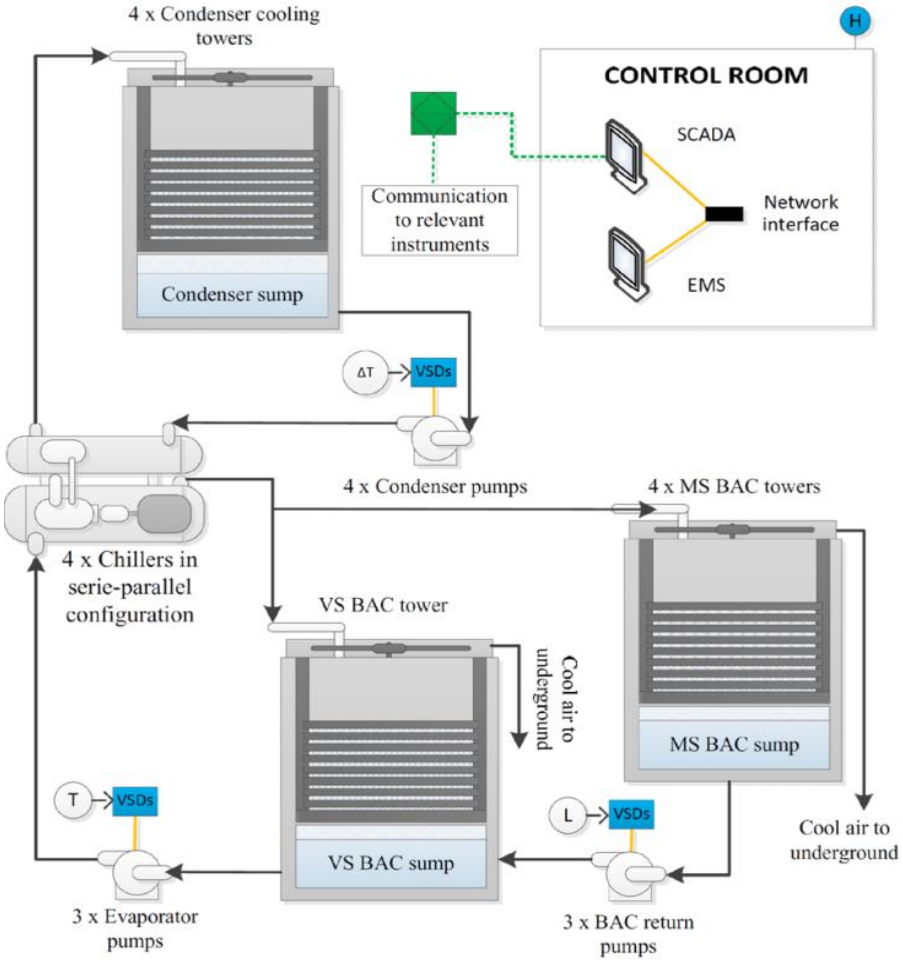

Figure 2.11. Layout of underground cooling system integrated with variable flow equipment [38].

In recent years, another strategy has been instigated in Chinese mines which is based on extracting the cold from the underground water inrush to cool the warm airflow [12]. In summer,

High-temperature Exchange Machinery System (HEMS) is able to provide cooling to the working environment as well as buildings. The system also helps to provide the extracted heat from water inrush for buildings and showers in winter [39]. Figure 2.12 shows the layout of this system comprising of closed-loop water as well as open-loop air circulation systems. Since the refrigeration plant (chilling water) and air cooling station are located at different levels, a pressure transition is also installed to reduce the pressure when reaching lower levels. Qi et al. [40] reported the operational effects of this system for Sanhejian coal mine, China for a depth of 1000m. They indicated that the airflow temperature at a point of the working face decreased from 38°C to 30°C. This method is claimed to bring about environmental benefits and economic sustainability in addition to energy management. A similar thermal energy management system was introduced by Niu [41] where a heat recovery system was utilized during winter. A two-stage cooling system was proposed that made use of the lower underground cooling requirements in winter, to run the heat pumps in heating conditions by recovering heat from the low temperature mine return air and mine water.

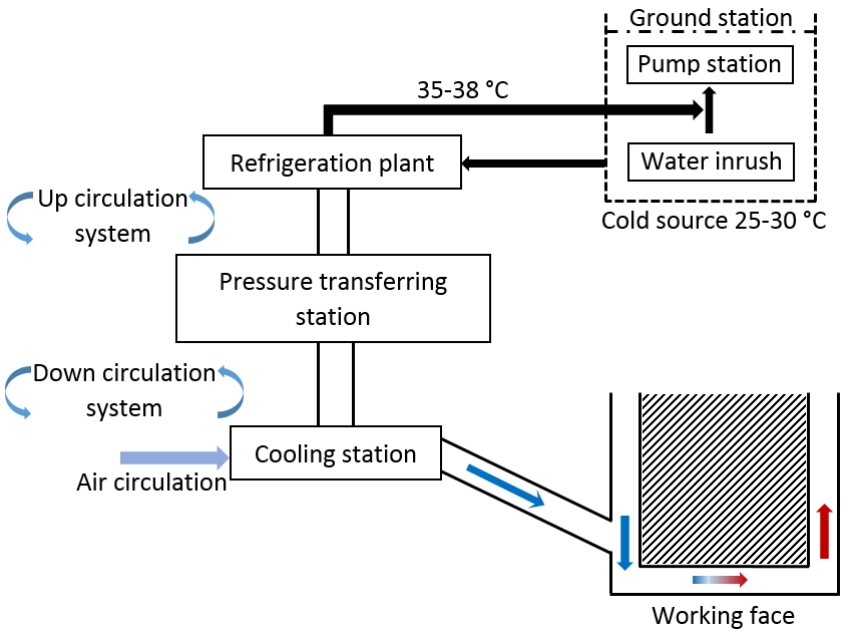

Figure 2.12. Schematic of HEMS cooling system [42].

Aside from the aforementioned strategies, Schutte et al. [43] focused on improving the efficiency of pre-cooling towers and its effect on the refrigeration performance. The energy efficiency project included replacing the film fill inside the tower with splash type fills to rectify the clogging inside the tower. In the next phase, the large fans were retrofitted by four smaller fans that required lower maintenance. These implementation added up to a daily power saving of 1 MW. Outlet temperature also dropped by 4°C as the tower performance enhanced.

2.5 Conclusions

This chapter presented an overview of the common trends in mine ventilation and refrigeration as well as more recent energy efficiency and optimization practices in underground cooling. Despite all the recent developments in South African mines, many Australian mines are still lacking a mining code of practice for heat management in mines. If the sources of heat in underground environment is measured in an accurate way, a suitable cooling strategy can be proposed which is an inevitable fact with the increase in depth of mines in future. Energy efficiency and optimization strategies will address the concerns of management in terms of functionality and cost-effectiveness of these strategies. The cooling requirement of an underground environment might change hour-by-hour or shift-by-shift with the change in number of equipment, workers and operations. Demand-side Management (DSM) systems introduced, are sample methods to resolve this issue. Introduction of novel monitoring systems, implementing control strategies to obtain cooling-on-demand, thermal energy recovery from available resources and improving the performance of current cooling plants are the main ways to achieve this goal. Previous case studies acknowledge that large financial benefits can be acquired if refrigeration plant of a mine is optimized.

Chapter 3 Fluid Dynamics and heat transfer characteristics of ice slurries

Ice slurry refers to a binary solution (such as alcohol, glycol, etc.) mixed with small ice particles with an average diameter of 1 mm or smaller (Figure 3.1) [44]. Releasing large latent heat of fusion during melting of ice particles gives interesting features to this type of flow. Rapid cooling rate, intensive-energy density and eminent heat transfer capability make ice slurry a promising coolant as compared to the common single-phase fluids [45, 46].

Figure 3.1. Microscopic photograph of a sample ice slurry [44].

A number of review studies were carried out on the behaviour and applications of ice slurry in the last decade. In 2003, Ayel et al. [47] conducted a review focusing on the rheology and heat transfer of ice slurry flows. Later in 2005, Kitanovski et al. [48] critically reviewed the research work done before 2002 on the fluid dynamics of ice slurry flows. They announced the effects of particle shape, size and time behaviour, numerical works on flow pattern, and effect of heat transfer on the pressure drop as the areas requiring more elaborative research. Bellas and Tassou [49] presented an overview of various industrial applications of ice slurry including mine refrigeration. They outlined the capital cost and energy consumption of ice production to be the major deterrents of using this technology in different areas imposing the need for further research and development. In the same year, other reviews were published focusing on physical properties and applications of ice slurry including those by Egolf et al. [50], Davies [51].

In this chapter, more recent literature on fundamental flow behaviour in terms of fluid dynamics and heat transfer as well as application in heat exchangers will be presented chronologically. The literature will be classified into two groups of experimental and numerical works.

3.1 Experimental studies

The doctoral thesis of Melinder [52] has been commonly used as the pioneer reference for determining the thermophysical properties of aqueous solutions and ice slurry. This work presents exhaustive data from experimental measurements of density, viscosity, specific heat and thermal conductivity of ice slurries and anti-freeze solutions. The findings have been also endorsed by the International Institute of Refrigeration (IIR) as a credible reference for characterization of this secondary refrigerants. As proposed by Melinder [53], using properties of the anti-freeze depressant and ice, ice mass fraction and enthalpy of ice slurry can be obtained.

3.1.1 Rheology of ice slurries

The fact that ice slurries demonstrate non-Newtonian flow characteristics is well indicated in the literature. Due to the complex flow structure, there is not a unanimous consent on the most accurate rheological model for ice slurry flows. The rheological flow properties of a fluid is governed by the relationship between the shear stress and shear rate. Shear-thinning fluid shows a decreasing viscosity with an increase in the shear rate. The other category of fluids show shear-thickening behaviour that includes a rise in viscosity with an increase in the shear rate. When the fluid shows a minimum stress threshold (referred to as yield stress), that must be overcome before the fluid is able to flow. When the exerted stress exceeds the yield stress, stress-strain relationship may be linear (Bingham plastic) or non-linear (Herschel-Bulkley). Table 3.1 gives a summary of the most common rheology models that has been used to characterize the ice slurry flows.

Monitero and Bansal [54] reviewed the research on ice slurry rheology and pressure drop in pipes. They conducted a comparative analysis on various available rheological models for ice slurry flows using the available data. They concluded that any of Bingham, Casson or Herschel-Bulkley models can be used among which the last model owned the highest accuracy. Figure 3.2 displays their analysis using the pressure drop data from the work of Grozdek et al. [46] to compare the various rheological models.

Table 3.1 Most common rheology models used for ice slurry flows.

Model	Equations		
Bingham	$\tau = \tau_y + \mu_\infty \dot{\gamma}$	$\mu(\dot{\gamma}) = \frac{\tau_y}{\dot{\gamma}} + \mu_\infty$	$\mu(\tau) = \frac{\tau}{\tau - \tau_y}\mu_\infty$
Power Law	$\tau = K\dot{\gamma}^n$	$\mu(\dot{\gamma}) = K\dot{\gamma}^{n-1}$	$\mu(\tau) = K^{1/n}\tau^{(n-1)/n}$
Herschel-Bulkley	$\tau = \tau_y + K\dot{\gamma}^n$	$\mu(\dot{\gamma}) = \frac{\tau_y}{\dot{\gamma}} + K\dot{\gamma}^{n-1}$	$\mu(\tau) = \tau\left(\frac{K}{\tau - \tau_y}\right)^{1/n}$

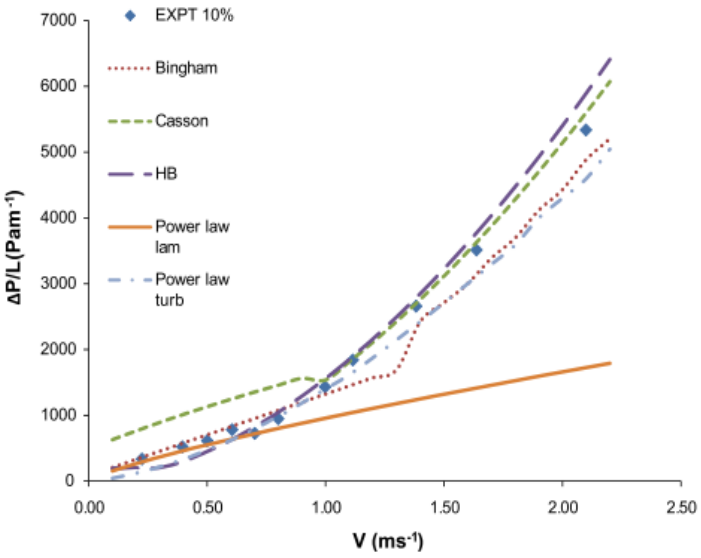

Figure 3.2. Analysis of experimental data by Grozdek et al. [46] for different rheological models (mass concentration of 10%) [54].

Niezgoda-Żelasko and Żelasko [55] used the Bingham plastic rheology model to investigate the pressure drop of ice slurries flowing through channels with various cross sections. They stated that the critical Reynolds number for such ice slurry flows falls between 1800 and 3000.

Stokes et al. [56] characterized the rheology of sucrose-based ice suspensions using a vane geometry rheometer. The rheological properties were determined using Herschel-Bulkley model. The tested ice slurries were found to be highly shear-thinning owing a large zero-shear viscosity.

Mika [57] also focused at the friction coefficient for ethylene-water ice slurry within sudden contractions and expansions. They reported different rheological observations for the flow as:

Bingham for low shear rate region and power-law for high shear rate regions. However, the author suggested a Herschel-Bulkley model to be used for the whole low and high shear rate regions.

Mellari [58] investigated the effects of ice concentration and additive concentration on the rheology and pressure drop of monopropylene glycol ice slurry in straight pipes using the power law model.

Trabelsi et al. [59] experimentally constructed the rheograms for ethylene glycol and propylene glycol at high concentrations, and determined the rheological characteristics of the ice slurry based on an Artificial Neural Network model. They also presented correlations for the rheological parameters in terms of the additive initial concentration and ice volume fraction.

Table 3.2 presents a summary of studies on the rheology of various ice slurries using implementing different models.

Table 3.2 Summary of literature on rheology models used for ice slurries

Authors	Carrier fluid	Ice fraction	Rheology model
Vuarnoz et al. [60]	10.6% ethylene alcohol	10%	Bingham
Niezgoda-Żelasko and Żelasko [55, 61-64]	10.6% ethylene alcohol	3.4%-29.8%	Bingham
Wang et al. [65]	10.6% ethylene alcohol	5.3%-31.5%	Bingham/Power Law
Mellari et al. [66]	5-24% monopropylene glycol	5%-25%	Power Law
Mellari [58]	5-24% monopropylene glycol	5%-25%	Power law
Mika [57, 67]	10.6% ethylene alcohol	5%-15%	Herschel-Bulkley
Stokes et al. [56]	52%-66.3% sucrose solution	9%-29%	Herschel-Bulkley
Illán and Viedma [68]	9% NaCl brine	5%-26%	Herschel-Bulkley
Trabelsi et al. [59]	5-24% ethylene alcohol/5-24% Monopropylene glycol	5%-65%	Herschel-Bulkley

3.1.2 Ice slurry performance in heat exchangers

Martinez and Braga [69] investigated the performance of a plate heat exchanger working with glycol-water ice slurry as the coolant. They found an increase of 25% in the heat transfer coefficient and provided correlations for Nusselt (*Nu*) and friction factor (*f*).

Lee and Sharma [70] tested a double pipe heat exchanger while operating with ice slurry. They also reported an increase of heat transfer rate with the increase in mass flux. However, they outlined that enhancement was more pronounced for low mass flux and more gradual for high mass fluxes.

Grozdek et al. reported their experimental results on pressure drop [46] and heat transfer [71] of ethanol-water ice slurry flow in a horizontal tube. It was deduced that pressure drop is a transient phenomenon that increases with the ice mass fraction and velocity and ice particles cause delay in laminar-to-turbulent transition. In terms of heat transfer, the maximum heat transfer rate was observed for laminar flow to be up to twice as that of the single-phase solution.

In another experiment by Illán and Viedma [72], performance of sodium chloride-water ice slurry in a corrugated heat exchanger was studied. The authors concluded that dependence of ice slurry performance on operating conditions make it difficult to come up with a general correlation. They added that heat exchanger performance enhanced by increasing the mass flow rate of hot fluid mass flow rate and deteriorated by increasing the ice slurry mass flow rate.

Performance of ice slurry in two types of heat exchangers (plate and tubular) was explored by shire et al. [73]. The authors claimed that the practical pumping power is less than that predicted by theoretical rheology models. An exponential dependence on ice mass fraction was announced for pressure drop in heat exchangers. Figure 3.3 shows the reported pressure drop in terms of ice mass fraction and flow rate.

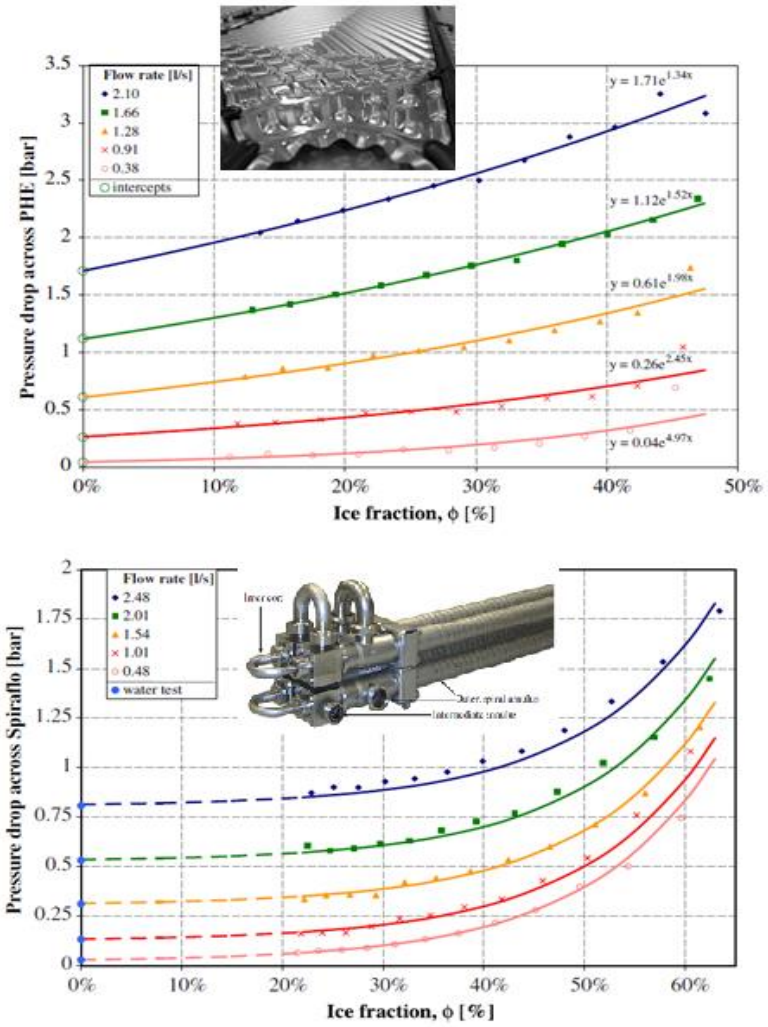

Figure 3.3. Pressure drop in terms of ice mass fraction for plate (top) and tubular (bottom) heat exchangers [73].

In the experimental work of Kousksou et al. [74], heat transfer of ice slurry flow through a horizontal tube was tested which showed that heat transfer improvement is more substantial for lower mass flow rates. Kumano et al. also explored the fluid dynamics [75] and thermal performance [76] of ice slurry flow in a narrow tube. It was noted that friction factor increased with the increase in ice packing factor (IPF) in case of laminar flow while for turbulent this parameter showed a negligible change but then increased for higher IPFs. They suggested that ice slurry flow can be treated as a non-Newtonian fluid via power-law model. A correlation was also proposed for laminar ice slurry flow *Nu* in terms of Reynolds (*Re*), IPF and diameter ratio.

The only study considering the use of ice slurry in shell-and-tube heat exchangers belongs to Renaud-Boivin et al. [77]. They showed that the overall heat transfer coefficient and effectiveness of a shell-and-tube heat exchanger can be increased by 50% and 18%, respectively as a result of using

ice slurry as the refrigerant. The authors also verified the validity of the existing correlations for Nu and friction factor were evaluated for laminar and turbulent flow inside the heat exchanger.

Different behaviours were detected by Haruki and Horibe [77] in terms of heat transfer for laminar and turbulent flows of ice slurry inside a helically-coiled heat exchanger. In case of laminar flow, heat transfer rate exceeded that of water due to latent heat of ice particles. On the other hand, heat transfer was less than water for turbulent flow. Correlations were proposed for heat transfer/friction coefficients of ice slurry in terms of dean number (*De*), curvature ratio and IPF with accuracies of 13.1% and 9.5%, respectively. To get a clear picture of the flow pattern, the authors also did a flow visualization for different inlet velocities and curvature ratios. For both small and large curvature ratios, there was concentrated region of ice particles on the top. However, with the increase in curvature ratio, concentrated region on the outside section of the wall disappeared and particles moved toward the central region.

Friction and pressure drop of ice slurry through bends and elbows was also investigated by Niezgoda-Żelasko and Żelasko [63]. They also mentioned that local flow resistance through curved pipes is characterized by curvature ratio and *De*.

Fernández-Seara and Diz [78] performed heat transfer and pressure drop measurements for ice slurry flow through an offset strip-fin heat exchanger. Slight increase in heat transfer and exponential growing trend were reported with the increase in ice mass fraction.

Niezgoda-Żelasko and Żelasko [64] recently studied the heat transfer of ice slurry inside a rectangular tube and a tube with slit cross-section. At some velocities, heat transfer of ice slurry fell below that of the carrying liquid. The reason behind this observation was mentioned as the change in the thermo-physical properties of ice slurry along with the change in ice mass fraction that in turn influences the flow pattern. Stronger effect of ice mass fraction on heat transfer for laminar flow compared to that for turbulent case was also mentioned in this study. It was discussed that under laminar conditions higher near-wall conduction exists along with the micro-convection around the particles. However, with the increased momentum for turbulent case, the effect of micro-convection is downgraded. This phenomenon was claimed to be irrespective of shape of cross sections. Figure 3.4 shows the measured heat transfer coefficients for both channels in terms of inlet velocity and ice mass fraction.

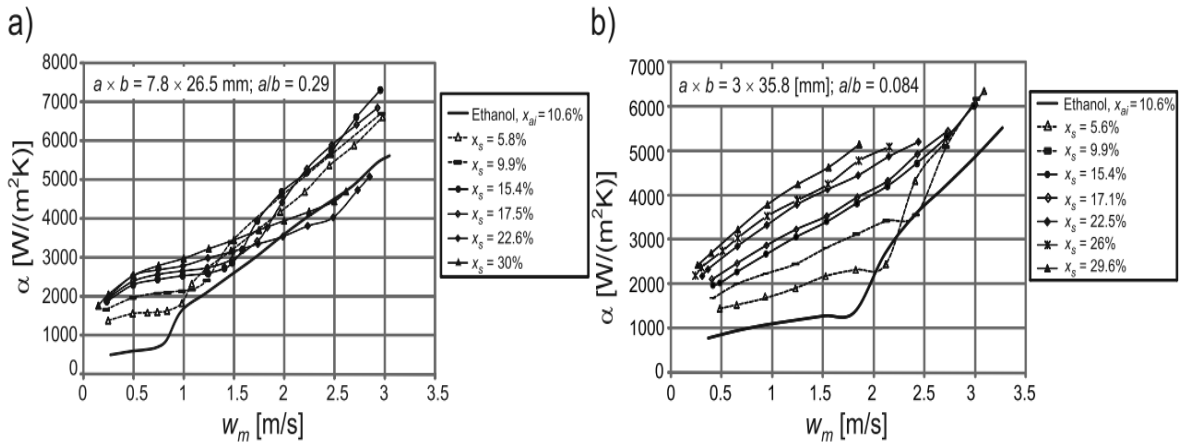

Figure 3.4. Experimental heat transfer coefficients in terms of inlet velocity for various ice mass fractions in (a) rectangular channel and (b) slit channel [64].

Recently, Singh and Kachhawaha [79] conducted studied the pressure drop and heat transfer of propylene glycol and ethylene glycol ice slurries in a plate heat exchanger. An increase of up to 300% was outlined for the measured pressure drop for ice slurry compared to that of chilled water. On the other side, thermal performance augmented by up to 100%. It was also suggested that thermo-hydraulic modelling (TH) method can estimate the values of pressure drop and heat transfer coefficient with a maximum deviation of 15%.

3.2 Numerical studies

Looking into the mainstream of ice slurry literature shows that numerical modelling of ice slurry flow is not exhaustive as the experiments done on this area. Only a few papers were found on the numerical modelling of ice slurry flow all of which were carried out for the simple geometry of straight tubes. The main reason is that the numerical simulation of ice slurry requires modelling complex characteristics at the same time. These characteristics include multiphase structure, non-Newtonian rheology and phase change during heat transfer. Each of these phenomena adds to the complexity of numerical models as well as the required computational time.

3.2.1 Single-phase approach

The very first study on ice slurry modelling seems to be the work by Niezgoda-Żelasko and Żelasko [61]. In this study, ice slurry was treated to be single-phase behaving as a non-Newtonian fluid via Bingham rheological model. This approach is less expensive in terms of computational requirements and can include the simultaneous melting of ice particles. However, accurate knowledge on the thermo-physical properties of the mixture is vital for this method. One can benefit from this

approach when modelling homogenous mixtures with known rheological behaviour. It was found that single-phase approach gave a solution with a relative deviation of 16% but overestimated the pressure drop. The authors outlined that Euler approach could provide results within 10% accuracy as compared with experiments.

Same authors simulated the heat transfer of ice slurry flow inside a horizontal tube considering the melting of ice particles [80]. Validating their results with experiments, they used enthalpy-porosity approach to take into account the effect of phase change in their computations. For laminar flow they used the Herschel-Bulkley rheological model. Figure 3.5 demonstrates the comparison between their numerical and experimental results for heat transfer coefficient.

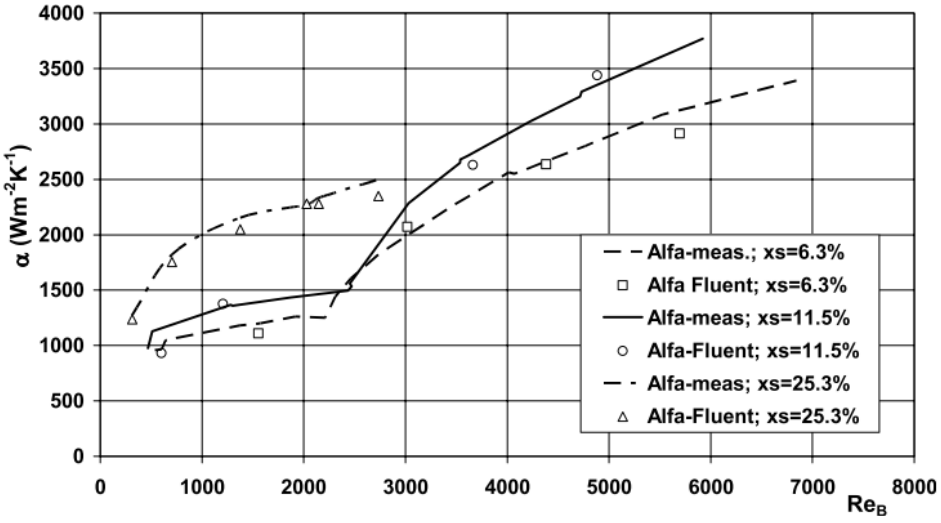

Figure 3.5. Comparison of numerical and experimental values of heat transfer coefficient for ice slurry flow inside horizontal tube [80].

Enthalpy-porosity method was also used by Kousksou et al. [74] with the aid of finite difference method for a two dimensional problem. Effects of heat flux and mass flow rate was explored for the flow numerically and experimentally. Similar to previous studies, heat transfer enhancement was more notable for low mass flow rates.

Mellari et al. [66] also did a numerical study on fluid dynamic behaviour of ice slurry using Ostwal-de Waele rheological model for a laminar single-phase problem. Pressure drop values from experiments and numerical simulations were compared as well. It was found that experimental pressure drop is about 14% less than that predicted by numerical results. The authors also recommended to use multiphase models to make their method more precise.

Onokoko et al. [81] used a different single-phase approach by assuming Newtonian behaviour of propylene glycol ice slurry in a straight pipe. They considered the species transport based on a diffusion model, where gradients of viscosity and volume fraction may induce particle flux. However, the turbulent dispersion was not taken into account. Figure 3.6 shows the velocity field and ice volume fraction distribution obtained by this method in their study.

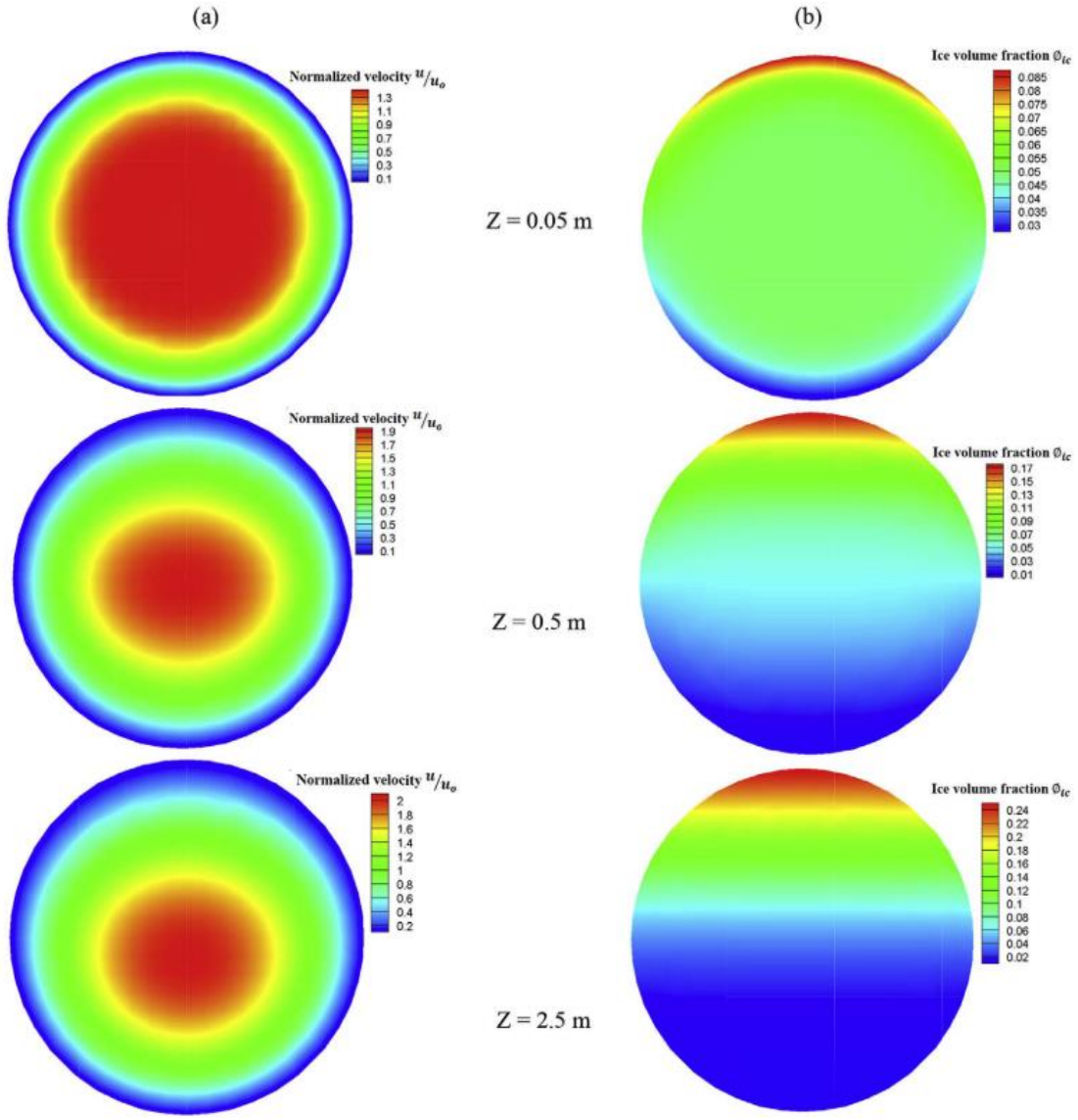

Figure 3.6. Simulated (a) normalized velocity and (b) ice volume fraction at different axial positions for laminar flow of ice slurry in straight pipe by Onokoko et al. [81] using single-phase approach integrated with diffusion model for species transport.

Bordet et al. [82] extended the model of [81] by including a turbulent dispersion term with four different turbulence closure models. The study focused on the prediction of the concentration

distribution by various turbulence closures. The RNG k-ε model gave a more homogenous concentration profile due to the over-dissipation of kinetic energy levels in the viscous sublayer.

The single-phase numerical method used in the two last above-mentioned studies provided satisfactory results while being computationally inexpensive. However, the model did not solve the fluid and solid velocities independently.

3.2.2 Multiphase approach

There are various multiphase models for particular flows including Discrete Phase Model (DPM), mixture and Eulerian all of which are known to be numerically expensive. Effect of particle mass fraction and size and thermo-physical properties of both phases are accounted. These models are of interest particularly for simulating the flow in curved structures and bends. For Euler model, one has to provide the thermo-physical properties of the carrier fluid plus the density and size of solid particles. However, for the case of mixture model the dynamic viscosity of particles is also needed.

Wang et al. [83] implemented Euler multiphase models to simulate ice slurry flow inside horizontal/vertical straight and elbow pipes with no phase change considerations. They claimed that ice slurry flow can be effectively simulated using Euler-Euler model with an accuracy of about ±20% in pressure drop findings. They discovered a three-region flow inside the horizontal tubes as high concentration on top, uniform concentration in centre and low concentration on the bottom. For vertical flows, a more homogenous nature was detected yet with particles being repelled from the wall. Besides, the authors outlined that for ice slurry flow through a 90° bend, secondary flow is shaped which intensifies the mixing and makes the flow more uniform. Figure 3.7 shows their simulated secondary flow and particle concentration for different cross sections of the elbow pipe.

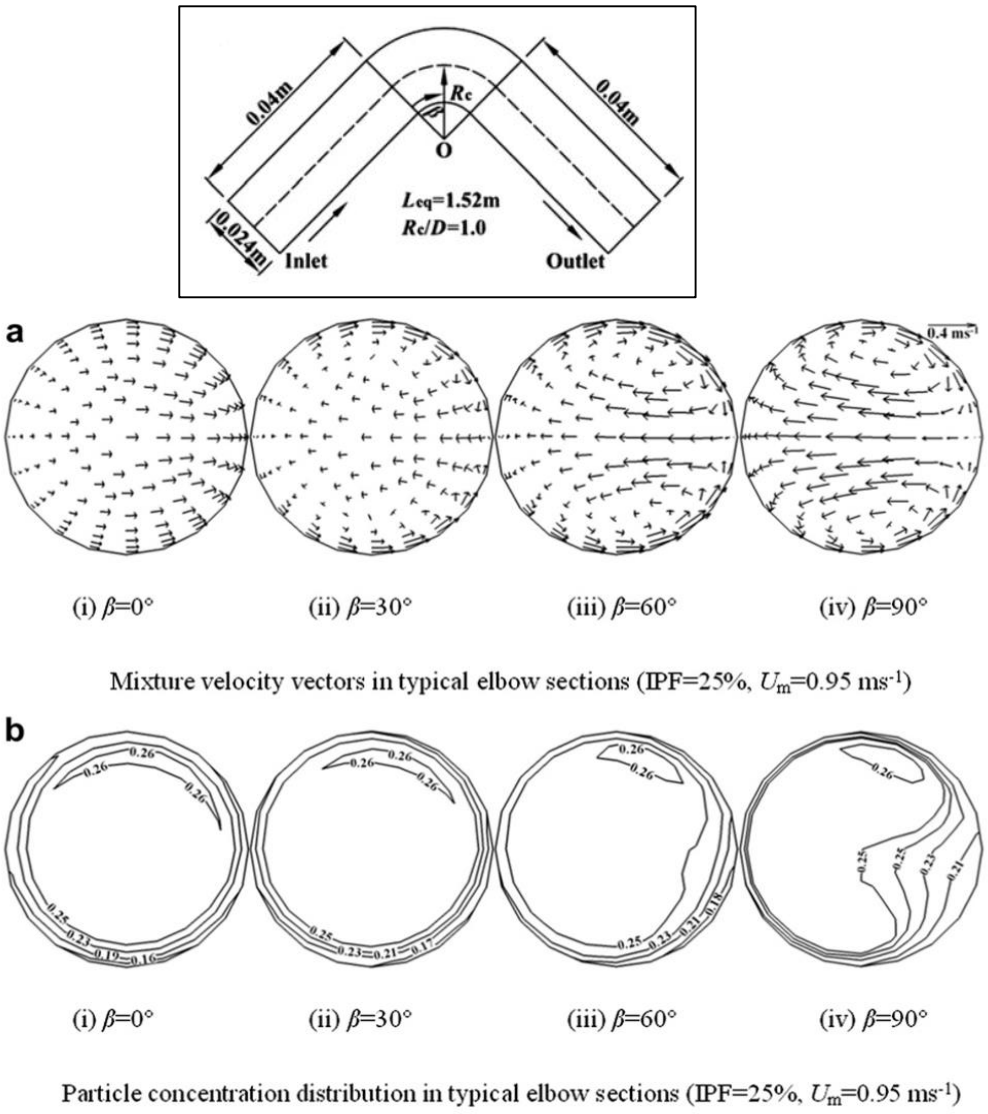

Figure 3.7. Simulated (a) velocity and (b) particle distribution at different cross sections of an elbow [83].

Eulerian multiphase approach was implemented by Tian et al. [84] to investigate the influence of parameters such as IPF, particle size and pipe diameter on the ice blockage phenomenon. It was concluded that reducing the pipe diameter lessens the ice blockage probability. Ice blockage is known to happen when ice slurry flow changes it state from suspension to moving-bed. In this study, the authors evaluated the critical velocity for this transition in terms of changes in IPF. Maximum critical velocities took place at IPFs 30-35% for different particle diameter sizes. Since the unbalance of buoyancy and gravity causes the creation of moving-bed flow, the authors also recommended that to delay the transition wall roughness can be decreased through nano-fluorocarbon coating.

Ice slurry flow in a straight tube was recently modelled by Zhang and Shi [85] using Euler-Euler approach coupled with heat and mass transfer models. Their work consisted of two main parts: modelling homogenous/heterogeneous isothermal flow; and heat transfer with phase change. For the

first part, without adopting the heat and mass transfer, it was shown that at lower inlet velocities particles tend to concentrate on the top section of the wall. However, the increase in inlet velocity and turbulence intensity, the particles were driven away from the walls and a more homogeneous flow was formed. In the presence of heat transfer (heat flux of 120 kW/m^2 and phase change, four regions were identified along the pipe as shown in Figure 3.8. In region I, thermal development occurred and wall temperature and mass transfer rate between two phases rose dramatically. Melting of particles mainly took place near the wall, and heat transfer coefficient increased rapidly. In region II, a constant mass transfer existed and fully developed region of ice slurry began leading to melting of ice particles in the centre as well. This region is characterized by constant heat transfer coefficient. In the third region, ice volume fraction near the wall decreased resulting in reduction of mass transfer. Finally, in region IV a zero particle volume fraction was reached near the wall with a decrease in mass transfer. This was the reason behind an increase in sensible heat absorption and heat transfer coefficient.

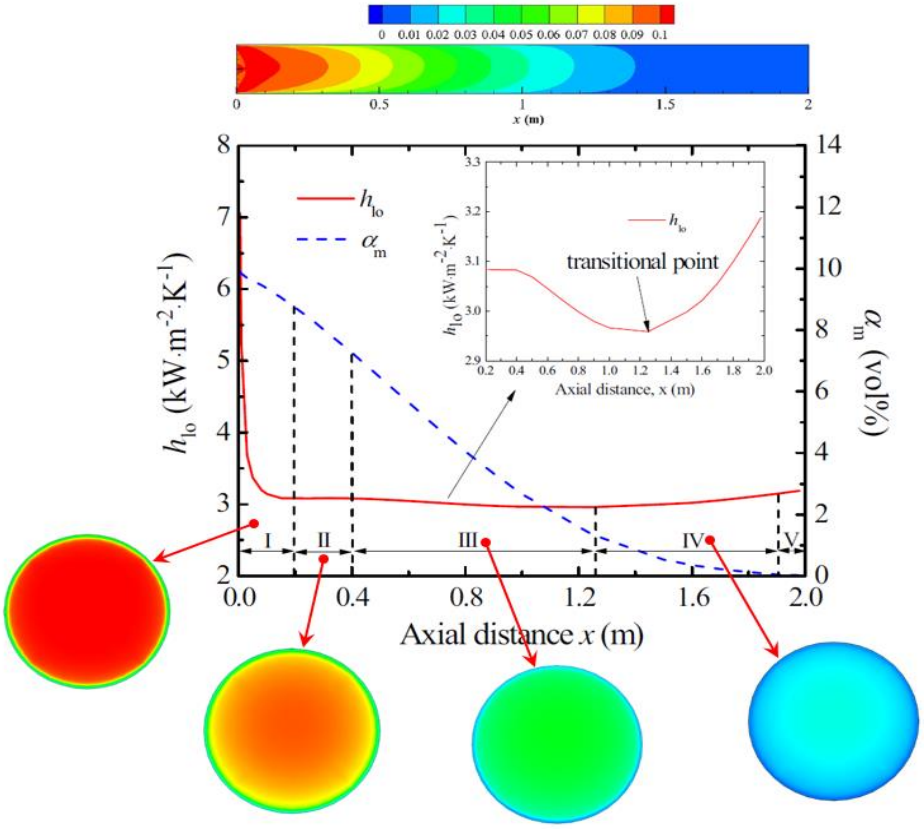

Figure 3.8. Various regions of ice slurry flow inside horizontal tube with heat and mass transfer simulated by Zhang and Shi [85]

Heat transfer through a finned tube heat exchanger operated with sodium chloride ice slurry, was investigated numerically and analytically by Long et al. [86]. The Volume of Fluid (VOF) method was used taking into account the phase change of ice particles using enthalpy-porosity method.

It was previously mentioned that ignoring the turbulent dispersion could result in a uniform particle distribution at any pipe cross-section. This may explain the uniform distribution of solid particles and insignificant impact of secondary flows on the heterogeneous ice slurry in 90º bends presented by Wang et al. [87]. Their study also investigated the validity of different turbulence models as well as various rheology models. It was concluded that centrifugal forces do not affect the particle distribution within the ice slurry in a significant way.

Rawat and Pathikar [88] also used Eulerian approach to model the isothermal ethanol-based ice slurry flow in a horizontal straight pipe. They reported that with an increase in particle diameter ice slurry flow becomes more heterogeneous. It was also stated that the increase in particle diameter and ice volume fraction leads to higher repletion forces from the wall. The same numerical approach was used by Liu et al. [89] for isothermal ice slurry in a horizontal pipe. They also developed models for the ice slurry viscosity and velocity.

3.3 Conclusions

In this chapter, a thorough review of the state-of-the-art literature on fluid dynamics and heat transfer characteristics of ice slurries was conducted. A large portion of the available literature focuses on experimental investigation of rheology and flow of ice slurries in straight pipes. Due to the temperature-sensitive nature of ice slurries, the results of rheology studies show many uncertainties. More experimental data is required to acquire precise flow patterns as well as hydraulic and thermal characteristics of ice slurries. Despite the existence of an exhaustive collection of experimental studies, the numerical work in this area needs to be developed further to elucidate the behaviour of ice slurry in applications. Since the visualization of ice slurry flows is a daunting task, simulations can make a substantial contribution to the flow characterisation of this complex mixtures. No previous study has investigated the relationship between ice particle diameter, flow disturbance and pressure drop in a curved geometry. These parameters could affect the interaction and collision of solid particles and induce the flow transition from the moving-bed layer to the suspension layer.

The following chapter has been published in the form of a journal article:

- **Amin Kamyar**, Saiied M Aminossadati, Christopher R Leonardi. *Thermo-hydrodynamics of a helical coil heat exchanger operated with a phase-change ice slurry as a refrigerant*. Heat Transfer Engineering. https://doi.org/10.1080/01457632.2018.1428989

Candidate's Contribution to the authorship:

Authorship activities	Contribution
conception and design of the project	80%
analysis and interpretation of the research data	80%
drafting significant parts of the publication or critically reviewing	80%

Chapter 4 Thermo-hydrodynamics of a helical coil heat exchanger operated with a phase-change ice slurry

4.1 Introduction

Heat exchangers are used to achieve a required amount of heat transfer between two or more fluids. These devices are widely used in a multitude of applications such as air conditioning and refrigeration systems and other thermal processing plants. Thermal engineers are continuously searching for techniques to simultaneously improve the performance and decrease the bulkiness of heat exchangers.

Many techniques such as increasing the heat transfer surface area or intensifying the flow turbulence have been introduced to enhance the thermal performance of heat exchangers. It has also been shown that introducing a helical coil in heat exchangers can increase the heat transfer rate and improve the heat exchanger performance. Thanks to the coiled tube geometry, centrifugal forces induce a secondary flow and longitudinal vortices that lead to rises in local heat transfer coefficient around the periphery of the tube [90].

Combining the enhanced performance of coiled tubes with the superior heat transfer capability of ice slurry flows is one way to improve the thermal performance of heat exchangers. Some numerical studies have presented the modelling of Newtonian phase change material (PCM) slurries in helical geometries. Languri and Rokni [91] investigated the velocity and temperature field for a PCM slurry in a planar spiral coil using enthalpy-porosity method with the aid of ANSYS FLUENT solver. Using the same approach, Kurnia et al. [92] simulated the laminar flow of microencapsulated PCM slurry inside coiled ducts with square cross sections. Zhao et al. [93] also performed a parametric study for laminar flow of PCM slurry inside a circular tube with constant wall temperature via enthalpy-porosity method. All in all, the method has been shown to give acceptable results when modelling PCM slurries.

The analysis of the second law of thermodynamics and irreversibility is a useful means of identifying thermodynamically efficient processes. When the heat transfer is part of a power cycle such as refrigeration, the irreversibility influences the mechanical power input [94]. Current studies on ice slurry in heat exchangers mainly focus on the heat transfer and pressure drop characteristics. The irreversibility, produced as a result of using this type of thermal energy storage, still needs to be analysed before being used as a feasible secondary refrigerant.

Strub et al. [95] theoretically evaluated the exergetic efficiency of ethanol-water based ice slurry in a simplified heat exchanger. They concluded that concentrated solutions without ice are preferable to less concentrated solutions. Another study by Bouzid et al. [96] provided an analytical solution to

the entropy generation problem in a two dimensional laminar flow of ice slurry. They expressed an increasing trend of entropy generation with the mass fraction of ice.

There is an exhaustive collection of experimental research on the behaviour of ice slurry as coolant in heat exchangers. Nonetheless, the numerical work in this area needs to be developed further to elucidate the behaviour of ice slurry in applications. To the best of the authors' knowledge, no studies have so far numerically investigated the performance of melting ice slurry flow inside a helical coil tube. In this chapter, thermo-hydrodynamic as well as the entropy generation characteristics of laminar flow of melting ice slurry through a helical coil subjected to uniform wall heat flux is numerically studied. The effect of parameters such as the initial ice mass fraction and *Dean* number (*De*) on the fluid friction, the heat transfer rate and entropy generation are investigated.

4.2 Model development

The computational domain for the present study is a double-turn helical coil tube (Figure 4.1). The main geometrical parameters of the modelled copper tube include the inner radius of the tube (r), the radius of the coil (R) and the coil pitch (b). Various axial positions in the coil are specified by the angle (β) measured across the length of the tube (inlet and outlet correspond to $\beta = 0°$ and $\beta = 720°$, respectively). It has been specified that $r = 12.0$ mm, $R = 266.4$ mm and $b = 50.0$ mm.

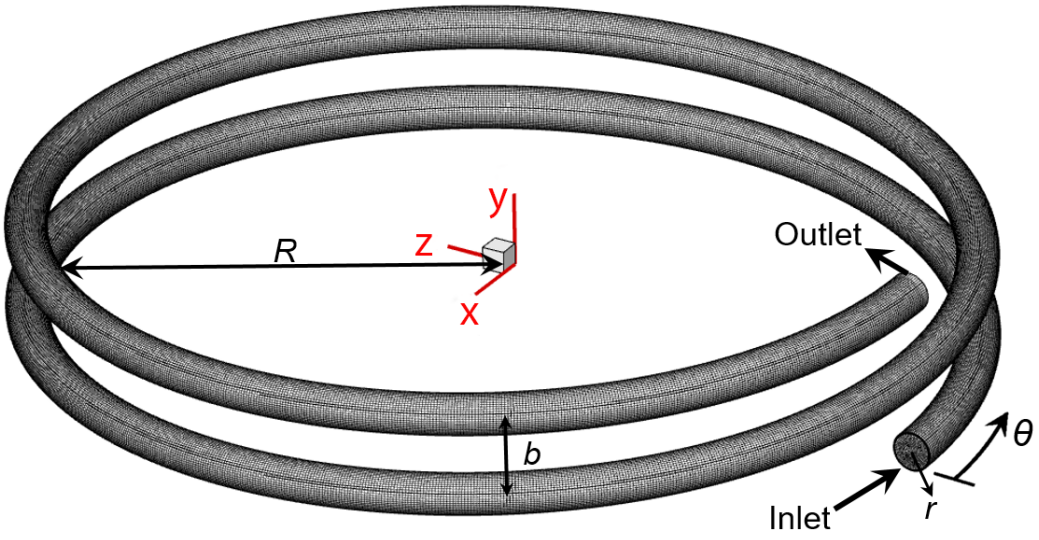

Figure 4.1. Schematic of the meshed double-turn helical-coil heat exchanger modelled in this study.

4.2.1 Governing equations

The flow field and convective heat transfer along with phase change of ethyl-alcohol ice slurry is considered in the double-turn helical coil tube. The mixture is assumed to be three-dimensional, incompressible, laminar and steady. The governing equations of continuity and momentum are given as,

$$\nabla.(\rho_{is}\vec{v}) = 0 \tag{4.1}$$

$$\nabla.(\rho_{is}\vec{v}\vec{v}) = -\nabla P + \nabla.[\mu_{is}(\nabla\vec{v}) + (\nabla\vec{v})^T] \tag{4.2}$$

in which $\vec{v}$ is the velocity, P is the pressure, ρ_{is} is the density and μ_{is} is the dynamic viscosity of ice slurry.

In order to model the thermal transport along with melting process for the ice slurry, enthalpy-porosity method is implemented [80]. For such a problem, the energy equation can be written in the following form:

$$\frac{\partial}{\partial t}(\rho_{is}.H_{is}) + \nabla.(\rho_{is}\vec{v}H_{is}) = \nabla.(k_{is}\nabla T) + S \tag{4.3}$$

In this equation, T is the mixture temperature, k_{is} is the thermal conductivity of ice slurry, and H_{is} is the mass enthalpy of ice slurry calculated as,

$$H_{is} = h_{ref} + \int_{T_{ref}}^{T} c_{p,is}dT + \omega H_l \tag{4.4}$$

where h_{ref} is the reference enthalpy and $c_{p,is}$ is the heat capacity of ice slurry. Furthermore, H_l is the latent heat of ice slurry and ω is the liquid fraction. In this method, melting starts at a certain solidus temperature ($T_{solidus}$) and once a certain liquidus temperature ($T_{liquidus}$) is reached in the field, only liquid phase is present. Accordingly, the liquid fraction changes from 0 to 1 and is calculated using the following relation [97]:

$$\omega = \begin{cases} 0, & T < T_{solidus} \\ \dfrac{T - T_{solidus}}{T_{liquidus} - T_{solidus}}, & T_{solidus} < T < T_{liquidus} \\ 1, & T_{liquidus} < T \end{cases} \tag{4.5}$$

In this numerical method, the partially solidified region (mushy region) is considered as a porous medium. For each cell, the computed liquid fraction equals the porosity of that cell. Thus, a region which is fully solidified, has a porosity of zero. In the case of forced convection, a term is

added to the energy equation that accounts for pressure drop caused by the solid phase conditions. This term, which brings in the relationship between the porosity and the change in momentum in the mushy zone is expressed as [98]:

$$S = \frac{(1-\omega)^2}{(\omega^3 + z)} A_{mush}(\vec{v} - \vec{v}_p) \tag{4.6}$$

where A_{mush} is the mushy zone constant (100000), z has the constant value of 0.001, and $\vec{v}_p$ denotes the velocity of the solid phase conditions.

These coupled equations are solved by ANSYS Fluent using the SIMPLE algorithm and second order upwind discretization. Convergence criteria of 10^{-5} for the continuity and momentum equations and 10^{-8} for the energy equation is employed. The temperature (T_{in}) and velocity (u_{in}) of the ice slurry are specified at the inlet (corresponding to a specific *Reynolds* number) whereas a uniform pressure is selected as the boundary condition for the outlet. Assuming a $T_{liquidus}$ = 268.39 K for ethanol ice slurry, T_{solidus} is calculated in such a way that the liquid fraction calculated by Eq. (5) corresponds to the value of (1 - α_s) for $T = T_{in}$ at the inlet. A uniform heat flux of 2000 W/m^2 is also applied to the wall of the double-turn helical coil tube.

4.2.2 Thermophysical properties of ice slurry

In this study, ethyl alcohol 10.6% has been considered as the freezing point depressant blended with water as the carrier fluid. When a certain aqueous solution is cooled down below the freezing point, ice crystals will be formed and separation of the mixture will occur (assuming that process is taking place in equilibrium). Three ice mass fractions ($\alpha_{s,m}$) of 5%, 10% and 15% were considered for ice particles. Thermophysical properties of such a mixture depend on the properties and concentrations of ice, the liquid solution, and as a result the concentration of ethanol and the mixture temperature. Melinder [99] presented a polynomial equation to obtain the different properties of the aqueous solution,

$$F = \sum C_{IJ}(x - x_m)^I (y - y_m)^J \tag{4.7}$$

in which F is the property of the alcohol solution (denoted by subscript l) to be determined, $0<I\leq5$, $0<J\leq3$, and C_{IJ} is the coefficient for each term. The freezing point temperature or alcohol concentration can be chosen as the input parameter, x, and the fluid temperature as the input parameter, y. x_m and y_m have constant values. This form of equation is used to obtain the thermal conductivity ($k_{c,l}$), density (ρ_l) and specific heat ($c_{p,l}$) of the pure alcohol solution. For the case of

dynamic viscosity (μ_l), the logarithmic form of the same polynomial is used. Further details about the coefficient values can be found in the work of Melinder [99]. The properties of ice slurry are then obtained using the ethyl alcohol solution properties by Eq. (4.7) and properties of ice as explained in the following section.

Thermophysical properties of ice are calculated in terms of temperature using the equations presented in Table 4.1 [100].

Table 4.1. Property relations of ice in terms of temperature T (°C) [100].

Property	Relation
Density (kg/m^3)	$\rho_s = 917 - 0.13T$
Specific heat (J/kg K)	$c_{p,s} = 2.12 + 0.008T$
Thermal conductivity (W/m K)	$k_{c,s} = 2.21 - 0.012T$

Having calculated the above parameters, the density of ice slurry can be determined as,

$$\rho_{is} = \frac{1}{\frac{\alpha_{s,m}}{\rho_s} + \frac{1-\alpha_{s,m}}{\rho_l}} \tag{4.8}$$

where $\alpha_{s,m}$ and ρ_l denote the ice mass fraction and density of the aqueous solution, respectively.

The presence of solid particles leads to an increase in the thermal conductivity. This was accounted for by the model [101],

$$\frac{k_{c,is}}{k_{c,is(v=0)}} = \begin{cases} 1 + 3(\alpha_s)Pe_s^{1.5}, & Pe_s < 0.67 \\ 1 + 1.8(\alpha_s)Pe_s^{0.18}, & 0.67 \leq Pe_s \leq 250 \\ 1 + 3(\alpha_s)Pe_s^{1/11}, & 250 < Pe_s \end{cases} \tag{4.9}$$

where $k_{c,is,(v=0)}$ and $k_{c,is}$ denote the thermal conductivities of static and moving slurries, respectively. α_s is the volume fraction of ice particles, and $k_{c,is,(v=0)}$ is calculated using the Maxwell-Tareff model [102] as,

$$k_{c,is(v=0)} = k_{c,l}\left[\frac{2k_{c,l} + k_{c,s} - 2\alpha_s(k_{c,l} - k_{c,s})}{2k_{c,l} + k_{c,s} + \alpha_s(k_{c,l} - k_{c,s})}\right] \tag{4.10}$$

where $k_{c,l}$ and $k_{c,s}$ denote the thermal conductivities of ice and ethanol solution, respectively.

The *Peclet* number of solid particles (Pe_s) is defined as,

$$Pe_s = \frac{(\nabla v) d_s}{D_T} \tag{4.11}$$

where d_s is the average ice particle diameter (0.12 mm) , v is the axial velocity and D_T is the thermal diffusivity calculated as,

$$D_T = \frac{k_s}{\rho_s c_{p,s}} \tag{4.12}$$

The specific heat of ice slurry ($c_{p,is}$) is calculated as,

$$c_{p,is} = \alpha_{s,m}.\, c_{p,s} + \left(1 - \alpha_{s,m}\right) c_{p,l} \tag{4.13}$$

The relations for the properties of the aqueous solution, ice and ice slurry (eq. (4.7) - (4.13)) were written in C language and introduced into the solver as User Defined Functions (UDFs) to reflect the change in properties with temperature and mass concentration.

4.2.3 Rheology and hydrodynamics analysis

Ice slurry is considered as a non-Newtonian fluid. Therefore, Bingham plastic model is applied to determine the pressure drop of ice slurry flows in tubes [54]. The *Reynolds* number for the non-Newtonian ice slurry can be expressed as [103],

$$Re = \frac{d^{n_B} u_{in}^{2-n_B}}{K_B 8^{n_B - 1}} \tag{4.14}$$

where K_B and n_B are the consistency index and the flow behaviour index for the Bingham fluid, respectively. These parameters depend on various factors such as rheological properties, mean flow velocity, mean wall shear stress and geometrical constants. For circular pipes, these two factors are obtained using the expressions [103],

$$K_B = \tau_w \left[\frac{\mu_p}{\tau_w \left(1 - \frac{4}{3}\varepsilon + \frac{1}{3}\varepsilon\right)} \right]^{n_B} \tag{4.15}$$

$$n_B = \frac{1 - \frac{1}{3}\varepsilon - \frac{1}{3}\varepsilon^2 - \frac{1}{3}\varepsilon^3}{1 + \varepsilon + \varepsilon^2 + \varepsilon^3} \tag{4.16}$$

In these equations μ_p is the plastic viscosity, τ_w is the average shear stress at the wall, and the dimensionless parameter ε is the ratio of yield stress to shear stress at the wall (τ_p/τ_w). The following equations are used to obtain the values of these parameters [55]:

$$\mu_p = 0.0035 + 0.0644(\alpha_{s,m}) - 0.7394(\alpha_{s,m})^2 + 5.6963(\alpha_{s,m})^3 - 19.759(\alpha_{s,m})^4 + 26.732(\alpha_{s,m})^5 \quad (4.17)$$

$$\tau_p = 0.013 - 1.4284(\alpha_{s,m}) + 73.453(\alpha_{s,m})^2 - 394.64(\alpha_{s,m})^3 + 835.82(\alpha_{s,m})^4 \quad (4.18)$$

The wall shear stress can be calculated using the, Buckingham equation for a laminar flow of ice slurry treated as a Bingham plastic fluid:

$$\frac{8u_{in}}{d_i} = \frac{\tau_w}{\mu_p}\left[1 - \frac{4}{3}\varepsilon + \frac{1}{3}\varepsilon^4\right] \quad (4.19)$$

Due to the nature of the flow through helical coils, the transition criterion from laminar to turbulent regions differs from that in straight tubes. Furthermore, the onset of turbulence of non-Newtonian fluids in coiled tubing is further delayed which makes the transition to turbulent flow to be even more gradual. Thus, a relation for the critical *Reynolds* number inside the coil as suggested by Zhou and Shah [104] can be used to obtain a lower limit for the transition criteria for non-Newtonian flow inside the coil:

$$Re_c = 2100\left[1 + 12\left(\frac{r}{R}\right)^{0.5}\right] \quad (4.20)$$

The critical *Reynolds* number (Re_c) for this study is equal to 7,448. All the studied cases are set to be laminar according to this critical value.

The *Dean* number (*De*) is also introduced to elucidate the effects of curvature and centrifugal forces on heat transfer and friction factor throughout the curved tubes [105]. It is defined as:

$$De = Re\sqrt{\frac{r}{R}} \quad (4.21)$$

The friction factor (*f*) is obtained using the equation,

$$f = \frac{8\tau_w}{\rho_{is}U^2} \quad (4.22)$$

where *U* is the mass-flow-averaged bulk velocity of the fluid.

4.2.4 Heat transfer and entropy generation analysis

The average *Nusselt* number for the ice slurry flow is calculated as,

$$Nu_m = \frac{hd_i}{k_{is}} \tag{4.23}$$

where h is the mean convective heat transfer coefficient. This can be determined by the ratio of the exerted heat flux (q'') to the difference between the wall temperature (T_{wall}) and the mass-flow-averaged bulk temperature of the fluid (T_f),

$$h = \frac{q"}{T_{wall} - T_f} \tag{4.24}$$

In order to perform an exergy analysis, entropy generation due to pressure drop and heat transfer must be determined as well. By combining the first and second laws of thermodynamics, and using the numerical values of Nu_m and f, total entropy generation per unit length of the coil (E_{gen}) can be calculated as [106],

$$E_{gen} = \frac{(q')^2}{T_f^2 \pi k_{is} Nu_m + T_f q'} + \frac{\dot{m}_{is}^3 f}{T_f \rho_{is}^2 r^5 \pi^2} \tag{4.25}$$

Eq. (4.25) can be rewritten in non-dimensional form using the term q'/T_f (heat transfer rate per unit length to the bulk temperature of the fluid) resulting in a term called entropy generation number E_{gen}^* [107] as,

$$E_{gen}^* = \frac{1}{\left(T_f \pi k_{is} Nu_m / q'\right)+1} + \frac{f}{\left(\rho_{is}^2 r^5 \pi^2 q' / \dot{m}_{is}^3\right)} \tag{4.26}$$

The expression in Eq. (26) can be rewritten in the form of a two-term equation,

$$E_{gen}^* = E_T^* + E_P^* \tag{4.27}$$

where E_T^* and E_p^* denote the entropy generation numbers of heat transfer and fluid friction, respectively. In order to quantify the contribution of heat transfer on the overall entropy generation, Paoletti et al. [108] defined an irreversibility distribution parameter, the *Bejan* number,

$$E_{gen} = \frac{E_T^*}{E_{gen}^*} \tag{4.28}$$

which has values in the range of 0 to 1. *Be* = 0 and *Be* = 1 represent the two cases of fully friction-dominated and heat transfer-dominated irreversibilities. The mid-value of *Be* = 0.5 implies equal entropy generation rates from heat transfer and fluid friction.

4.3 Grid test and model validation

Figure 4.2 depicts a section of the mesh topology used in the simulation. The mesh density was varied to examine the grid independence of the numerical results. Mesh refinement was continued until a satisfactory difference was obtained between subsequent numerical results. For the grid test, it was considered that ice slurry with an ice mass fraction of 5% enters the tube with an inlet velocity corresponding to *De* = 200. The tube undergoes a constant heat flux of 2000 W/m^2. Table 4.2 presents the mesh sensitivity analysis for the tested grid cells and numerical results for the outlet temperature and average heat transfer coefficient (*h*). Finally, a mesh arrangement with 1,576,440 grid cells is chosen.

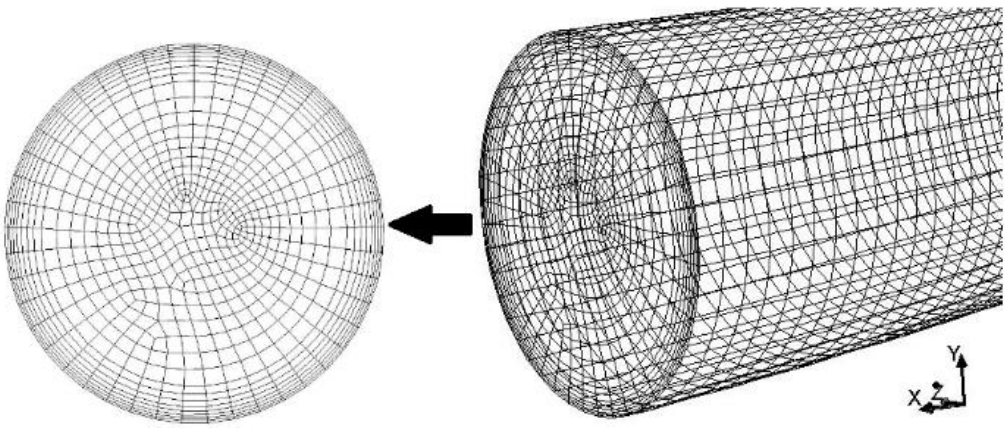

Figure 4.2. Mesh for the modelled heat exchanger.

Table 4.2. Results of the mesh sensitivity analysis.

No. of grid cells	Outlet Temperature (K)	h (W/m^2.K)
446,342	268.50	686.47
608,235	268.51	689.43
854,646	268.52	692.69
1,576,440	268.54	697.91
1,732,241	268.54	697.91
2,025,865	268.54	697.91

In order to validate the numerical results obtained by the model, the experimental study by Haruki and Horibe [109] is used. Their experiments were conducted for water-based ice slurry in a helical coil heat exchanger with various curvature ratios subjected to a heat flux of 2,400 W/m^2. The authors expressed an accuracy of 1.5% for the measured pressured drops and uncertainty of ≤14% for the average *Nusselt* number.

Figure 4.3 shows the comparison between the calculated unitary pressure drop and the experimental results for ice mass fractions of 5% and 20% at different average inlet velocities for the curvature ratio of $R/r = 22.2$. As noted, the numerical results are in acceptable agreement with the experimental data with a maximum deviation of 12.8%. A comparison between the numerical results and experimental data for average *Nusselt* number is also presented in Figure 4.4 for water-based ice slurry of 10% mass fraction with an inlet temperature of 2 ºC. A maximum deviation of 9.8% was found between the numerical and the reported experimental results.

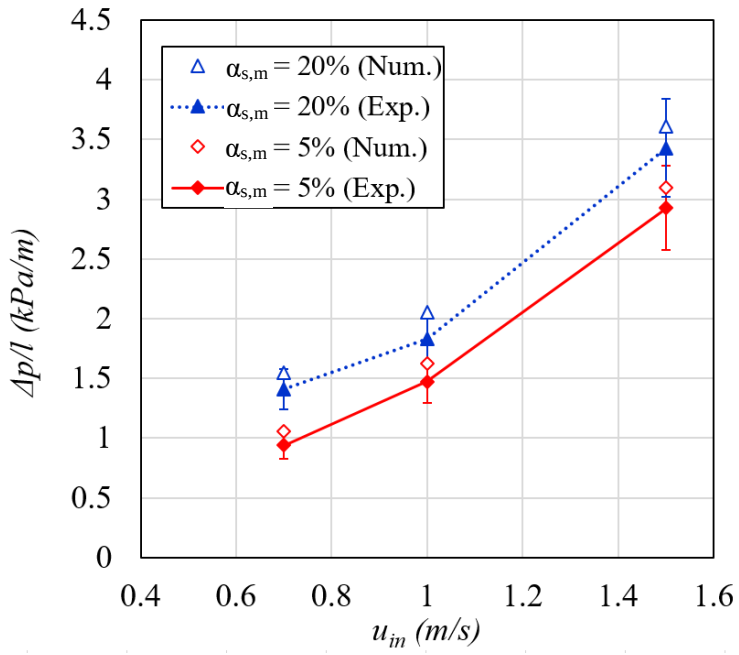

Figure 4.3. Unitary pressure drop (*Δp/l*): comparison of simulated results with experimental data from [109] for water-based ice slurry of 5% and 20% ice mass fractions.

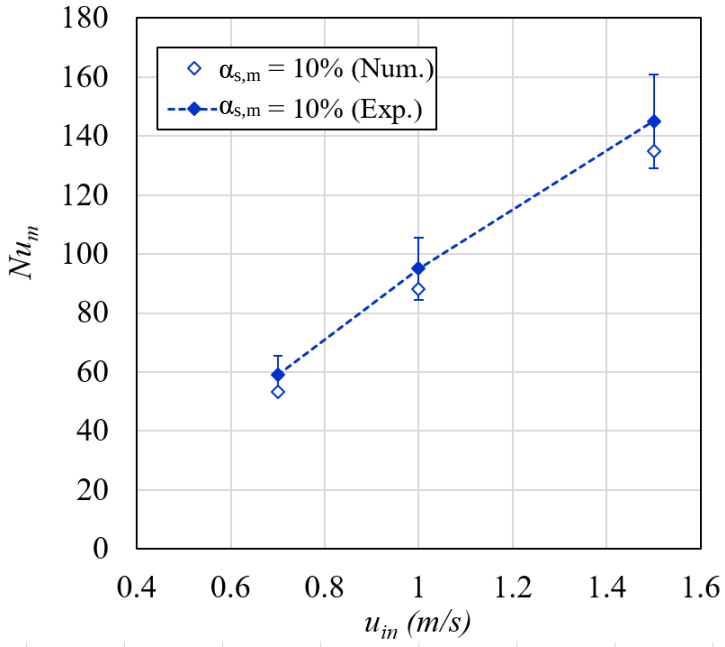

Figure 4.4. Average *Nusselt* number (Nu_m): comparison of simulated results with experimental data from [109] for water-based ice slurry of 10% ice mass fraction.

4.4 Results and discussion

4.4.1 Hydrodynamics

Figure 4.5 shows the variation of friction factor with respect to the ice mass fraction at various values of *De*. At a specific *De*, the results show insignificant variation of the friction factor with the change of ice mass fraction from 0% to 15%. However, the friction factor changes in an inverse manner relative to the values of *De*. For instance, at 15% mass fraction, this parameter wanes from 0.104 at *De* = 200 to 0.033 at *De* = 1000. It can be concluded that for laminar flow in the helical coil tube, the friction factor merely depends on the mass flow rate and the geometry (curvature ratio) of the heat exchanger. The behaviour of ethanol ice slurry was studied in an experimental work by Niezgoda-Żelasko and Żelasko [63] for bends and elbow pipes. They deduced that the friction coefficient of laminar ice slurry flow in these curved geometries is merely a function of *De* and curvature ratio. The curvature ratio is constant in this study. It should be noted that the ice mass fraction indeed changes as slurry moves through the heat exchanger. The results shown in this study are expressed in terms of average ice mass fraction.

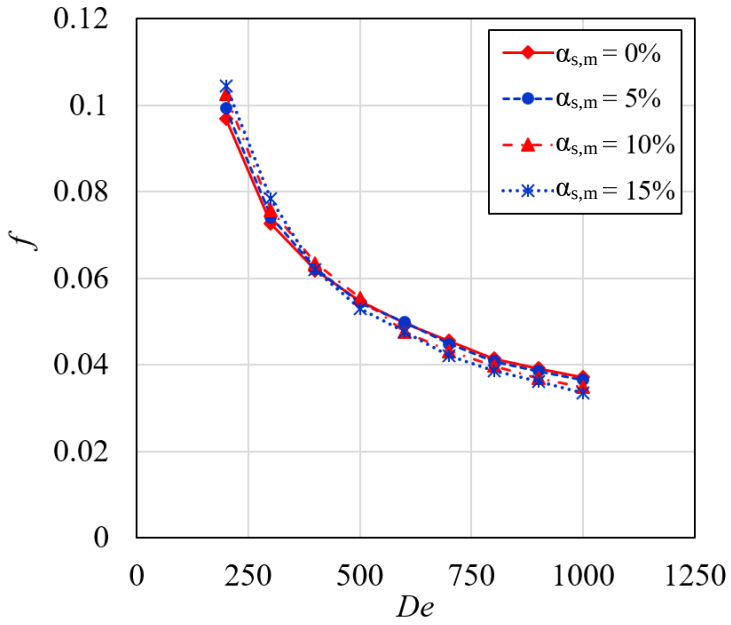

Figure 4.5. Computed friction factor (*f*) of ice slurry flowing through the helical coil at different ice mass fractions (α_s) and various *Dean* numbers (*De*).

Figure 4.6 shows the change of unitary pressure drop of the slurry flow through the heat exchanger in terms of *De*. As noted from the graph, the pressure drop increases with the increase in the *De* for a specific ice mass fraction. For instance, an increment from 215 to 1,393 Pa/m is observed for the minimum ice mass fraction of 5% when the inlet velocity is increased from 200 to 1,000. The increase in the pressure drop then becomes 1,864 to 7,760 Pa/m at 15% ice mass fraction for the same

range of *De*. Moreover, at a constant *De* the pressure drop tends to increase with an increase in the ice mass fraction. Another observation is that the rate of increase in the pressure drop increases as one increases the ice mass fraction. This implies that higher pumping power is needed when the ice mass fraction is increased within the flow. The pressure drop in ice slurry flows has been the subject of conjecture due to the complex structure of the flow. Some studies [47, 110] have similarly reported an increase in pumping requirements after using ice slurries while some others outlined a reduction in the pressure drop [111, 112].

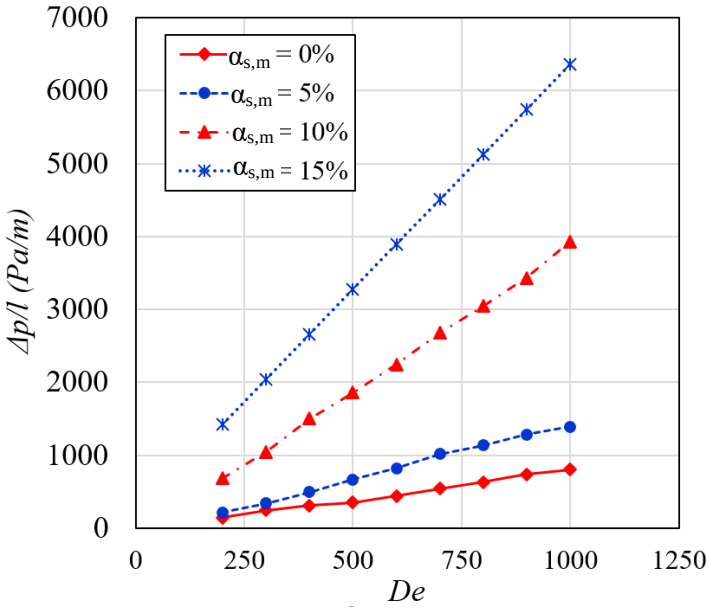

Figure 4.6. Unitary pressure drop ($\Delta p/l$) as a function of *Dean* number (*De*) and ice mass fraction (α_s).

4.4.2 Flow patterns

The increase in the pressure drop is a result of the flow behaviour in curved structures. In general, the pressure drop for a particular flow in a curved tube is higher than that in a straight tube at the same flow rate and tube length [113]. This is the result of both friction and momentum exchange due to the change in direction of the fluid and the creation of a secondary flow. This phenomenon is clearly shown in Figure 4.7 (a). The outer side is shown by **O** while the inner side is shown by **I** symbols. Various sections along the length are represented by the angle (θ) measured from the inlet plane. The vectors demonstrate the effect of centrifugal force on the fluid structure at different cross sections of the coil heat exchanger. The curvature of the coil creates centrifugal force acting on the ice slurry leading to higher velocities near the outer wall. The other expected effect is the addition of ice particles and the natural increase in the dynamic viscosity (increased values of yield shear stress) which intensifies the pressure drop to a further extent. The increase in the ice mass fraction affects the friction factor as both the plastic viscosity and the yield stress have a direct relation with the amount of ice content. This, in turn, affects the non-Newtonian behaviour of the ice slurry [58]. If the minimum pumping power is required, the inlet velocity is recommended to be kept as low as possible but still high enough to attain the required cooling requirements.

Figure 4.7 (b) demonstrates the change in the liquid mass fraction distribution throughout the coil tube via contours in different cross sections for the inlet ice mass fraction of 15%. As the ice slurry moves forward and a higher heat transfer rate is obtained, a larger proportion of the ice content undergoes phase change which adds to the liquid mass fraction. The contours also show that due to the intensified mixing inside the helical coil, the penetration of higher values of temperature into the central region is augmented. Higher temperatures in the centre lead to the melting of some of the ice in the central region as compared to straight tubes, where phase change mainly occurs within the near-wall region.

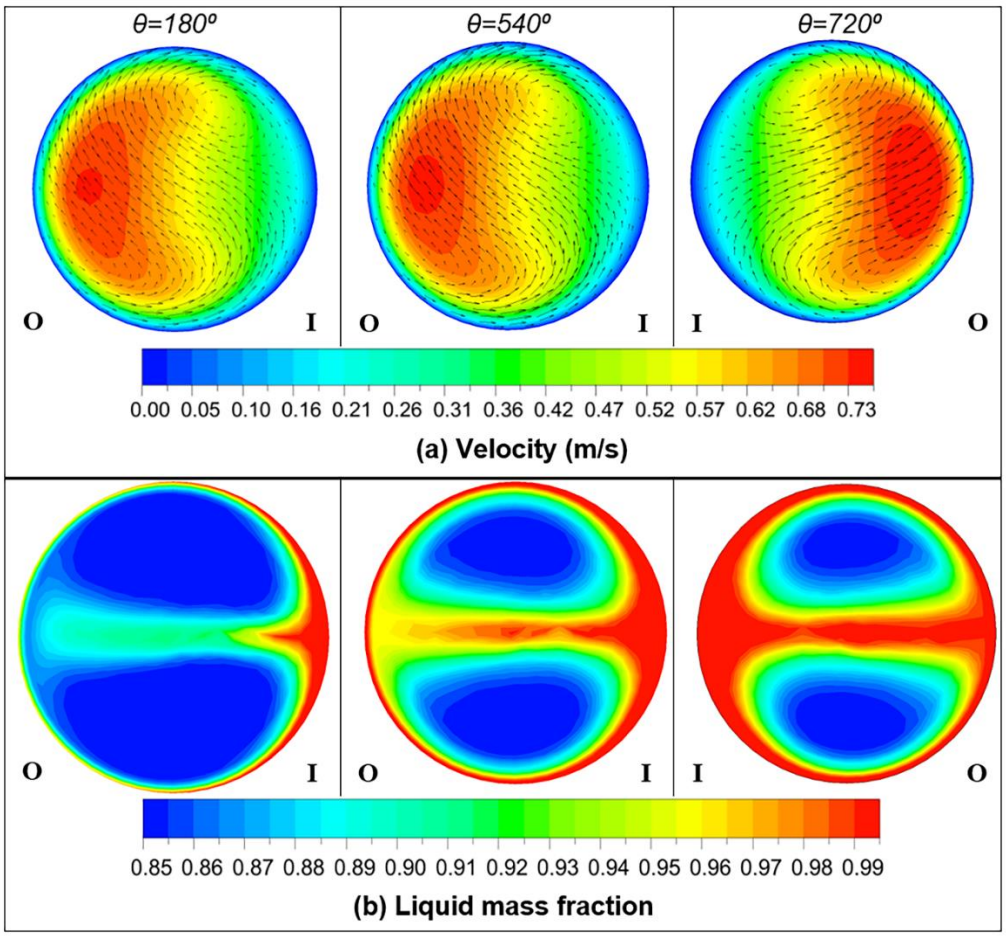

Figure 4.7. Contours of (a) velocity and (b) liquid mass fraction of ice slurry flow at various cross sections (in terms of θ) at ice mass fraction (α_s) of 15% and *De*=1,000.

4.4.3 Thermal performance

The effect of ice slurry on the heat transfer capability of the helical coil tube is displayed in Figure 4.8. Ice slurry induces enhancements in the thermal performance of the heat exchanger by increasing the heat transfer coefficient (*h*) compared to the pure liquid solution. The increase in *h* is a function of both *Dean* number and the ice mass fraction. This coefficient is improved from 638 to 960 W/m^{2}K at the lowest *De* (200) while it rises from 1,496 to 1,977 W/m^{2}K at the maximum *De* (1000). The positive effect of ice slurry on the thermal performance has also been observed in previous studies [62, 77]. As mentioned before, the behaviour of ice slurry flow was particularly investigated for a helical coil heat exchanger by Haruki and Horibe [109]. They reported an increase in the heat transfer coefficient for the laminar regime but a drop in heat transfer capability with the change of flow to turbulent conditions and an increase in the curvature ratio.

The increase in *h* in the helical coil heat exchanger can be explained by two phenomena. The first is the increased thermal conductivity of the mixture which is due to the presence of solid particles

in the moving slurry. The second effect stems from the geometry of the helical coil tube that is characterized by the secondary flows that intensify the mixing caused by centrifugal forces and further improve the heat transfer. In addition, the increase of velocity (*De*) induces an increase in the inertial force and consequently causes the ice slurry to flow uniformly through the central region of the helical coil pipe. As the eccentric force pushes a major part of the flow to the outer near-wall region (Figure 4.7 (b)), the heat can be more effectively transferred towards downstream. In the case of laminar flow through straight pipes, even small heat fluxes are sufficient to melt the ice within the near-wall layer. This creates a structure with properties of the carrying liquid near the wall. Consequently, heat transfer to the core of the fluid, where more solid phase is present, is delayed [62]. Thus, helical coil geometry can be a potential technique to resolve this issue.

The computed *Nusselt* numbers for the different studied cases are shown in Figure 4.9. Nu_m of ice slurry increases with *De*, however, small differences are obtained between the Nu_m of ice slurry and that of the pure liquid solution at lower values of ice mass fraction. The higher Nu_m is associated with the 15% ice mass fraction starting from 35 at *De* = 440 reaching up to 71 at *De* = 1,000.

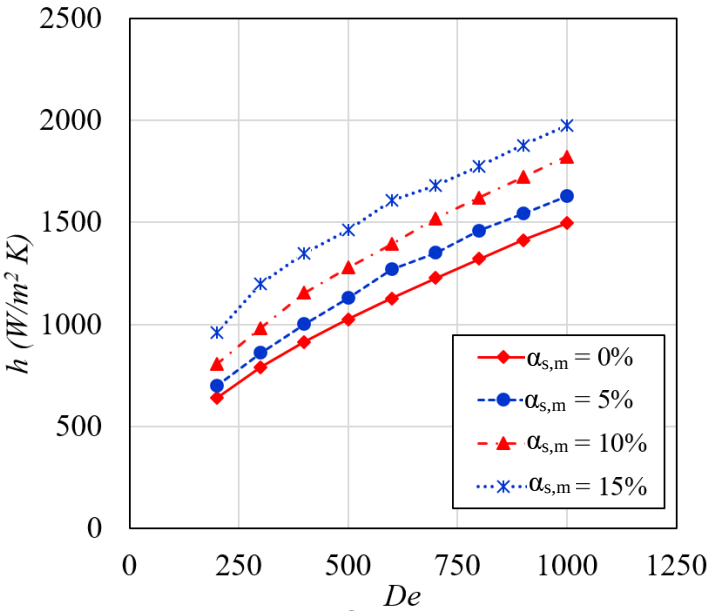

Figure 4.8. Average convection heat transfer coefficient (*h*) as a function of *Dean* number (*De*) and ice mass fraction (α_s).

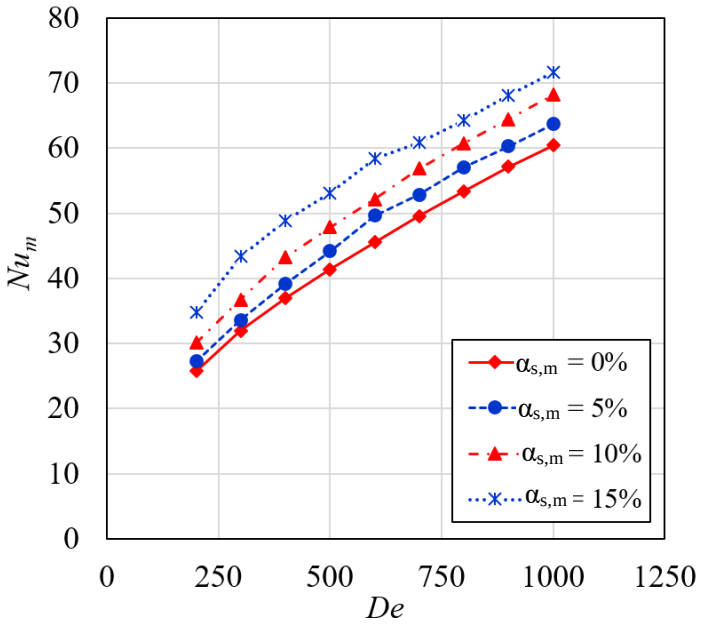

Figure 4.9. Computed average *Nusselt* number (Nu_m) as a function of *Dean* number (De) and ice mass fraction (α_s).

4.4.4 Entropy generation

The observed heat and momentum transport of ice slurry flow inside the helical coil tube has a significant influence on the irreversibility and entropy generation. In this section, the effects of hydrodynamic and thermal characteristics of the ice slurry on the entropy generation in the helical coil tube are investigated. Similar to all thermodynamic systems, the entropy in the helical coil tube is a product of the irreversibilities due to heat transfer with finite temperature differences as well as the friction of the flow. Figure 4.10 shows the values of the frictional entropy generation number (E_P^*) with respect to *Dean* number for different ice mass fractions. As De increases, the fluid friction substantially increases which causes the friction irreversibility to increase. This explains the growing trend of E_P^* for a specific mass fraction. However, with addition of ice particles and a non-Newtonian viscosity a sharp rise is detected for ice slurries with higher mass fractions. As theoretically expected, E_P^* reaches its maximum at the highest De for the ice mass fraction of 15%.

Figure 4.11 shows the values of heat transfer entropy generation number (E_T^*) with respect to De for different ice mass fractions. In general, the values of entropy generation due to heat transfer are considerably larger than those from frictional entropy generation. This might be due to the fact that the influence of thermal process (including convection and melting) on the increase in entropy is greater than the influence of friction. As opposed to fluid friction, the heat transfer enhancement causes reduction in the entropy generation. The results show that E_T^* decreases as De increases. With

the increase in *De*, the heat transfer improvement makes the temperature gradients in the flow fields mild and as a result the irreversibility due to heat transfer drops. A similar thermodynamic behaviour was also reported by Ko and Ting [114] for a helical coil tube.

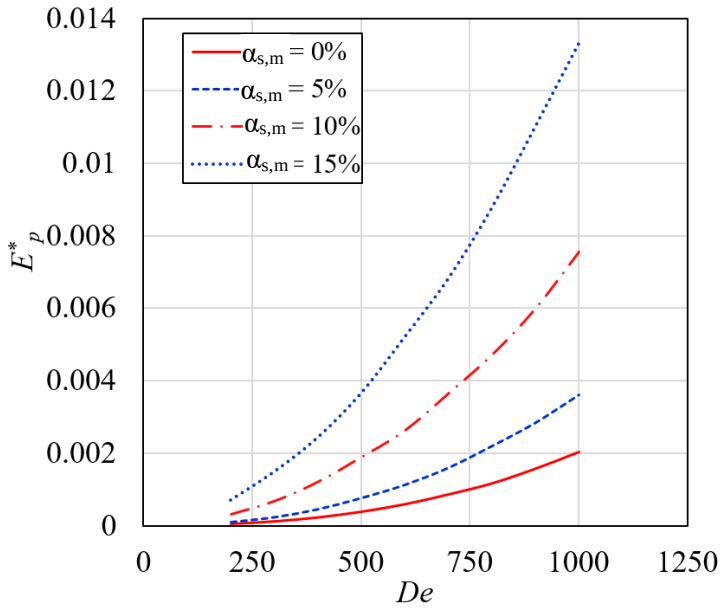

Figure 4.10. Partial entropy generation number due to friction (E_P^*) in terms of ice mass fraction (α_s) and *Dean* Number (*De*).

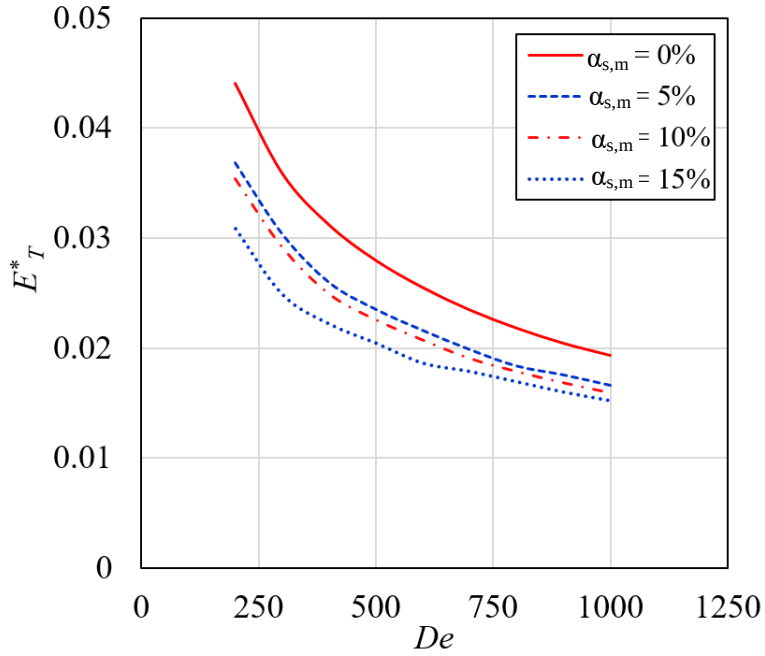

Figure 4.11. Partial entropy generation number due to heat transfer (E_T^*) in terms of ice mass fraction (α_s) and *Dean* Number (*De*).

The opposite effects of increase in *Dean* number and ice mass fraction on the irreversibilities from the friction and heat transfer make it possible to seek an optimal trade-off to get the minimal entropy generation. The total entropy generation number (E_{gen}^*) is presented in Figure 4.12. For pure ethanol solution, the total entropy generation keeps decreasing with an increase in the mass flow rate. This behaviour implies the dominance of heat transfer irreversibility over the whole range of values of mass flow rate (or *De*). On the other hand, ice slurries of 10% and 15% show a different trend. For both of these cases, the total entropy generation reaches its minimum before starting to rise. This indicates that before a certain mass flow rate (or *De*), the heat transfer irreversibility is the dominant source of entropy generation while after this point, the fluid friction becomes more substantial. For ice mass fraction of 10%, this point is located at *De* = 800 (marked by the triangle) whereas, for the ice mass fraction of 15%, the minimum value occurs at *De* = 600 (marked by the circle). It is noteworthy that E_{gen}^* can be considered as a function of geometry parameters such as the curvature ratio and heat flux [115]. A wider range of *De* that includes the turbulent regimes as well might shed more light on the optimum values of entropy generation. Bearing this in mind, an optimisation study would be beneficial to find the most efficient design of helical tube heat exchangers operating with ice slurry.

The evolution of *Be* with *De* as shown in Figure 4.13, further expounds the thermodynamic characteristic of ice slurry in the helical tube. As *De* increases, the value of *Be* decreases monotonically for all values of ice mass fraction. This also implies that the contribution of the fluid

friction to the entropy generation becomes more significant in higher mass flow rates. It also noted that for all the cases, the value of *Be* is greater than 0.5. This suggests that E_T^* is larger than E_P^* for all the studied cases.

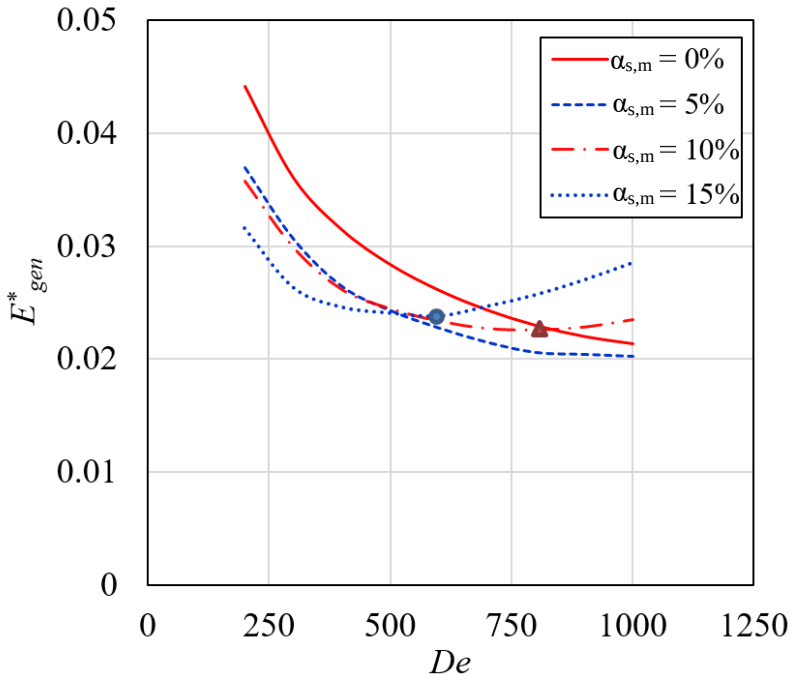

Figure 4.12. Total entropy generation number (E^*_{gen}) of ice slurry in terms of ice mass fraction (α_s) and *Dean* Number (*De*).

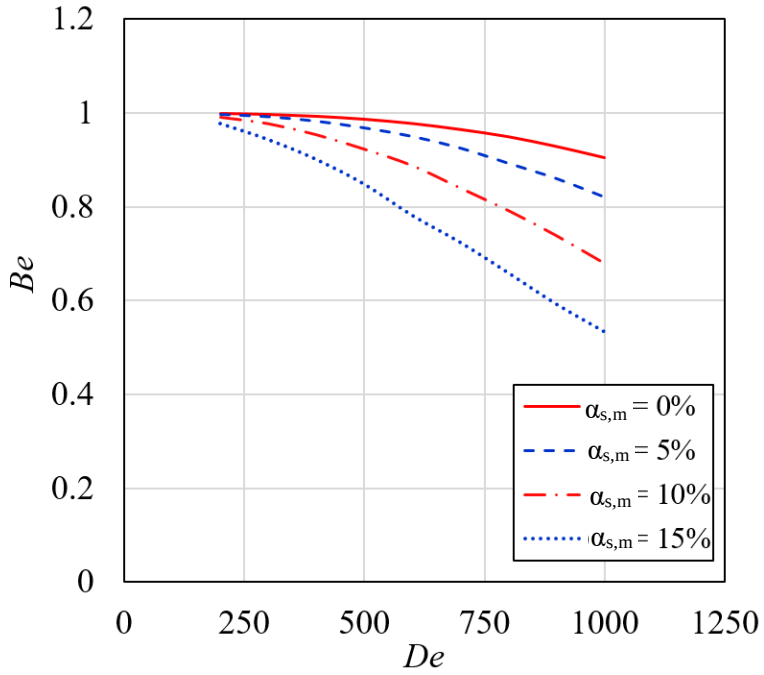

Figure 4.13. Effect of *Dean* Number (*De*) and ice mass fraction (α_s) on *Bejan* number (*Be*).

4.5 Conclusions

In this chapter, the flow of non-Newtonian ethanol-based ice slurry through a double-turn helical coil heat exchanger is numerically investigated. Ice slurry is treated as a Bingham plastic with rheology parameters defined as functions of the ice mass fraction. The melting of the solid phase is simulated using enthalpy-porosity method. The effects of ice mass fraction of ice and *Dean* number on the thermal and hydrodynamic performance of the heat exchanger are explored. According to the numerical results, the existence of ice imposes a rise in the pressure drop. On the other hand, the introduction of ice slurry induces improvements in the heat transfer coefficient via melting and convection processes. In addition to the ice melting, the secondary flows produced by the geometry further intensify the thermal and hydraulic effects. It is also noted that changes in the heat transfer and pressure drop impose rises in the entropy generation. The major proportion of the induced irreversibility is attributable to the heat transfer. However, the entropy generation analysis for ice mass fractions of 10% and 15% showed an optimal trade-off between the frictional and thermal irreversibilities where the entropy generation was minimum. For a thermal system composed of helical coiled heat exchangers operated with ice slurries, the optimal mass flow rates can be considered to achieve the best exergy utilisation.

The following chapter has been submitted in the form of a journal article and is currently under review:

- **Amin Kamyar**, Saiied M Aminossadati, Christopher R Leonardi, Agus P Sasmito, Sebastien Poncet. *Flow characterization of monopropylene glycol ice slurry through a horizontal U-bend: Part I: A numerical approach*. International Journal of Refrigeration. (**Under review**)

Candidate's Contribution to the authorship:

Authorship activities	Contribution
conception and design of the project	70%
analysis and interpretation of the research data	70%
drafting significant parts of the publication or critically reviewing	70%

Chapter 5 Flow characterization of monopropylene glycol ice slurry through a horizontal U-bend: A numerical approach

5.1 Introduction

Thermal energy storage systems have attracted significant interest amongst design engineers in various industries [116]. Ice slurry is increasingly used as a form of thermal energy storage due to its high energy storage density, fast cooling rate and high heat transfer coefficient [2]. Ice slurry is a mixture of liquid water, an anti-freeze depressant and microscale ice particles. It is classified as a pumpable Phase Change Material (PCM) with numerous interesting transport characteristics. Various aspects of ice slurry such as production, storage and transport properties including rheology, hydrodynamics and heat transfer have been comprehensively reviewed and reported in the literature [45, 54, 117].

The flow behaviour of ice slurry is generally very complex due to the existence of ice particles. Thus, the flow patterns and hydrodynamics of ice slurries must be well understood prior to the design of transport lines. This requires investigation of the flow behaviour of ice slurry flows through different piping components.

As far as multiphase modelling is concerned, mixture and Euler-Euler methods have been the most commonly implemented approaches for modelling ice slurry flows. Wang et al. [118] used a mixture model to simulate isothermal ice slurry flows through rectangular and circular pipes.

The disturbance of ice slurry flows by curved geometries is an important phenomenon that enhances the interaction and collision of solid particles and induces the saltation of particles from the moving-bed layer to the suspension layer [84]. Visualising the ice slurry flow through the U-bend and analysing the change in the structure due to centrifugal forces helps us to understand the hydrodynamics of ice slurry in helical coil heat exchangers. This implies the importance of modelling the role of centrifugal forces in the mixing occurring within ice slurry flows. To the best of the authors' knowledge, no previous study has investigated the relationship between ice particle diameter, flow disturbance and pressure drop in a curved geometry. Clarifying the effect of particle diameter on the pressure drop and flow structure is important, especially when selecting the ice slurry generation technique.

5.2 Numerical Model

5.2.1 Computational Domain

The model geometry is presented in Figure 5.1a. It shows a U-bend pipe with a diameter of D = 25 mm. The length of the inlet section is $L = 50D$ to ensure that the flow entering the bend is fully developed. The length of the exit section is also $L = 50D$. The different cross-sectional locations along the bend are specified via defining the angle, β, commencing from the bend inlet. Figure 5.1b shows the implemented grid used in the numerical model. A grid-independence study was also carried out in order to select the appropriate mesh density, and this found that a total of 578,984 cells was sufficient. Grid refinement was also used near the wall, to capture the complex flow characteristics.

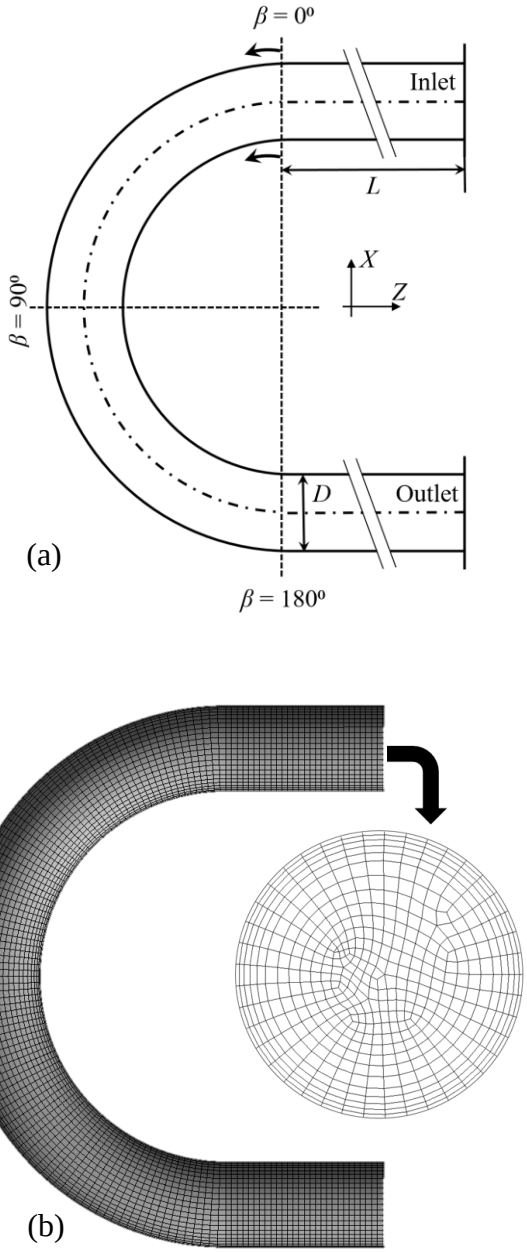

Figure 5.1. (a) The geometry of the U- bend and (b) the implemented grid used in the numerical model.

5.2.2 Governing equations

The Euler-Euler multiphase model was used to simulate the ice slurry flow in ANSYS FLUENT 17.0. The granular version of this approach enables to take the friction and collision between the solid particles into account. These phenomena are of great importance for ice slurry flows as they are not dilute systems. Setting a maximum packing limit is also possible with this approach which is favourable for modelling flows with particulate secondary phases. The solid (*s*) and liquid (*l*) phases are treated as interpenetrative continua along with interphase momentum exchange. This is applied in the way that $\alpha_l + \alpha_s = 1$, where α_l and α_s denote the volume fractions of the liquid and solid

phases, respectively. Each phase satisfies the conservation laws of mass and momentum individually, with the coupling facilitated by pressure and inter-phase exchange coefficients.

The conservation of mass for both phases is written as,

$$\nabla.(\alpha_i \rho_i \vec{v}_i) = 0 \tag{5.1}$$

where *i* can be either *s* or *l*.

The momentum equation for the fluid phase is,

$$\nabla.(\alpha_l \rho_l \vec{v}_l \vec{v}_l) = -\alpha_l \nabla P + \nabla.\bar{\bar{\tau}}_l + \alpha_l \rho_l \vec{g} + \vec{F}_D + \vec{F}_L + \vec{F}_{TD} \tag{5.2}$$

where $\bar{\bar{\tau}}_l$ is the liquid phase stress tensor, which is expressed in terms of the liquid dynamic viscosity (μ_l) and unit vector ($\vec{I}$) as,

$$\bar{\bar{\tau}}_l = \alpha_l \mu_l [\nabla \vec{v}_l + (\nabla \vec{v}_l)^T] - \frac{2\alpha_l \mu_l (\nabla.\vec{v}_l)\vec{I}}{3} \tag{5.3}$$

The momentum equation for the solid phase is,

$$\nabla.(\alpha_s \rho_s \vec{v}_s \vec{v}_s) = -\alpha_s \nabla P - \nabla P_s + \nabla.\bar{\bar{\tau}}_s + \alpha_s \rho_s \vec{g} + \vec{F}_D + \vec{F}_L + \vec{F}_{TD} \tag{5.4}$$

where, $\bar{\bar{\tau}}_s$ is the solid phase stress tensor, which is expressed as,

$$\bar{\bar{\tau}}_s = (-P_s + \gamma_s \nabla.\vec{v}_s)\vec{I} + \alpha_s \mu_s [\nabla \vec{v}_s + (\nabla \vec{v}_s)^T] - \frac{2\alpha_s \mu_s (\nabla.\vec{v}_s)\vec{I}}{3} \tag{5.5}$$

The bulk viscosity (γ_s) accounts for the resistance of solid particles to compression and expansion [119]. This is expressed as,

$$\gamma_s = \frac{4}{3}\alpha_s \rho_s d_s g_0 (1 + e_{ss}) \left(\frac{\theta_s}{\pi}\right)^{1/2} \tag{5.6}$$

The shear viscosity of solid particles (μ_s) is defined as the sum of collisional ($\mu_{s,col}$) and kinetic ($\mu_{s,kin}$) viscosities [120],

$$\mu_s = \underbrace{\frac{4}{5}\alpha_s\rho_s d_s g_0(1+e_{ss})\left(\frac{\theta_s}{\pi}\right)^{1/2}}_{\mu_s} + \underbrace{\frac{10\rho_s d_s\sqrt{\pi\theta_s}}{96\alpha_s(1+e_{ss})g_0}\left[1+\frac{4(1+e_{ss})g_0\alpha_s}{5}\right]^2}_{\mu_{s,col}} \tag{5.7}$$

In equations (6) and (7), d_s is the particle diameter, e_{ss} is the restitution coefficient, and g_0 is a radial distribution function that specifies the probability of particle-particle collisions [121],

$$g_0 = \left[1-\left(\frac{\alpha_s}{\alpha_{s,max}}\right)^{1/3}\right]^{-1} \tag{5.8}$$

where $\alpha_{s,max}$ is the maximum volume fraction of solid phase taken as 0.63.

In the Eulerian model, granular temperature (θ_s) is obtained using the kinetic theory of granular flow and is proportional to the kinetic energy of moving particles. The transport equation for granular temperature is derived in terms of the energy generated by the solid stress tensor, $\left(-P_s\vec{I}+\bar{\bar{\tau}}_s\right).\nabla\vec{v}_s$, as [122],

$$\frac{3}{2}\nabla.\left(\alpha_s\rho_s\vec{v}_s\theta_s\right) = \left(-P_s\vec{I}+\bar{\bar{\tau}}_s\right).\nabla\vec{v}_s + \nabla.\left(k_{\theta_s}\nabla\theta_s\right) - \lambda_{\theta_s} + \varphi_{ls} \tag{5.9}$$

The solid pressure, P_s, is expressed as,

$$P_s = \alpha_s\rho_s\theta_s + 2\rho_s(1+e_{ss})\alpha_s^2 g_0\theta_s \tag{5.10}$$

The term k_{θ_s} is defined as the diffusion coefficient given by [122],

$$k_{\theta_s} = \frac{15 d_s\alpha_s\rho_s\sqrt{\pi\theta_s}}{4(41-33\eta)}\left[1+\frac{12}{5}\eta^2(4\eta\text{-}3)\alpha_s g_0 + \frac{16}{15\pi}(41-33\eta)\eta\alpha_s g_0\right] \tag{5.11}$$

where,

$$\eta = \frac{1}{2}(1+e_{ss}) \tag{5.12}$$

The term λ_{θ_s} is the collisional dissipation energy, which accounts for the dissipated energy within the solid particles as a result of particle-particle collisions [119],

$$\lambda_{\theta_s} = \frac{12(1-e_{ss}^2)g_0}{d_s\sqrt{\pi}}\rho_s\alpha_s^2\theta_s^{3/2} \tag{5.13}$$

Finally, $\varphi_{ls} = -3\delta_{ls}\theta_s$ represents the kinetic energy due to random fluctuations of particle velocity [121].

Drag force between the phases plays a substantial role in particulate flows [123]. This component is given by,

$$\vec{F}_D = \delta_{sl}(\vec{v}_s - \vec{v}_l) \tag{5.14}$$

where δ_{sl} is the solid-liquid momentum exchange coefficient which is calculated as [124]:

$$\delta_{sl} = \begin{cases} \dfrac{3C_D\alpha_s\alpha_l\rho_l|\vec{v}_l - \vec{v}_s|\alpha_l^{-2.65}}{4d_s} & (\alpha_s < 0.2) \\ \dfrac{150\alpha_s^2\mu_l}{\alpha_l d_s^2} + \dfrac{1.75\rho_l\alpha_s|\vec{v}_l - \vec{v}_s|}{d_s} & (\alpha_s \geq 0.2) \end{cases} \tag{5.15}$$

where C_D is the drag coefficient formulated as,

$$C_D = \frac{24}{\alpha_l Re_s}[1 + 0.15(\alpha_l Re_s)^{0.687}] \tag{5.16}$$

and Re_s is the relative *Reynolds* number defined by

$$Re_s = \frac{\rho_l d_s|\vec{v}_l - \vec{v}_s|}{\mu_l} \tag{5.17}$$

Lift force is another dominant force affecting the concentration distribution within the solid-liquid mixtures. Lift force stems from the velocity gradients in the liquid phase. This force is directly related to the size of solid particles. Larger particles result in increased lift being exerted on the solid phase. This force is expressed as [125],

$$\vec{F}_L = C_L\rho_l\alpha_s(|\vec{v}_l - \vec{v}_s|) \times (\nabla \times \vec{v}_l) \tag{5.18}$$

where C_L is the lift coefficient which is taken to be 0.2 in this study [126].

The interphase turbulent momentum transfer is crucial in modelling the solid-liquid mixtures. Turbulent dispersion is the driving mechanism that forces near-wall particles towards the centre of the pipe from high-concentration regions. If this force is not taken into account, the particle distribution in the central region may not be captured accurately, resulting in a uniform solid volume fraction distribution in the centre. The turbulent dispersion force is formulated as [127],

$$\vec{F}_{TD} = C_{TD}\delta_{sl}\frac{\mu_{tl}}{\rho_l\sigma_{sl}}\left(\frac{\nabla\alpha_s}{\alpha_s} - \frac{\nabla\alpha_l}{\alpha_l}\right) \tag{5.19}$$

where μ_{tl} is the turbulent viscosity of the liquid phase, C_{TD} is the turbulent dispersion force coefficient taken as 1 [85], and σ_{sl} is the dispersion *Prandtl* number assigned as 0.9.

In order to choose the most appropriate model that can capture the turbulent features of the ice slurry, mixture and per-phase *k*-*ε* turbulence models were tested. The *k*-*ε* mixture model is based on using the mixture properties and velocities to model the important features of the turbulent flow. This model is sufficiently accurate for stratified (or almost stratified) two-phase flows and when the density ratio between phases is close to unity. In this model, the equations for *k* and *ε* are expressed as [128],

$$\frac{\partial}{\partial t}(\rho_m k) + \nabla.(\rho_m \vec{v}_m k) = \nabla.\left(\left(\mu_m + \frac{\mu_{t,m}}{\sigma_k}\right)\nabla k\right) + G_{k,m} - \rho_m \varepsilon \tag{5.20}$$

and

$$\frac{\partial}{\partial t}(\rho_m \varepsilon) + \nabla.(\rho_m \vec{v}_m \varepsilon) = \nabla.\left(\left(\mu_m + \frac{\mu_{t,m}}{\sigma_\varepsilon}\right)\nabla \varepsilon\right) + \frac{\varepsilon}{k}\left(C_{1\varepsilon} G_{k,m} - C_{2\varepsilon}\rho_m \varepsilon\right) \tag{5.21}$$

In these equations, mixture density (ρ_m), mixture viscosity (μ_m) and mixture velocity ($\vec{v}_m$) are calculated as,

$$\rho_m = \sum_{i=1}^{N} \alpha_i \rho_i \tag{5.22}$$

$$\mu_m = \sum_{i=1}^{N} \alpha_i \mu_i \tag{5.23}$$

$$\vec{v}_m = \frac{\sum_{i=1}^{N} \alpha_i \rho_i \vec{v}_i}{\sum_{i=1}^{N} \alpha_i \rho_i} \tag{5.24}$$

where indices *i* can be *s* or *l* referring to the solid and liquid phases, respectively.

The turbulent viscosity for the mixture ($\mu_{t,m}$) is given by,

$$\mu_{t,m} = \rho_m C_\mu \frac{k^2}{\varepsilon} \tag{5.25}$$

The production of turbulence kinetic energy, $G_{k,m}$, is expressed as

$$G_{k,m} = \mu_{t,m}(\nabla\vec{v}_m + (\nabla\vec{v}_m)^T) : \nabla\vec{v}_m \tag{5.26}$$

The per-phase *k*-ε turbulence approach is based on solving separate transport equations of *k* and ε for each phase. The averaged fluctuating quantities are obtained via an eddy viscosity model. The Reynolds stress tensor for the liquid phase is given as

$$\bar{\bar{\tau}}_l = -\frac{2}{3}\left(\rho_l k_l + \mu_{t,l}\nabla\vec{v}_l\right)\bar{\bar{I}} + \mu_{t,l}(\nabla\vec{v}_l + (\nabla\vec{v}_l)^T) \tag{5.27}$$

where turbulent viscosity ($\mu_{t,l}$) is defined as

$$\mu_{t,l} = \rho_l C_\mu \frac{k_l^2}{\varepsilon_l} \tag{5.28}$$

with $C_\mu = 0.9$.

Turbulent predictions are written as;

$$\begin{aligned}\frac{\partial}{\partial t}(\alpha_l\rho_l k_l) + \nabla.(\alpha_l\rho_l\vec{v}_l k_l) \\ = \nabla.\left(\alpha_l\frac{\mu_{t,l}}{\sigma_k}\nabla k_l\right) + \left(\alpha_l G_{k,l} - \alpha_l\rho_l\varepsilon_l\right) \\ + \sum_{s=1}^{N}\delta_{sl}(C_{sl}k_s - C_{ls}k_l) - \sum_{s=1}^{N}\delta_{sl}(\vec{v}_s - \vec{v}_l).\frac{\mu_{t,s}}{\alpha_s\sigma_s}\nabla\alpha_s \\ + \sum_{s=1}^{N}\delta_{sl}(\vec{v}_s - \vec{v}_l).\frac{\mu_{t,l}}{\alpha_l\sigma_l}\nabla\alpha_l\end{aligned} \tag{5.29}$$

$$\begin{aligned}\frac{\partial}{\partial t}(\alpha_l\rho_l\varepsilon_l) + \nabla.(\alpha_l\rho_l\vec{v}_l\varepsilon_l) \\ = \nabla.\left(\alpha_l\frac{\mu_{t,l}}{\sigma_\varepsilon}\nabla\varepsilon_l\right) + \frac{\varepsilon_l}{k_l}\left(C_{1\varepsilon}\alpha_l G_{k,l} - C_{2\varepsilon}\alpha_l\rho_l\varepsilon_l\right) \\ + C_{3\varepsilon}\left(\sum_{s=1}^{N}\delta_{sl}(C_{sl}k_s - C_{ls}k_l) - \sum_{s=1}^{N}\delta_{sl}(\vec{v}_s - \vec{v}_l).\frac{\mu_{t,s}}{\alpha_s\sigma_s}\nabla\alpha_s\right. \\ \left. + \sum_{s=1}^{N}\delta_{sl}(\vec{v}_s - \vec{v}_l).\frac{\mu_{t,l}}{\alpha_l\sigma_l}\nabla\alpha_l\right)\end{aligned} \tag{5.30}$$

In these equations $C_{sl} = 2$ and $C_{ls} = 2\left(\frac{\beta_{sl}}{1+\beta_{sl}}\right)$ where β_{sl} is the ratio of characteristic relaxation times. More information on turbulence modelling can be found in [128].

5.2.3 Boundary conditions

The simulation domain has three main boundaries, namely the velocity inlet, the wall, and the pressure outlet. At the inlet, uniform velocities and volume fractions of ice particles and carrier fluid are specified. A turbulent intensity of 5% was set at the inlet. Atmospheric pressure is assigned to the outlet.

A no-slip condition is set for the liquid phase at the wall, while the Johnson-Jackson boundary condition [129] is used to compute the solid tangential velocity ($\vec{v}_{sw}$) and granular temperature at the wall (θ_{sw}). For this condition, the losses in the tangential and parallel momentum equations of solid particles are taken into account through the specularity coefficient (ϕ_w) and the particle-wall restitution coefficient (e_{sw}). According to this method,

$$\vec{v}_{sw} = -\frac{6\mu_s\alpha_{s,max}}{\sqrt{3}\pi\phi_w\rho_s g_0\sqrt{\theta_{sw}}}\frac{\partial\vec{v}_{sw}}{\partial n} \tag{5.31}$$

and

$$\theta_{sw} = -\frac{k_{\theta_{sw}}}{\gamma_w}\frac{\partial\theta_{sw}}{\partial n} + \frac{\sqrt{3}\pi\phi_w\rho_s\alpha_s\vec{v}_{sw}^2 g_0\theta_{sw}^{3/2}}{6\alpha_{s,max}\gamma_w} \tag{5.32}$$

where $\gamma_w = \frac{\sqrt{3}\pi(1-e_{sw}^2)\rho_s\alpha_s g_0\theta_{sw}^{3/2}}{4\alpha_{s,max}}$.

The values for ϕ_w and e_{sw} are usually obtained through sensitivity analysis. In this study, values of 0.015 and 0.9 were assigned to the specularity and particle-wall restitution coefficients, respectively [85].

5.2.4 Solution strategy

The governing equations are discretised using the finite volume integral method. Second order upwind discretisation and Quick schemes were implemented for momentum and volume fraction equations, respectively. The convergence criteria are based on the residuals of different variables. The phase-coupled SIMPLE algorithm was utilized to solve the discrete equations. To improve the convergence, all of the volume fraction equations for both liquid and solid phases were solved. This was done as an alternative to solving the volume fraction equation for the solid phase initially and setting the volume fraction of the liquid phase to the complement. The initial time step was set to be 10^{-3} s. The convergence criterion for the momentum equation was assigned to be 10^{-5}, while for the volume fraction and turbulence equations a convergence criterion of 10^{-4} was used. An initial solution was obtained for the flow field, without considering the volume fraction equation.

5.3 Model validation and benchmarking

5.3.1 Solid velocity profiles

In order to ensure the accuracy of the numerical model, two sets of benchmark studies were completed.

The first benchmark study was based on a comparison of the solid velocity (u_s) profiles against the experimental results of Vuarnoz et al. [60] and the numerical results of Wang et al. [118] (Figure 5.2a). The numerical simulations were conducted for 10.3% ethanol-based ice slurry flowing in a straight pipe with a length of 1 m and a diameter of 23 mm. The particle diameter was taken as 0.1 mm. The ice volume fraction and the inlet mas flow rate were set to be 16% and 0.5 kg/s, respectively. The numerical results are obtained using both mixture and per-phase turbulence models. It is noted that both turbulence models demonstrate symmetrical solid velocity profiles, as observed by the experimental results. It is also evident that the solid velocity profiles obtained by the current numerical model are more accurate than those obtained by Wang et al [118] in the central region. However, the numerical model by Wang et al. [118] shoes smaller deviation from the experimental data in the near-wall regions. It is noteworthy that the per-phase turbulence model is more accurate than the mixture turbulence model despite being computational more expensive.

The second benchmark study was developed by comparing the numerical results for normalized solid velocity profile (u_s/u_{in}) with the experimental results obtained by Stamatiou and Kawaji [130] (Figure 5.2b). The numerical simulations were conducted for upward flow of 6.2% NaCl-water based ice slurry in a 0.305 × 0.61 × 0.025 m vertical rectangular channel, and with a mass fraction of 1.9%, an inlet velocity of 0.159 m/s and a particle diameter of 0.1 mm. The results show that there is a good agreement between the experimental and numerical results for both mixture and per-phase turbulence models.

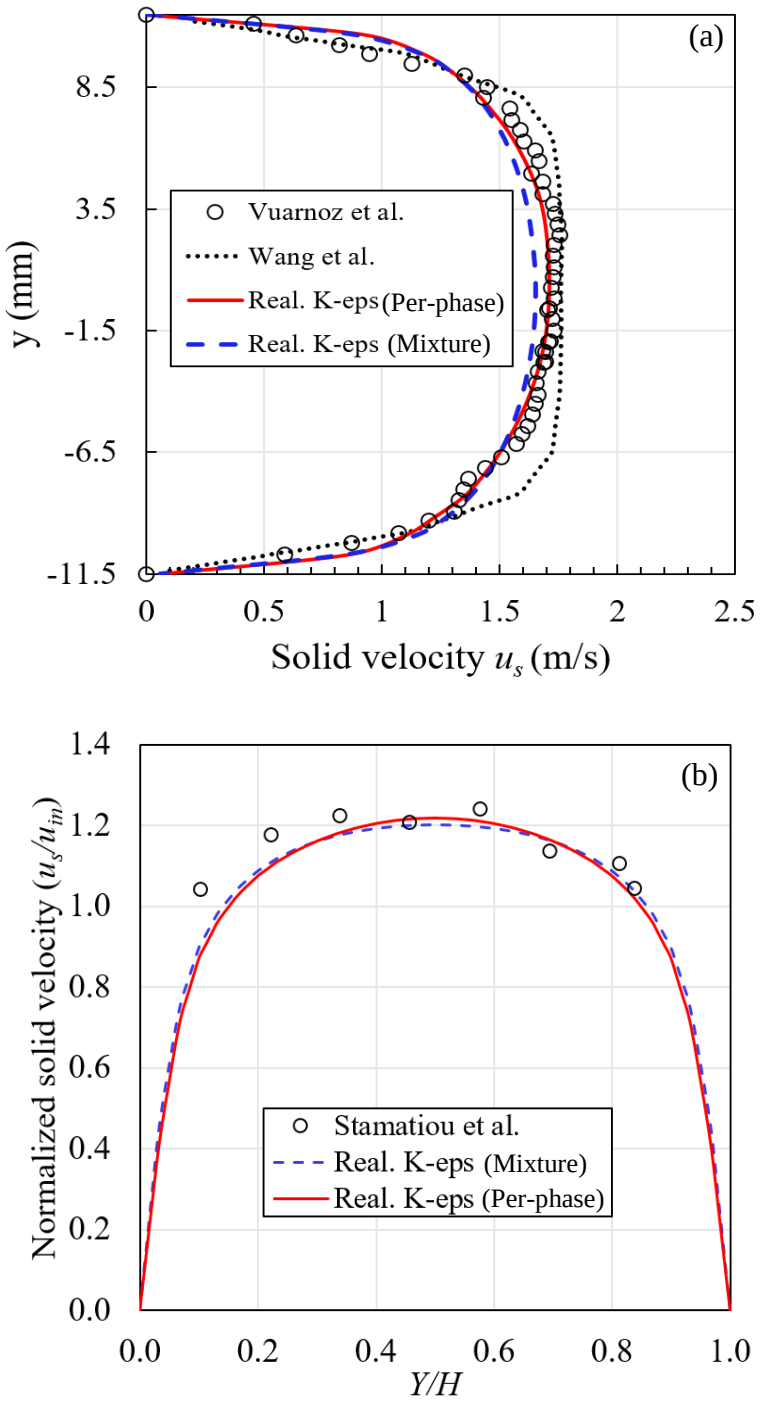

Figure 5.2. (a) Comparison of numerical results for solid velocity with the experiments [60] and simulations [118] for a straight pipe; (b) Comparison of numerical results of normalized solid velocity with the experiments [130] for a vertical channel.

5.3.2 Pressure drop

The numerical model was further validated against a series of new experiments fully described in Chapter 6. The variations of pressure drop with the ice slurry flow rate for two different ice volume fractions of 5% and 15%, are presented in Figure 5.3. The experiments were done for 5%

monopropylene glycol solution. The average particle diameter was estimated using a dual-view image processing. For the purpose of validation an average particle diameter of 0.1 mm was set for the simulations. The error bars denote the relative errors of ±12% for each experimental point. It is noted from the figure that there is an acceptable agreement between the numerical values and experimental measurements. The increase in the ice volume fraction, causes the viscosity of the ice slurry to increase. As a result, the ice slurry with a higher volume fraction of ice, results in more pressure drop and pumping requirements.

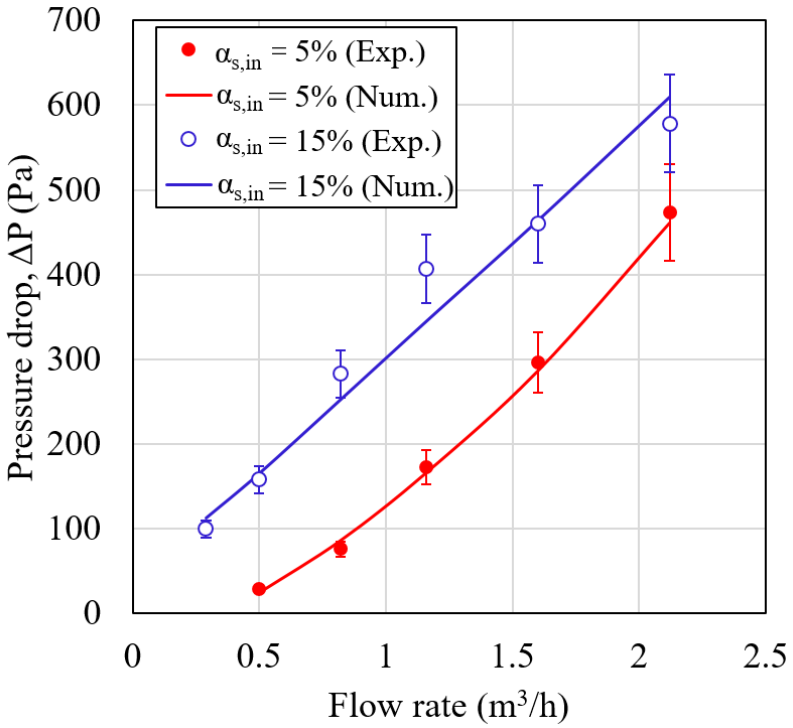

Figure 5.3. Validation of numerical results against experiments in terms of pressure drop of ice slurry for 5% and 15% ice volume fraction.

5.4 Results and discussion

5.4.1 Concentration distribution

The effect of different parameters such as inlet velocity, particle diameter and ice volume fraction on the concentration distribution along the bend are presented. In general, due to the centrifugal forces exerted on the flow in a bend, the particles and liquid will be mixed and the particle distribution will be disturbed.

Figure 5.4 shows the contours of ice volume fraction at three different locations in the bend, corresponding to sections at β = 0º, β = 90º and β = 180º, for three different inlet velocities of u_{in} = 0.35 m/s, 0.54 m/s and 1.42 m/s. The velocity vectors are also shown for the centre cross section

(β = 90º) and outlet cross-section (β = 180º). It is evident that the secondary flows are intensified as the inlet velocity increases. The heterogeneous structure of the fluid observed at the inlet cross-section (β = 0º) is disturbed due to the secondary flows generated due to centrifugal forces at β = 90º and β = 180º. This is associated with higher lift forces, intensified inter-particle collisions and higher turbulent dispersion force. This behaviour is observed for all inlet velocities.

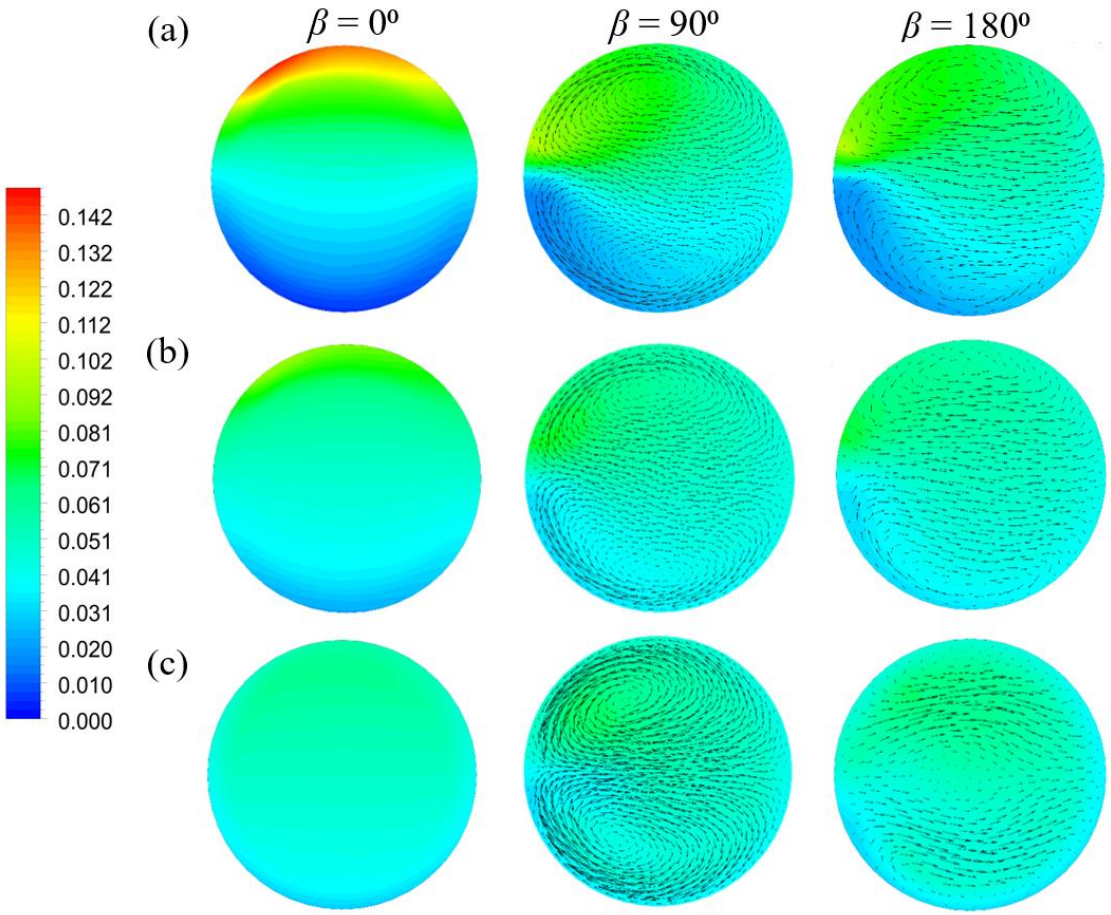

Figure 5.4. Contours of ice volume fraction at different locations (in terms of β) throughout the bend along with velocity vectors for $\alpha_{s,in}$ = 5% at (a) u_{in} = 0.35 m/s, (b) u_{in} = 0.54 m/s and (c) u_{in} = 1.42 m/s.

Figure 5.5 presents the top view of the mid-plane passing through the bend with the contours of (a) solid volume fraction (b) and solid velocity. The inlet velocity affects the horizontal ice volume fraction distribution such that higher volume fractions exist near the outer wall.

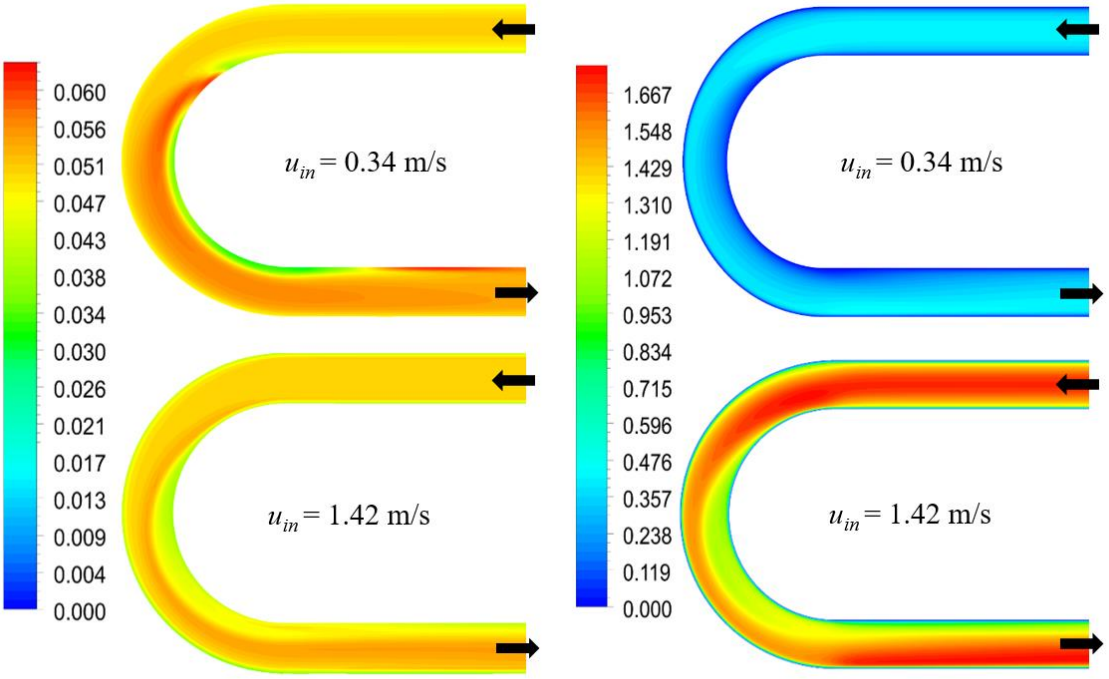

(a) Solid Volume fraction (b) Solid Velocity (m/s)

Figure 5.5. Contours of (a) solid volume fraction and (b) solid velocity at the horizontal mid-plane at different inlet velocities ($\alpha_{s,in}$ = 5%).

The effect of particle diameter on the concentration distribution is shown in Figure 5.6, where the normalized ice volume fraction is drawn against the vertical mid-axis for three particle diameters of d_s = 0.6, 0.8 and 1.2 mm at inlet (β = 0º), centre (β = 90º) and outlet (β = 180º) sections of the bend. It is noted that, for the same inlet velocity of 1.42 m/s, the fluid structure becomes more heterogeneous with increasing particle diameter. This stems from the fact that for the larger diameter, more ice particles are accumulated along the top section. However, a decrease of solid volume fraction near the wall is observed as the particle diameter increases. This emanates from the fact that larger particle diameter is associated with larger repulsive forces due to particle-wall collisions [85].

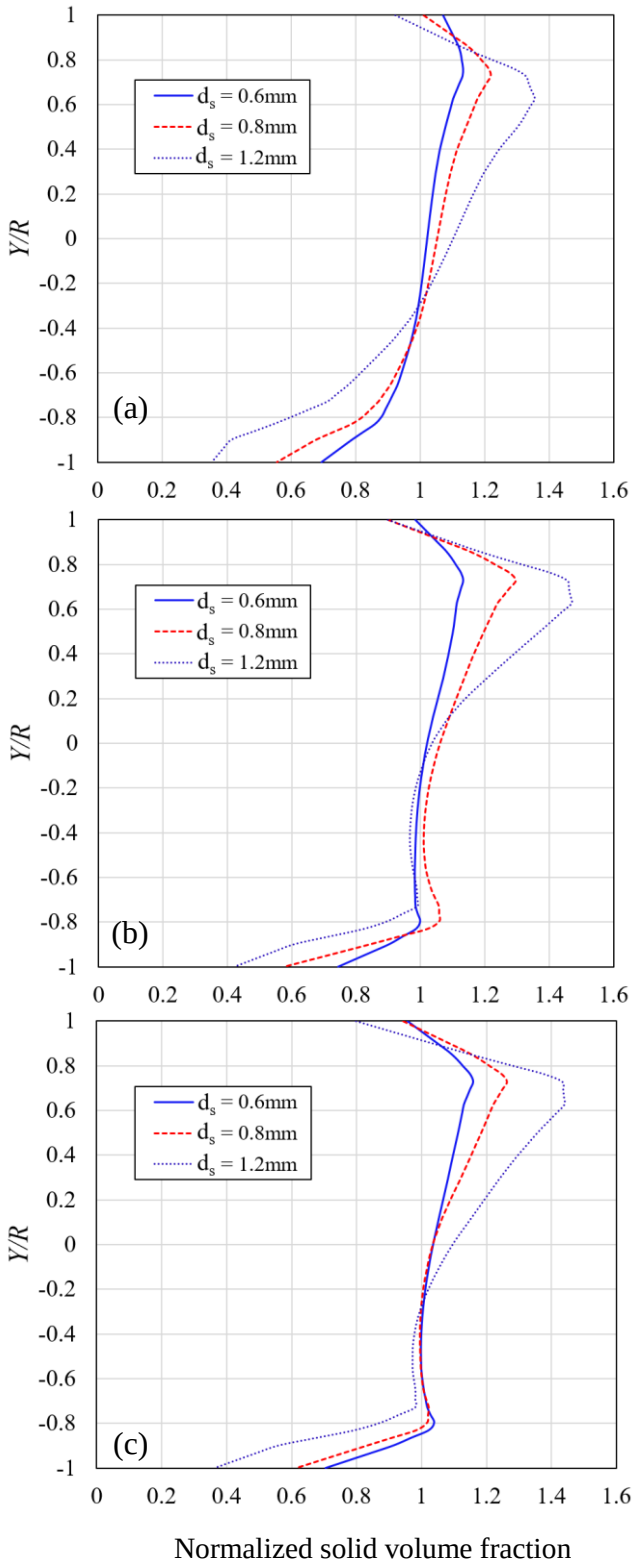

Figure 5.6. Radial distribution of normalized solid volume fraction across the vertical symmetry axis of (a) β = 0º, (b) β = 90º and (c) β = 180º of the bend for particle diameters of 0.6, 0.8 and 1.2 mm (u_{in} = 1.42 m/s and $\alpha_{s,in}$ = 20%).

Figure 5.7 shows the contours of turbulence kinetic energy for ice particles of 0.6 and 1.2 mm at different cross sections. As noted, the smaller diameter results in higher values of turbulence kinetic energy. This supports the observation that the ice slurry flow with smaller particle diameter exhibits a more homogenous structure. As the ice slurry enters the bend section, the turbulence kinetic energy of particles is further intensified due to the centrifugal force and the secondary flow. The effect of the secondary flow is more pronounced for the 0.6 mm particle diameter.

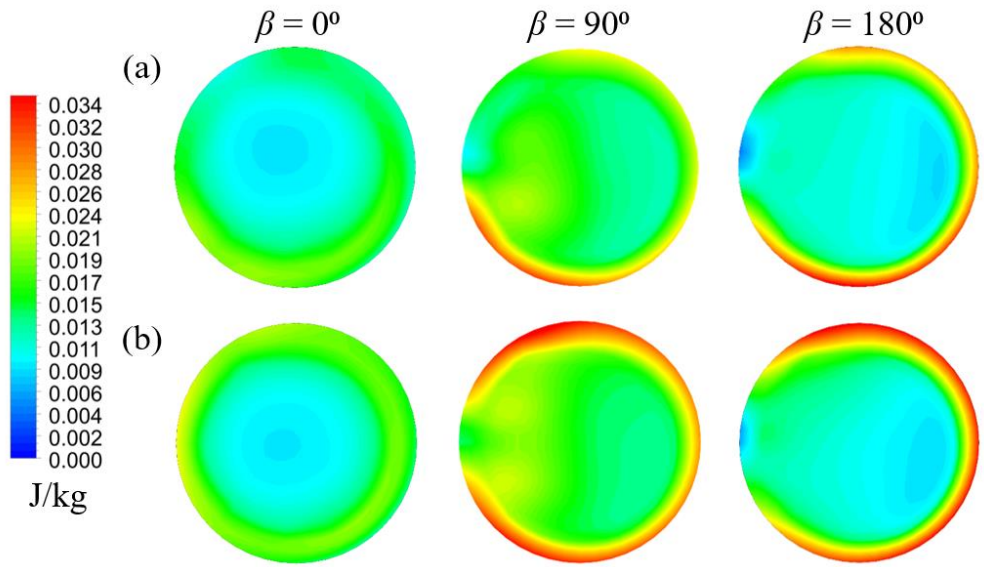

Figure 5.7. Contours of solid turbulence kinetic energy, *k*, at different locations throughout the bend for particle diameters of (a) 1.2 mm, and (b) 0.6 mm. For the two cases, u_{in} =1.42 m/s and $\alpha_{s,in}$ = 20%.

Figure 5.8 displays the effect of the inlet solid volume fraction on the profiles of normalized solid volume fraction at three vertical cross-sections of the U-bend and for an inlet velocity of u_{in} = 0.34 m/s. The results show that as the inlet solid volume fraction increases, the profile becomes more uniform due to the intensified inter-particle collisions which drives more particles into the central region of the pipe. The profile for the inlet solid volume fraction of $\alpha_{s,in}$ = 5% undergoes a substantial change as the ice slurry passes through the bend from inlet to the outlet, whereas for the 20% inlet solid volume fraction, the profile remains almost the same.

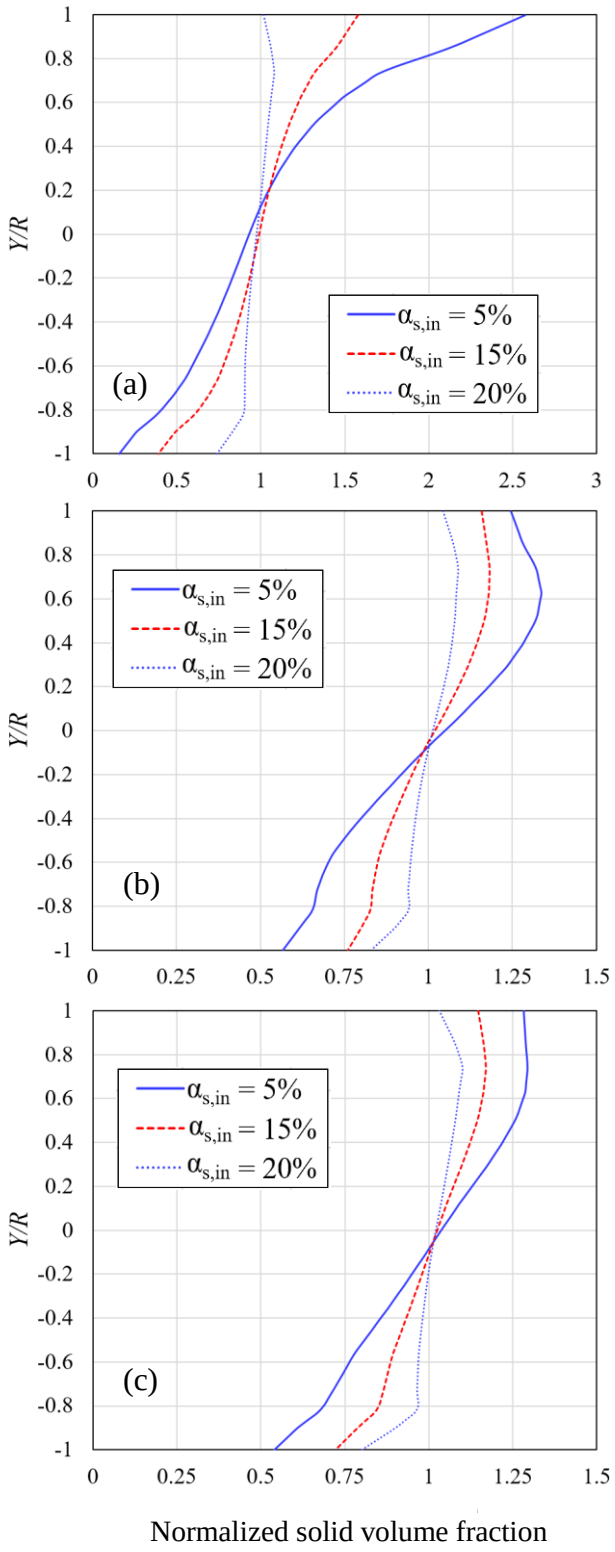

Figure 5.8. Radial distribution of normalized solid volume fraction across the vertical axis of (a) β = 0º, (b) β = 90º and (c) β = 180º of the bend for $\alpha_{s,in}$ = 5%, 15% and 20%. For all cases u_{in} = 0.34 m/s and d_s = 0.6 mm.

In general, there exists a difference between dilute and concentrated particulate flows in terms of the energy associated with each solid particle. This is depicted in Figure 5.9 where the energy of a particle at time t and $t + dt$ are denoted as E_t and E_{t+dt}, respectively. For the dilute case, particles exhibit random fluctuations creating a form of viscous dissipation and stress known as kinematic energy (φ_{ls}). In the case of a more concentrated flow, the collision of particles brings about an additional dissipation and stress known as collisional energy (λ_{θ_s}). This explains the more uniform nature of flows with higher concentrations. It is noteworthy, that with further increase of concentration (over 50%) another form of dissipation and stress will emerge as a result of particle-particle sliding contacts. Multiphase mixture models are usually incapable of considering these various cases.

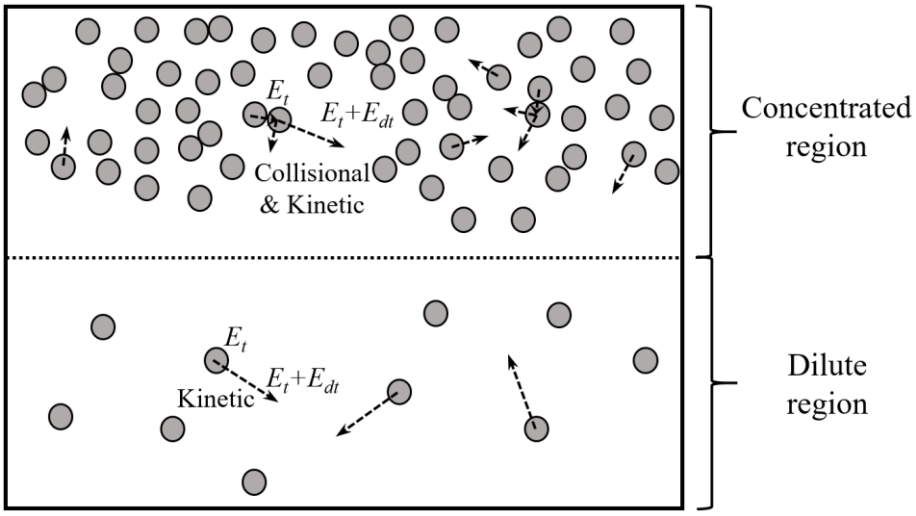

Figure 5.9. Pictorial explanation of the difference between dilute and concentrated cases in terms of the energy associated with solid particles.

5.4.2 Shear stress distribution

Figure 5.10 presents the distribution of solid shear stress at a volume fraction of 5% for different inlet velocities. In general, the solid shear stress increases with an increase in velocity. For the inlet cross section and at the lowest velocity, there is zero shear stress on the bottom of the wall. However, an increase in velocity spreads shear stress to the whole periphery of the wall. As the ice slurry enters the bend section, the distribution of shear stress is more significant on the right hand side of the wall where velocities are larger due to centrifugal forces and secondary flows. This induces higher kinetic and collisional components for the solid particles which in turn engender higher shear stresses. This shows how the wall stress distribution in a bend differs from that of a straight pipe. The change in ice volume fraction also influences the shear stress exerted on the wall.

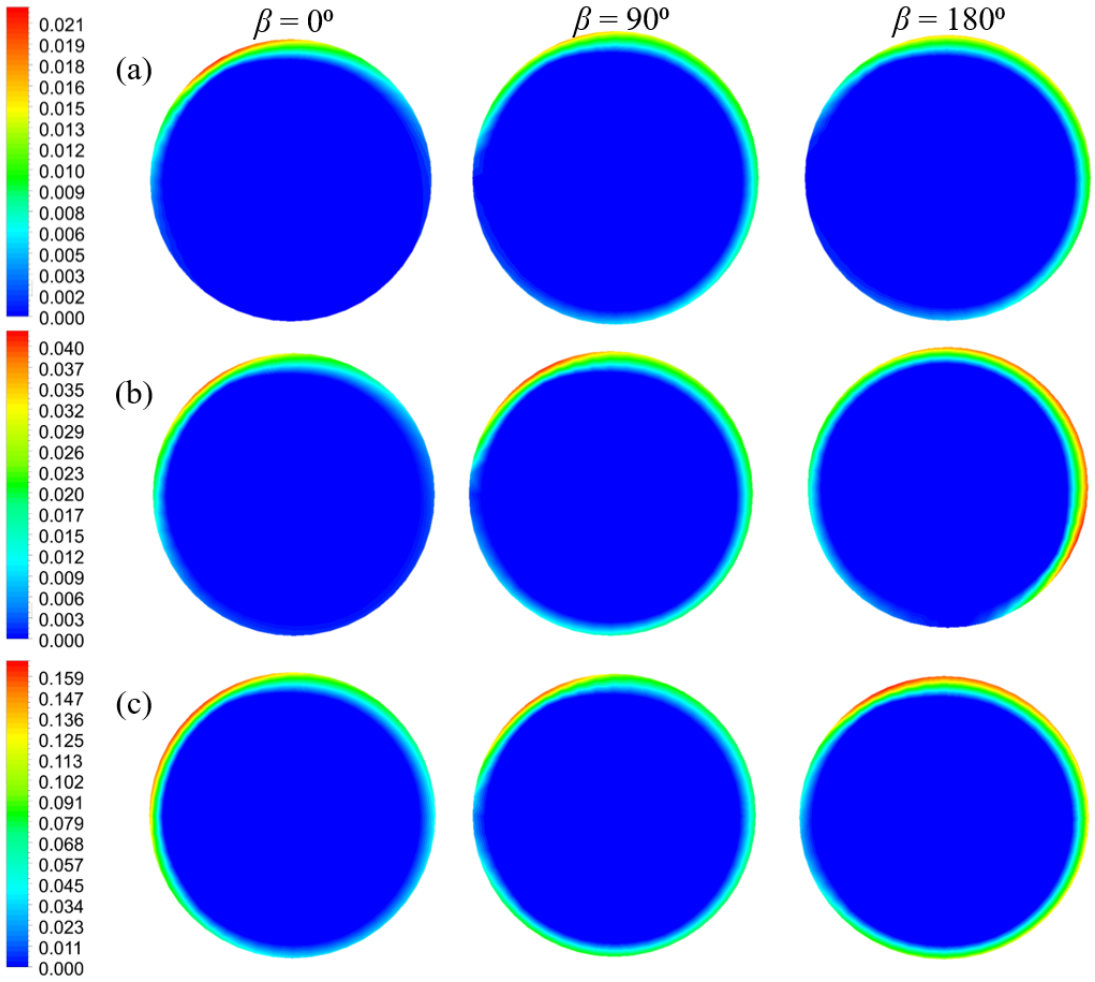

Figure 5.10. Contours of shear stress (Pa) due to ice particles at different locations throughout the bend for inlet velocities of (a) 0.34 m/s, (b) 0.55 m/s and (c) 1.42 m/s. Results obtained for $\alpha_{s,in}$ = 5% and d_s = 0.6 mm.

Figure 5.11(a, b) provide a comparison for the wall shear stress between two cases with different ice volume fractions of 10% and 20% with the same inlet velocity of u_{in} =1.42 m/s and diameter of 0.1mm It is clear that a higher volume fraction causes a higher wall shear stress. By increasing the ice volume fraction from 10% to 20%, the shear stress rises by approximately four fold. Figure 5.11(c, d) present the effect of particle diameter on the wall shear stress distribution throughout the U-bend for the same inlet velocity of u_{in} =1.42 m/s and the ice volume fraction of $\alpha_{s,in}$ = 20% . It is observed that a smaller particle diameter of d_s = 0.6 mm results in a slightly higher shear stress at the wall. This is an interesting fact as the wall shear stress directly affects the pressure drop. This implies the need for more investigation on the pressure drop at different velocities and for different particle diameters.

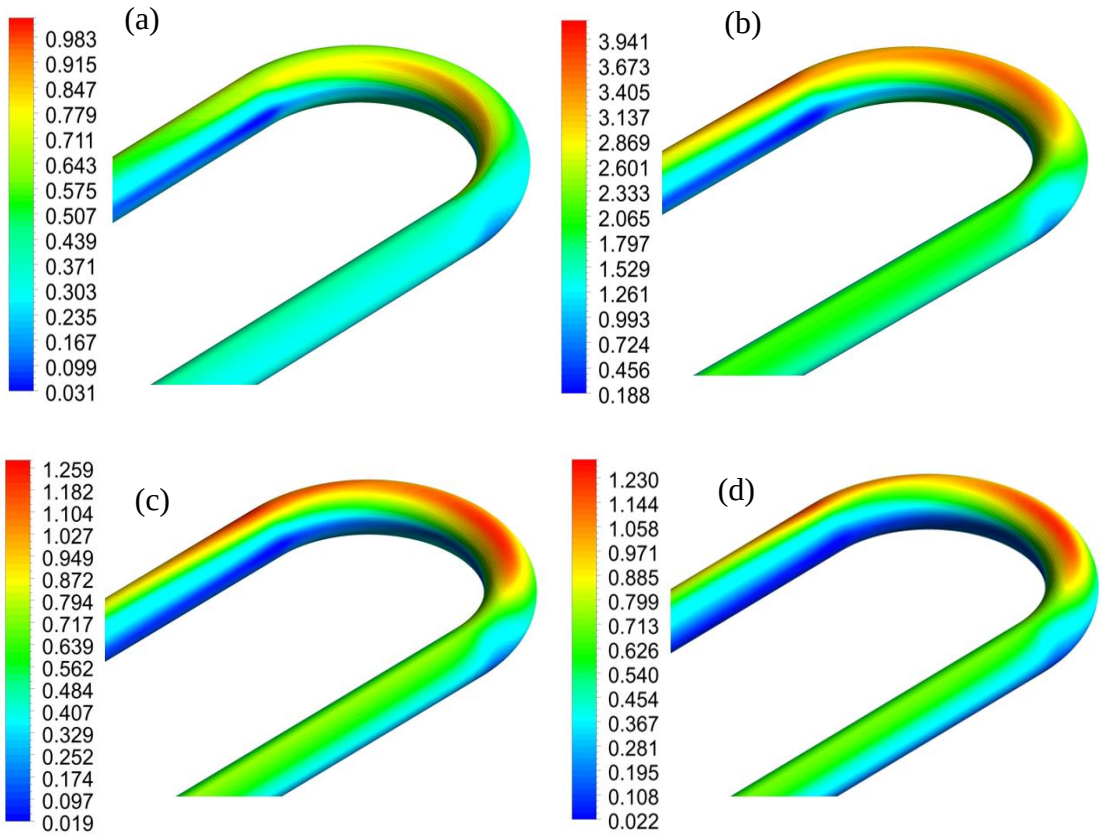

Figure 5.11. Contours of wall shear stress (Pa) at u_{in} =1.42 m/s (a) d_s = 0.1 mm, α_s = 10% (b) d_s = 0.1 mm, $\alpha_{s,in}$ = 20%, (c) $\alpha_{s,in}$ = 20% , d_s = 0.6 mm (d) $\alpha_{s,in}$ = 20% , d_s = 1.2 mm.

5.4.3 Pressure drop

Figure 5.12a presents the pressure drop in the bend at different flow rates and ice volume fractions. At any given flow rate, pressure drop increases with an increase in the ice volume fraction. It is also observed that for all ice volume fractions, the pressure drop increases as the flow rate increases. Thus, higher ice volume fractions and higher flow rates require higher pumping powers. This can be explained by the fact that a higher volume fraction brings about a higher shear stress at the wall as shown in Figure 5.11. Figure 5.12b shows the effect of particle diameter on the pressure drop of ice slurry flows in the bend. The pressure drops for ice volume fractions of 5% and 20% are presented for two particle diameters of 0.6 mm and 1.2 mm. The increasing trend of pressure drop with increasing velocity is observed for both particle diameters. It is also observed that for both values of ice volume fraction the finer particles result in lower pressure drops at lower flow velocities when compared to coarser particles. As the velocity increases, pressure drop values for 0.6 mm particles exceed those of 1.2 mm particles. The higher pressure drop of coarse particles at low velocities stems from the fact that the amount of particles moving in the bed is increased due to gravitational effects.

When it comes to fine particles at higher velocities, the pressure drop is primarily caused by a greater surface area causing more frictional losses [131]. This implies that the particle diameter should be considered, as it along with the flow rate can impact the pumping requirements.

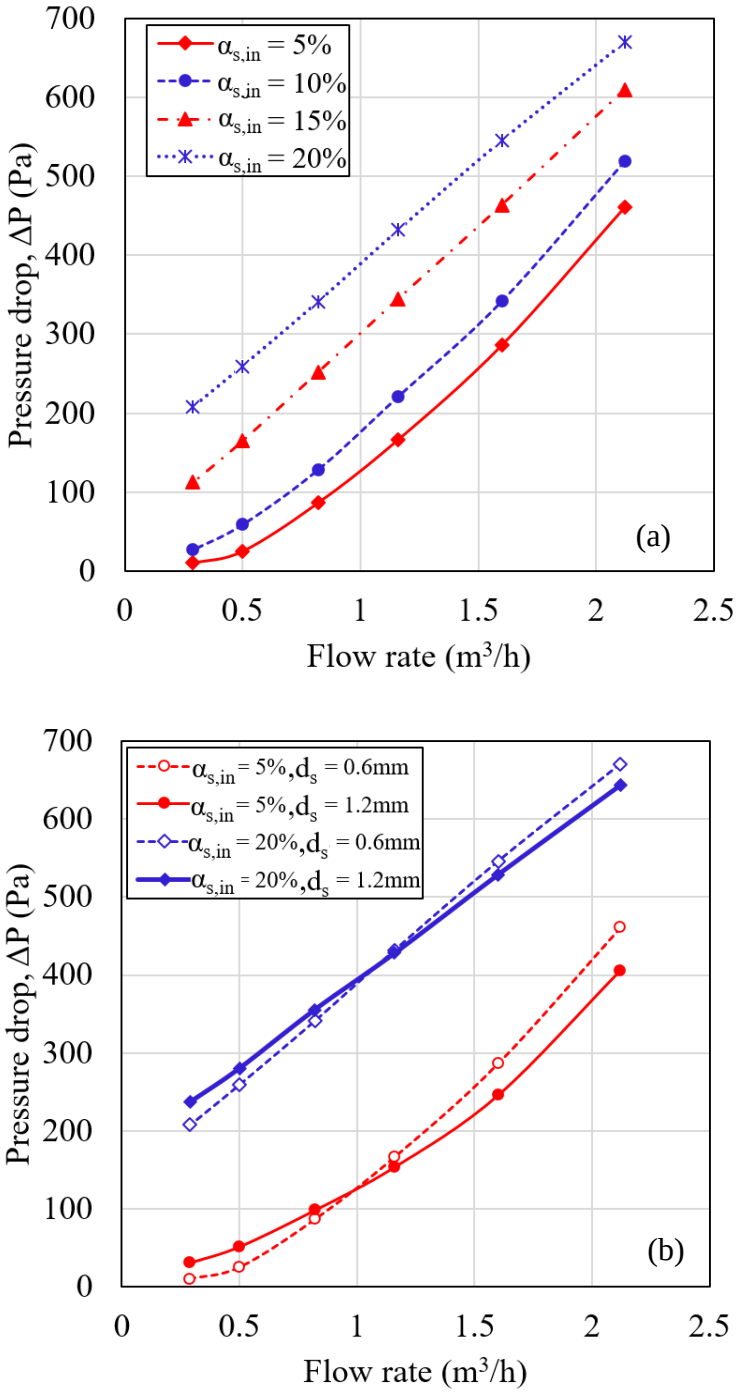

Figure 5.12. (a) Numerical values of pressure drop in the bend section for different flow rates and ice volume fractions. (b) Effect of particle diameter on the pressure drop in the bend for different flow rates with $\alpha_{s,in}$ = 5% and $\alpha_{s,in}$ = 20%.

5.4.4 Loss coefficients

The total loss coefficient of the U-bend, ζ, is usually expressed in terms of the total pressure drop in the bend as,

$$\zeta = \frac{\Delta P}{\left(\frac{\rho_{is} u_{in}^2}{2}\right)} \tag{5.33}$$

Figure 5.13 shows the variation of bend loss coefficient with the inlet velocity for different inlet ice volume fractions. The results show different trends for the bend loss coefficient for ice volume fractions of 5% and 10% compared with those for ice volume fractions of 15% and 20%. For low ice volume fractions (5% and 10%), there is a negligible change of loss coefficient as the inlet velocity increases. However, for high ice volume fractions (15% and 20%), a dramatic decrease in the loss coefficient is observed when the inlet velocity increases. The maximum loss coefficient is observed for the highest ice volume fraction and the lowest flow velocity. This is in accordance with previous findings [132] for flow of propylene glycol ice slurries through 90º bends.

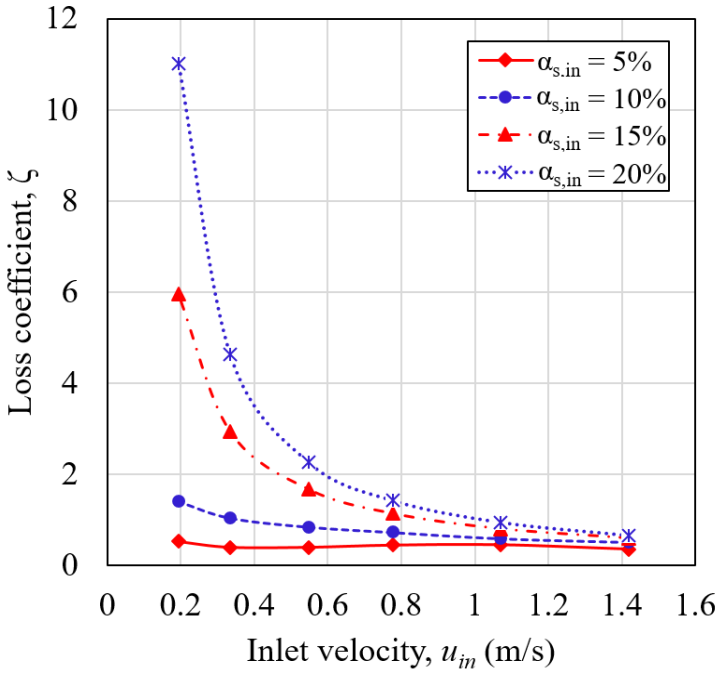

Figure 5.13. Variation of bend loss coefficient (ζ) with inlet velocity (u_{in}) at different ice volume fractions ($\alpha_{s,in}$).

5.5 Conclusions

In this chapter, the isothermal flow characteristics of monopropylene glycol ice slurry in a horizontal U-bend were investigated numerically. An Euler-Euler multiphase model based on the kinetic theory of granular flows was implemented to elucidate the flow behaviour of ice slurry passing through the bend. The numerical results were validated against numerical results published in the literature and present experiments. The secondary flow generated within the U-bend as a result of the centrifugal force was affected by the ice volume fraction and the particle diameter. This was due to the inter-particle interactions and different turbulent dispersion intensities. This in turn caused differences in the values of wall shear stresses. A higher ice volume fraction and a smaller particle diameter were associated with larger values of wall shear stress. It was observed that the particle diameter, the flow velocity and the ice volume fraction affected the pressure drop in the U-bend. The pressure drop increased with an increase in the ice volume fraction and the flow velocity. However, the effect of particle diameter was different for low values of flow velocity when compared with those at higher velocities. At low velocities, fine particles induced a lower pressure drop compared to coarse particles.

In Chapter 6, the experimental investigation of pressure drop of monopropylene glycol ice slurry in U-bends with different diameters at different flow rates is presented. The flow visualization of ice slurry flow in the straight pipe as well as the U-bend is also provided.

The following chapter has been submitted in the form of a journal article and is currently under review:

- **Amin Kamyar**, Saiied M Aminossadati, Christopher R Leonardi, Sebastian Gund, Michael Kauffeld. *Flow characterization of monopropylene glycol ice slurry through U-bends: Part II: An experimental approach*. International Journal of Refrigeration. (**Under review**)

Candidate's Contribution to the authorship:

Authorship activities	Contribution
conception and design of the project	70%
analysis and interpretation of the research data	70%
drafting significant parts of the publication or critically reviewing	70%

Chapter 6 Flow characterization of monopropylene glycol ice slurry through horizontal and vertical U-bends: An experimental approach

6.1 Introduction

There exists a limited number of experimental studies on ice slurry flows through geometries other than straight pipes. Mika [57] experimentally measured the pressure loss coefficients of pipe contractions and expansions for laminar flow of ethylene alcohol ice slurry. The authors also proposed that for more accurate prediction of ice slurry behaviour, different models should be implemented for low and high shear rate regions. Haruki and Horibe [109] studied the flow and heat transfer characteristics of water-based ice slurry in a helical coil heat exchanger. They also developed models for friction factor and Nusselt number in terms of different parameters. In another study, the local loss coefficients of ice slurry in pipe tees and flow drivers were determined by Mika [67] along with correlations for the laminar range. Nørgaard et al. [132] measured the pressure drop loss coefficients of ice slurry flow through various components such as elbows, bends, contractions and expansions. They found that the largest deviation for loss coefficients between the single-phase brine and ice slurry is more pronounced at high concentration and low flow velocity. Niezgoda-Żelasko and Żelasko [63] experimentally measured the flow resistance of ethanol-based ice slurry through 90º bends and, by considering the ice slurry as Bingham plastic fluid, were able to predict the loss coefficients.

The experimental investigation of ice slurry flow characteristics can be a challenging task due to the difficulties imposed by its complex structure. No previous research has experimentally measured the pressure drop and loss coefficients of ice slurry flows through U-bends. In this study, qualitative observations are made through visualization of ice slurry flow in the straight pipe and the U-bend section. The pressure drop and loss coefficients are also presented for vertical and horizontal orientations of U-bends. The effect of change in pipe diameter, ice volume fraction and flow rate on the pressured drop and loss coefficients are indicated.

6.2 Experimental Setup

A test bench was built in the refrigeration lab at HS Karlsruhe to visualize the flow patterns and to measure the pressure drop over the bend (Figure 6.1). It consists of an ice slurry generator **1** that is connected to a storage tank **2**. The storage tank is connected to the test section through five ball valves. Ice slurry is pumped with a centrifugal pump **3** through a Coriolis flow meter **4**. The ice slurry enters the inlet pipe **5** of the test section. A differential pressure sensor **6** is connected to the inlet **7** and the

outlet **8** of the bend. The ice slurry exits the test section through the outlet pipe **9** and is returned to the tank.

A scraper ice generator manufactured by Cooltech GmbH was used to produce the ice crystals. This generator is a double-walled steel tube inside which scrapers are mounted on a rotor. A refrigeration cycle provides a coolant that flows through the jacket of the generator. The ice crystals formed on the inner wall are then scraped off and pumped into the storage tank.

The piping was made of Polyvinyl Chloride (PVC) from GF Piping Systems. For the purpose of flow visualization, the inlet and outlet pipes and the bend were made of transparent material. The diameters for the bend tested in this study are shown in Table 6.1. The length of the inlet pipe was selected as $L_s = 50D$ to ensure that the flow entering the bend was fully developed. The experiments were conducted for horizontal and vertical orientations of the bend. In the case of vertical orientation, the flow entered the bend from the bottom. The tank had a storage capacity of 0.6 m^3, which was large in comparison to the piping test section including the bend. This kept the ice concentration stable throughout a measurement cycle. The Coriolis flow meter was a Proline Promass 80 F from Endress und Hauser AG. A Sitrans P310 from Siemens AG was used as differential pressure sensor. All signals were measured with an Agilent A34980A data logging device and evaluated in LabVIEW. The accuracy of mass flow measurement was ±0.15% and the accuracy of density measurement was equal to ±0.0005 g/cm^3. The accuracy of the differential pressure drop measurements was 0.075%.

Table 6.1. The dimensions of the tested pipes in the experiments

Type	Inner Radius, R (mm)	Pipe Diameter, d (mm)	Material
D25	62.5	25	PVC
D32	80	32	PVC

A mixture of water and 5% weight monopropylene glycol was used to generate the ice slurry. Table 6.2 includes the thermophysical properties of the material used in the experiments. The density of ice slurry was measured directly using the Coriolis flow meter. These values are presented in Table 6.3 for various ice volume fractions.

Table 6.2. Thermophysical properties of different phases [133].

Property	5% Monopropylene glycol	Ice particles
Freezing temperature (ºC)	-1.3	-
Density (kg/m^3)	1006.4	917
Specific Heat (J/kg ºC)	3780	2093
Thermal conductivity (W/m K)	0.57	2.25

Table 6.3. Measured density of ice slurry for various ice volume fractions.

	α_s = 0%	α_s = 5%	α_s = 10%	α_s = 15%	α_s = 20%
Density (kg/m^3)	1006.4	1001.5	996.6	991.8	987.1

The ice slurry concentration in the test section was controlled by the five valves and the mixing speed in the storage tank. The stirring process was maintained at low speed to produce a heterogeneous ice slurry concentration in the tank, a higher concentration of ice slurry could be harvested by controlling the top valve. Different volume fractions of ice slurry were obtained by mixing the flow from the top valve (high volume fraction) with that from the bottom valves (low volume fractions). The ice volume fraction was then calculated by:

$$\alpha_s = \frac{\rho_s(\rho_l - \rho_{is})}{\rho_{is}(\rho_l - \rho_s)} \tag{6.1}$$

where ρ_s, ρ_l and ρ_{is} denote the densities of ice, 5% monopropylene glycol solution and ice slurry, respectively.

The total loss coefficient of the U-bend, ζ, is expressed in terms of the pressure drop in the bend as,

$$\zeta = \frac{\Delta P}{\left(\frac{\rho_{is} u_{is}^2}{2}\right)} \tag{6.2}$$

The ice particles can have different sizes and shapes. The shape and size of particles can be affected by the agglomeration of particles and formed clusters over time. Agglomeration of particles

and the change in shape, affects the particle distribution and concentration in the cross section of a pipe. The shape of ice particles can also affect the solid-liquid interaction and inter-particle forces. In order to ensure that the change in particle size and agglomeration with time could be neglected, the particles were analyzed according to the method proposed by Koffler and Kauffeld [134]. They used the same ice slurry generation and storage facility to analyse the particle distribution via dual-view image processing. This method considered two parameters to analyse the particle distribution: the agglomeration size and the agglomeration degree. The agglomeration degree was assigned according to the number of particles in an agglomeration as single particle (level 0), 2 particles (level 1), 3-4 particles (level 2), 5-8 particles (level 3) and >8 particles (level 4). These parameters were monitored and analysed over the periods of 28, 48 and 72 hours of post-production time. It was shown that the particles tends to gain a spherical shape over time. In addition, the population of single particles (level 0) was the highest for all the tested time periods. However, the population of level 0 agglomeration increased with time and the 72-hour test period had the highest population of level 0 agglomeration. More information about this method can be found in the corresponding reference.

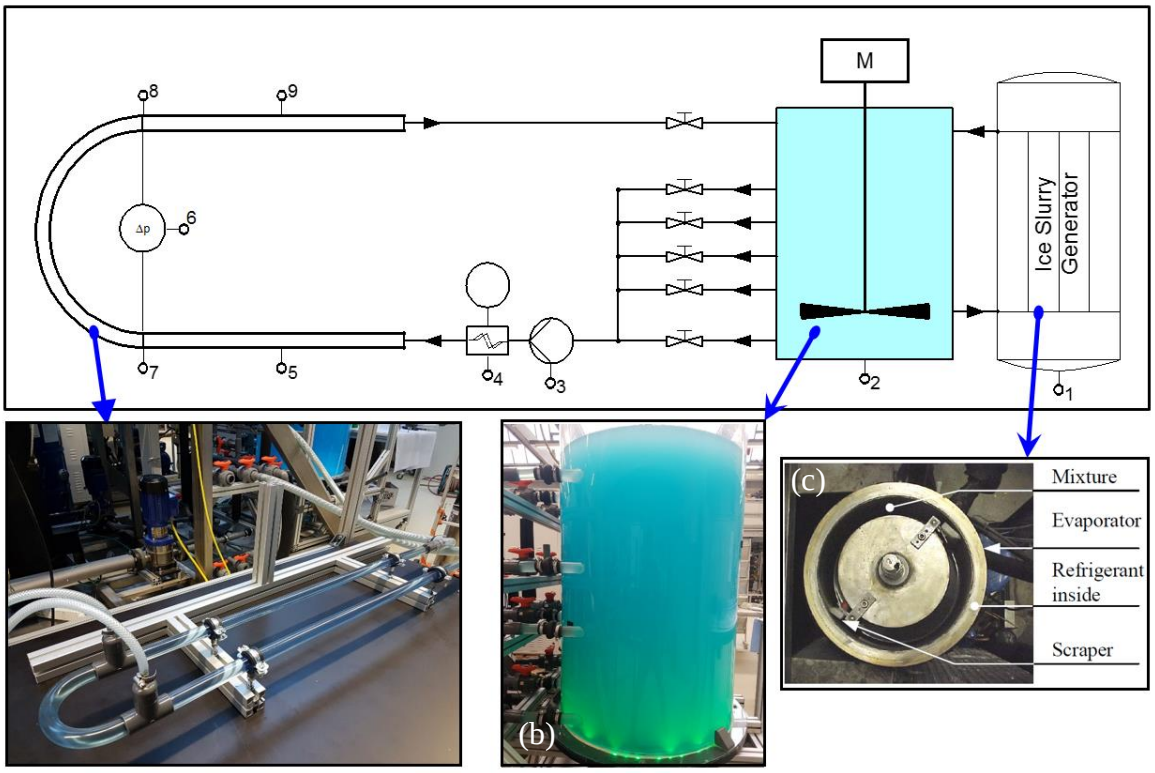

Figure 6.1. Schematic diagram of the experimental setup and photos of major components.

6.3 Results and discussion

6.3.1 Flow structure

To develop a clear comparison between the real physics of the ice slurry flow and the corresponding numerical simulation results, the particle distribution in the straight section of the pipe (10 cm just before the bend entrance) was analysed. Figure 6.2 shows the side-view photos of the flow at an ice volume fraction of 5% and various inlet velocities. On the right side, the illustrative sketches of the change in ice particle concentration are presented as well.

At a velocity of 1.42 m/s, the ice particles are uniformly distributed across the pipe diameter (Figure 6.2a). In this case, the ice slurry has a fully-homogeneous regime as a result of the high-intensity turbulence of the carrier fluid. In this flow regime, fluid-induced agitation and inter-particle collisions create symmetric flow and uniform particle distribution. When the inlet velocity is decreased to 1.1 m/s (Figure 6.2b), some degree of particle segregation occurs and a pseudo-homogeneous flow structure is observed. As the inlet velocity is reduced further (Figure 6.2c), the flow becomes heterogeneous and a low-concentrated region appears on the bottom of the pipe (below the dotted line). On top of this region (between the dashed and dotted lines), a thick compact layer moves forward. This compact layer shears a thin moving bed at the top of the pipe (above the dashed line) that advances with a relatively lower velocity. Lowering the velocity to 0.54 m/s causes the moving bed layer to become thicker (Figure 6.2d). At this velocity, there exists a region at the bottom of the pipe, where no ice particles are observed. However, random flocs of ice are found that move forward parallel to the top adjacent layer. Finally, at a velocity of 0.34 m/s, the whole region above the dashed line turn into a thick moving bed. In this case, the flocs of ice observed in the region between the dashed and dotted lines, display a swirling motion while moving forward (Figure 6.2e).

The observed phenomena are in agreement with previous findings [46] which imply the existence of a minimum allowable velocity to avoid moving (or stationary) bed regimes. Depending on the diameter of the pipe, the ice volume fraction and the mean ice particle diameter, transition of the flow regime will differ. Previously, minimum allowable velocities of 0.11 m/s to 0.32 m/s have been proposed by some researchers [67].

The main reason behind the separation of phases is the difference in the densities of ice particles and propylene glycol solution. However, higher velocities will induce higher turbulent dispersion which in turn brings about a more uniform concentration distribution [85]. At low velocities, cohesion forces are significant which cause the ice particles to coalesce and accumulate near the top region due to the difference in the densities of the phases. At higher velocities, the strong turbulent dispersion

within the flow does not allow the ice particles to coalesce. Consequently, the particles move forward separately without being agglomerated. Compared to other solid-liquid slurries where the gravity plays a remarkable role, cohesive forces dominate the flow structure of ice slurries [135, 136].

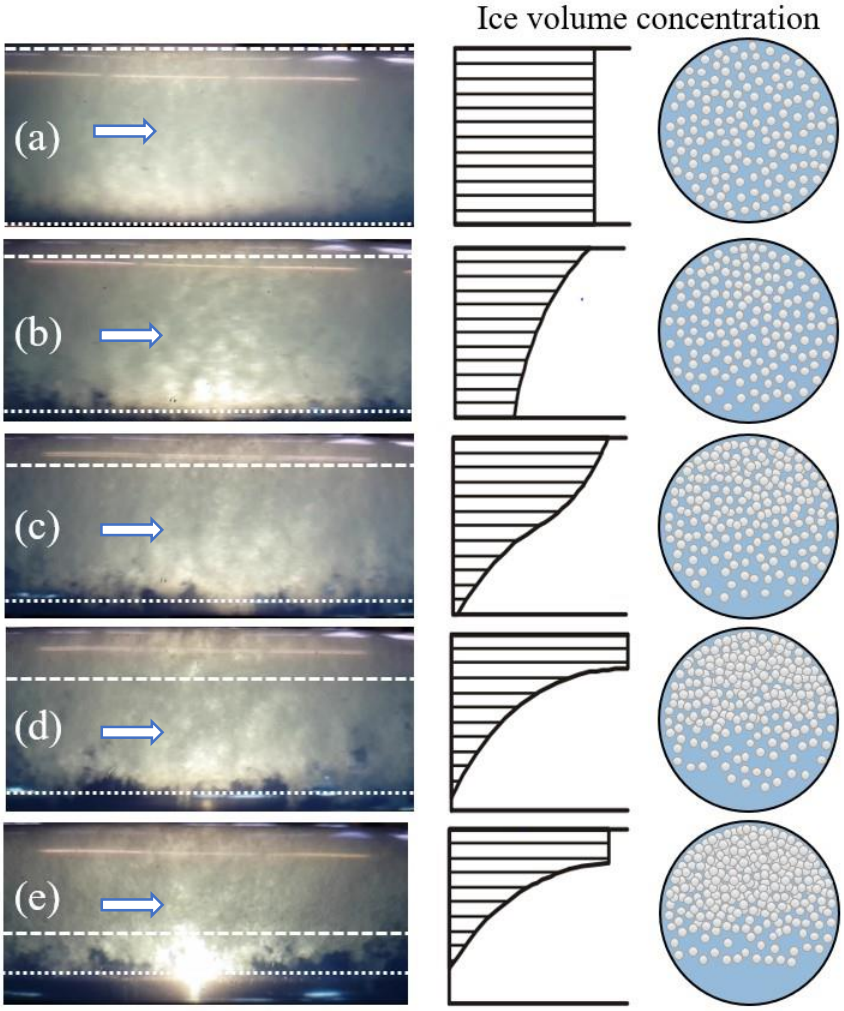

Figure 6.2. Flow visualization and illustrative sketch of the ice particle distribution in the straight section (length of 10 cm just before the bend inlet) for α_s = 5% , d = 32 m and inlet velocities of (a) 1.42 m/s, (b) 1.1 m/s, (c) 0.77 m/s, (d) 0.54 m/s and (d) 0.34 m/s.

A series of photos were also taken of the ice slurry flow through the horizontal bend at three different locations. For this purpose, a volume fraction of 15% and an inlet velocity of 0.4 m/s for the bend with a diameter of 25 mm were considered. Figure 6.3 shows these photos taken at the bend inlet, centre, and the outlet. As seen in the photos, there is a non-uniform distribution of particles when the ice slurry enters the bend section (Figure 6.3a). Once ice slurry advances through the bend, ice particles are driven towards the inner regions of the pipe. In Figure 6.3b, this is shown with the pointers indicating the direction of the observed particle movements due to the secondary flows created in the bend. Consequently, the mixture exiting the bend section has a more mixed structure

compared to the inlet location (Figure 6.3c). The bend increases the turbulence required to keep the ice particles fully dispersed. At the same inlet velocity and ice volume fraction, the bend induces a higher mixing rate compared to the straight pipe. This implies that for the same inlet conditions, the ice slurry through the bend needs a lower minimum allowable velocity to maintain a homogeneous suspension [137]. The effect of bend on the allowable minimum velocity and the transition of ice slurry flow regimes can be a subject of future investigations.

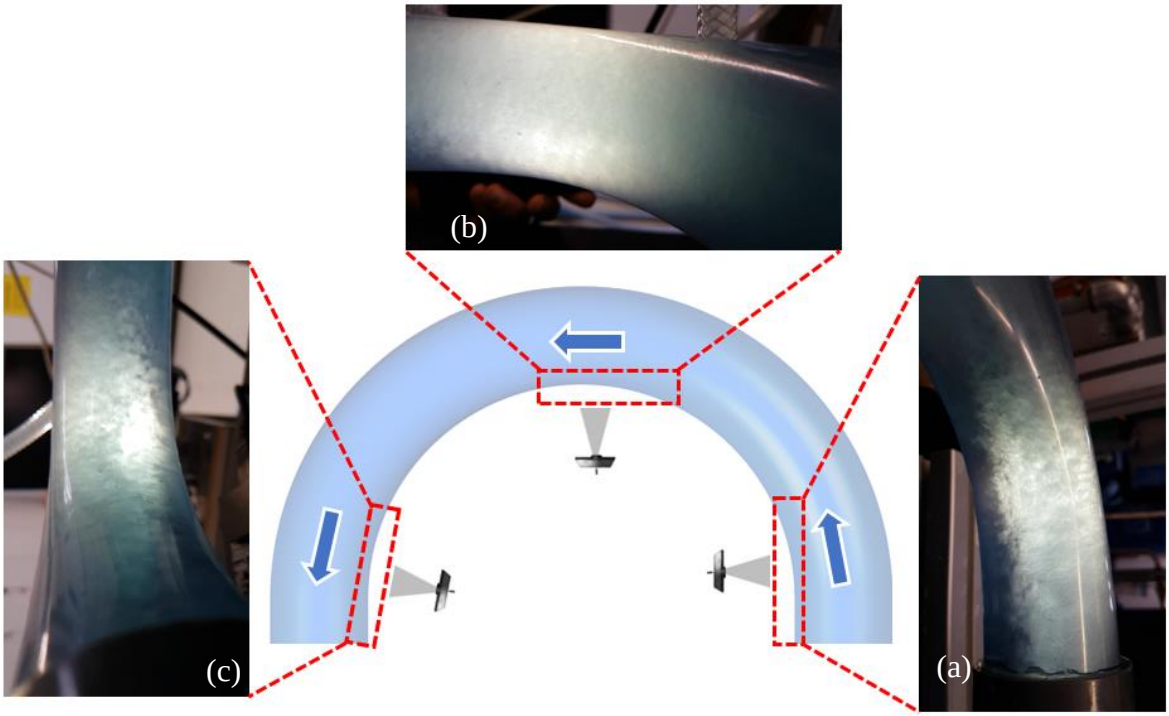

Figure 6.3. Flow visualization of ice slurry flow at different locations across the horizontal bend (d = 25 mm) at ice concentration of 15% and u_{is} = 0.4 m/s.

6.3.2 Horizontal U-bend

Figure 6.4a shows the pressure drop of ice slurry in the horizontal U-bend with the diameter of 25 mm. As can be seen, the pressure drop increases with an increase in the flow rate for all ice volume fractions. At a specific flow rate, the pressure drop increases with an increase in the ice volume fraction. Figure 6.4b presents the variation of loss coefficient with the inlet velocity for different ice volume fractions. For the ice volume fractions of 5% and 10%, the change in loss coefficient with the inlet velocity is insignificant. However, for the higher ice volume fractions (15% and 20%), a significant drop in the loss coefficient with the increase in inlet velocity id observed. Overall, the

highest loss coefficient is found for the highest ice volume fraction and the lowest velocity. A Similar trend was reported by [132] for propylene glycol ice slurry flow though a 90º bend.

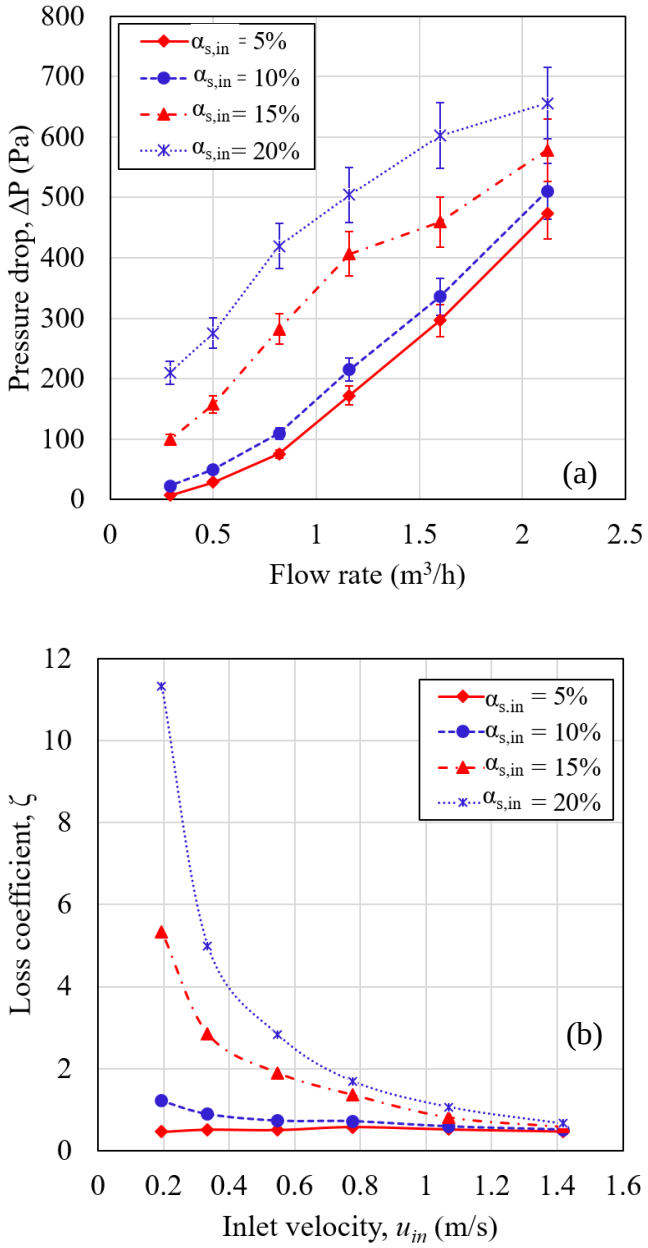

Figure 6.4. (a) Pressure drop of ice slurry flow in terms of flow rate and (b) loss coefficient in terms of inlet velocity for various ice volume fractions and pipe diameter of 25 mm for horizontal orientation.

The measured pressure drop of ice slurry though the horizontal bend with the diameter of 32 mm is shown in Figure 6.5a. Similarly, pressure drop increases with an increase in both flow rate and ice volume fraction. However, lower pressure drops are measured when pipe diameter is reduced from 25 mm to 32 mm.

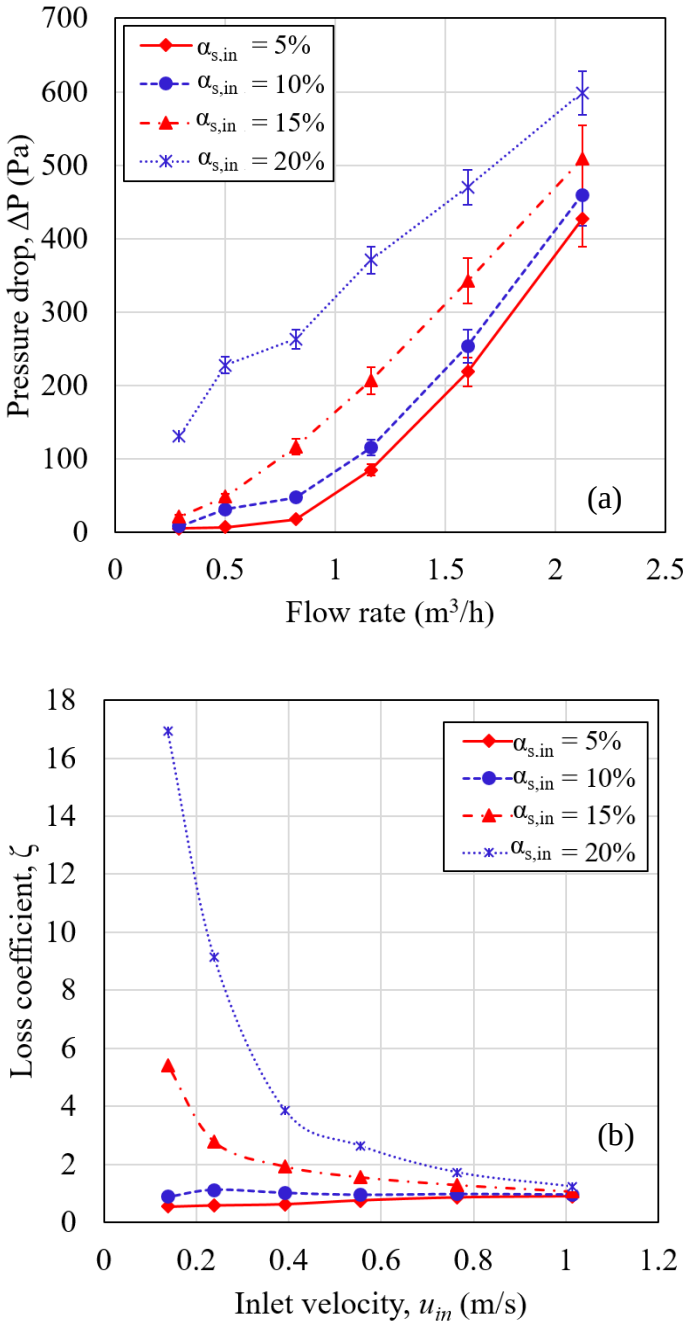

Figure 6.5. (a) Pressure drop of ice slurry flow in terms of flow rate and (b) loss coefficient in terms of inlet velocity for various ice volume fractions and pipe diameter of 32 mm for horizontal orientation.

It is noteworthy that although the pressure drop generally increases over the range of the tested flow rates, different parameters are responsible for the total pressure drop. The pressure drop of flows through bends stems from two factors: the change in direction due to geometry and fluid friction. For the case of the high-viscosity, particle suspensions such as ice slurry, the intensity of secondary flows depends on the concentration of ice particles. For higher ice volume fractions, the inter-particle

collisions are more intense and secondary flows are inhibited (lower mixing inside the bend). In this case, the major part of the pressure drop is due to the friction loss rather than the geometry loss [138].

6.3.3 Vertical U-bend

Figure 6.6 and Figure 6.7 show the pressure drop and loss coefficient of ice slurry for vertical orientation of the 25 mm and 32 mm U-bends for various flow rates, inlet velocities and ice volume fractions. The observed trends for the pressure drops of ice slurry in for the vertical orientation of the U-bend is similar to the one for the horizontal orientation. However, the loss coefficients for all the ice volume fractions decrease with the increase of inlet velocities. This is observed for both pipe diameters.

In addition to the fluid friction and the curved fluid path, the static pressure head adds to the total pressure loss. As observed from the graphs, the overall pressure loss for the vertical bend is higher than that measured for the horizontal bend. The observed difference in the trends for loss coefficients also stems from the elevation difference between the inlet and outlet of the bend. Even at low velocities for the ice volume fractions of 5% and 10%, a certain pumping power is required to overcome the pressure differences due to the change in the elevation (vertical bend).

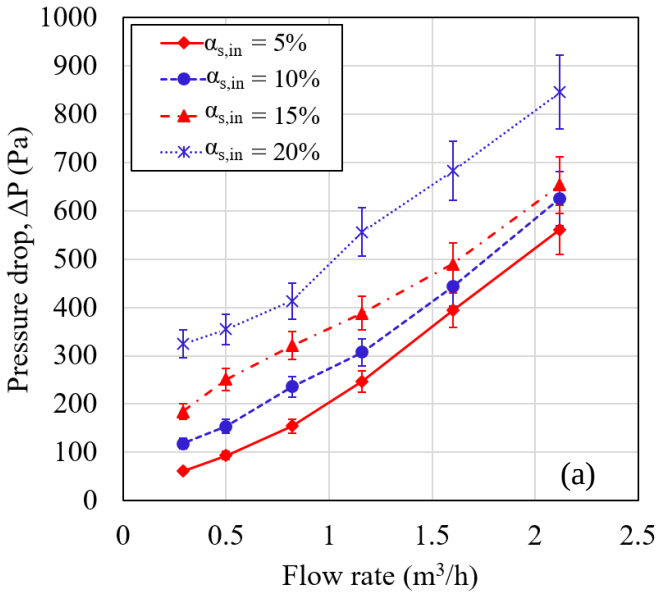

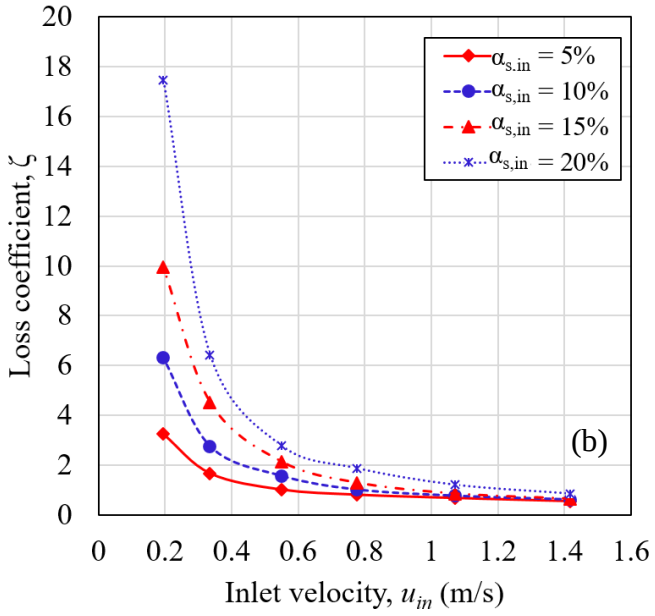

Figure 6.6. (a) Pressure drop of ice slurry flow in terms of flow rate and (b) loss coefficient in terms of inlet velocity for various ice volume fractions and pipe diameter of 25 mm for vertical orientation.

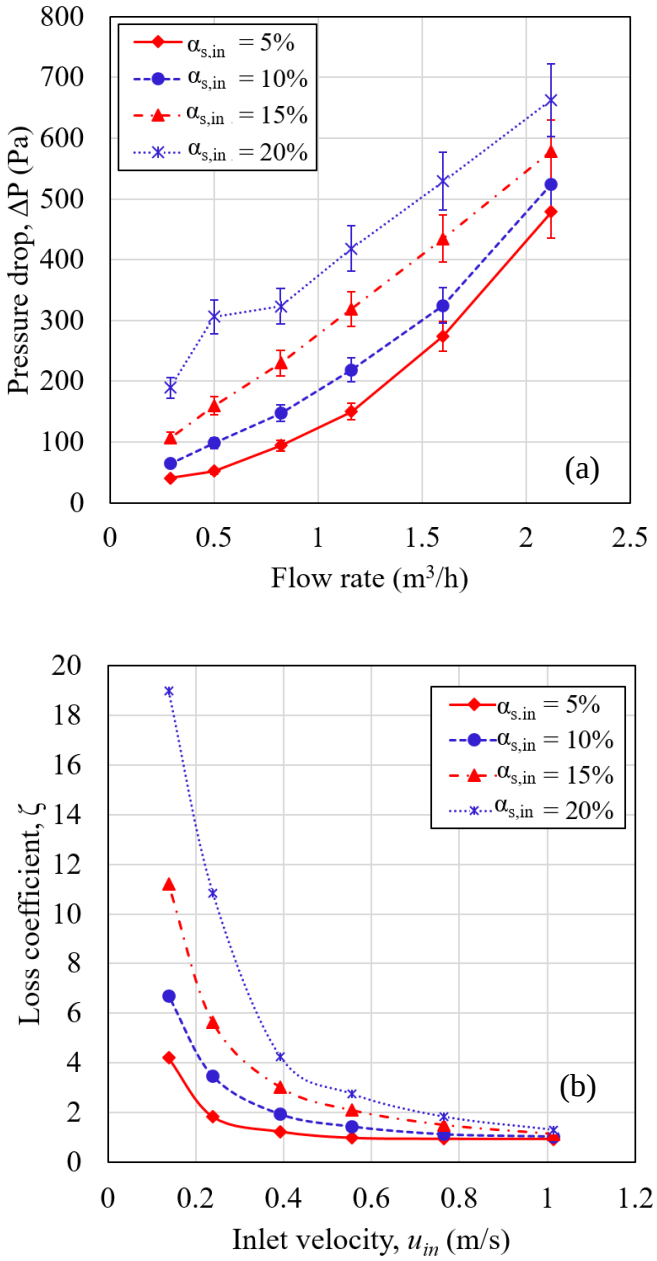

Figure 6.7. (a) Pressure drop of ice slurry flow in terms of flow rate and (b) loss coefficient in terms of inlet velocity for various ice volume fractions and pipe diameter of 32 mm for vertical orientation.

6.3.4 Rheological considerations

In order to elucidate the rheological behaviour of the modelled ice slurry, a non-Newtonian model was adapted for the ice slurry in accordance with the experimental results. The ice slurry in this study is treated as an Ostwald-de Waele power law fluid which has been successfully implemented previously for laminar and turbulent ice slurry flows [58, 66, 75]. In this model the wall shear stress is expressed as,

$$\tau_w = K_P \dot{\gamma}^{n_P} \tag{6.3}$$

where K and n represent the power law consistency index and flow index, respectively.

The flow index, $n_{P,}$ is determined as [139]:

$$n_P = \frac{d\left(ln\frac{d\Delta P}{4L}\right)}{d\left(ln\frac{8u_{is}}{d}\right)} \tag{6.4}$$

The consistency index is also obtained through the following expression,

$$\frac{d\Delta P}{4L} = K_P\left[\left(\frac{3n_P+1}{4n_P}\right)\left(\frac{8u_{is}}{d}\right)\right]^{n_P} \tag{6.5}$$

Table 6.4 presents the comparison between the calculated values of the flow index, n_P, and consistency index, K_P, with the experimental values presented by Mellari et al. [66] for the same concentration of monopropelyne glycol. As noted from the table, the experimental values are in a good agreement. The numerical values also confirmed the non-Newtonian characteristics of ice slurry flow, showing that increasing the ice volume fraction changes the slurry's behaviour from shear thickening to ($n_P > 1$) to shear thinning ($n_P < 1$) at this specific additive concentration.

Table 6.4. The rheological parameters of the ice slurry: Flow index, n_P from the experiments and the study of Mellari et al. [66], and the calculated consistency index, K_P.

	n_P (Exp.)	n_P [66]	K_P (Exp.)
α_s = 5%	1.9	1.7	1.20×10^{-5}
α_s = 10%	1.5	1.4	0.0009
α_s = 15%	0.85	0.90	0.10
α_s = 20%	0.59	0.62	0.81

6.4 Conclusions

In this chapter, flow characteristics of 5% monopropylene glycol ice slurry flowing through horizontal and vertical U-bends with two diameters were experimentally studied. The ice slurry flow was also visualized in the straight and curved sections of the pipe. The change of particular flow regime from homogenous to heterogeneous and moving-bed layer was observed and compared with numerical results. It was also seen that, for the bend section, the curved geometry induced more mixing of ice particles within the liquid phase. The pressure drop and loss coefficient were measured for two pipe diameters positioned at horizontal and vertical orientations. For all cases, pressure drop increased with an increase in flow rate and ice volume fraction. However, the larger pipe diameter showed a lower pressure drops. The loss coefficients decreased with an increase in the inlet velocity. For the horizontal orientation, the change in the loss coefficient was insignificant for lower ice volume fractions (5% and 10%). Rheology analysis of the flow confirmed the Power law behaviour of the non-Newtonian ice slurry. The results shed more light on the measures that needs to be taken when considering ice slurry transport for industrial applications such as mine cooling. A geometry such as a bend or helical coil delays reaching the moving-bed layer flow regime in coolant pipe lines. The more uniform (homogenous) flow of ice slurry ensures an enhanced cooling performance by bulk air coolers (such as in-stope heat exchangers) used in underground environments.

Chapter 7 Conclusions and Recommendations

7.1 Conclusions

In this thesis, thermal and hydrodynamic behaviour of ice slurry flow in curved geometries including helical coil heat exchangers and bends were investigated. The effects of various important parameters on the pressure drop, heat transfer and ice concentration distribution was investigated through Computational Fluid Dynamics (CFD) as well as experiments. The numerical part was conducted using ANSYS FLUENT for three-dimensional geometries of a helical coil heat exchanger and horizontal bends. A series of experiments were also conducted to validate the multiphase modelling results and also to visualize the flow and investigate more features of the ice slurry flows.

The literature review was conducted in two main sections. First, different mine cooling methods, challenges and new developments were thoroughly looked into. Many studies conclude that if the sources of heat in underground environment is measured in an accurate way, a suitable cooling strategy can be proposed which is an inevitable fact with the increase in depth of mines in future. Ice cooling plants using ice slurry or ice-on-coil systems are considered as potential strategies towards this goal. However, economics of ice slurry cooling systems are influenced by factors such as power tariffs, climate, geothermal gradient and heat from artificial sources. This implies that a techno-economic analysis of ice plants before implementation on any mine site is beneficial. Previous case studies also acknowledge that large financial benefits can be acquired if refrigeration plant of a mine is optimized.

The second section of the literature review focused on the state-of-the-art investigations of fluid dynamics and heat transfer characteristics of ice slurries. Looking into experimental and numerical studies of ice slurries show that the present results consist of significant uncertainties and deviations. The first indicator of this is that there is no unanimous agreement on the suitable rheology model to describe the hydrodynamics of ice slurries. The fact that the ice slurry production and storage method affects the ice particle size and shape, more experimental and numerical data is required to acquire precise flow patterns as well as hydraulic and thermal characteristics of ice slurries. There is an exhaustive collection of experimental research on the behaviour of ice slurry as coolant in heat exchangers. Nonetheless, the numerical work in this area needs to be developed further to elucidate the behaviour of ice slurry in applications. The disturbance of ice slurry flows by curved geometries is an important phenomenon that enhances the interaction and collision of solid particles and induces the saltation of particles from the moving-bed layer to the suspension layer. No previous study has investigated the relationship between ice particle diameter, flow disturbance and pressure drop in a curved geometry. Clarifying the effect of particle diameter on the pressure drop and flow structure is important, especially when selecting the ice slurry generation technique. In addition, The

experimental investigation of ice slurry flow characteristics can be a challenging task due to the difficulties imposed by its complex structure. No previous research has experimentally measured the pressure drop and loss coefficients of ice slurry flows through U-bends.

In the first stage of this thesis, thermo-hydrodynamic as well as the entropy generation characteristics of laminar flow of melting ice slurry through a helical coil subjected to uniform wall heat flux was numerically studied. The effect of parameters such as the initial ice mass fraction and *Dean* number (*De*) on the fluid friction, the heat transfer rate and entropy generation were investigated. Ice slurry was treated as a Bingham plastic with rheology parameters defined as functions of the ice mass fraction. The melting of the solid phase was simulated using enthalpy-porosity method. According to the numerical results, the existence of ice imposes a rise in the pressure drop. On the other hand, the introduction of ice slurry induces improvements in the heat transfer coefficient via melting and convection processes. In addition to the ice melting, the secondary flows produced by the geometry further intensify the thermal and hydraulic effects. The major proportion of the induced irreversibility is attributable to the heat transfer. However, the entropy generation analysis showed an optimal trade-off between the frictional and thermal irreversibilities where the entropy generation was minimum. A performance optimization can provide the best trade-off between the heat transfer and pressure drop of ice slurries in heat exchangers.

The flow behaviour of ice slurry is generally very complex due to the existence of ice particles. Thus, the flow patterns and hydrodynamics of ice slurries must be well understood prior to the design of transport lines. Therefore, in the next stage, the flow characteristics of monopropylene glycol ice slurry through a horizontal U-bend was numerically examined. An Eulerian two-phase model was used to investigate the effect of inlet flow velocity, particle diameter and ice volume fraction on the particle distribution and pressure drop throughout a horizontal U-bend. The numerical results were validated against numerical results published in the literature and present experiments. Due to the inter-particle interactions and different turbulent dispersion intensities, the secondary flow generated within the U-bend as a result of the centrifugal force was affected by the ice volume fraction and the particle diameter. A higher ice volume fraction and a smaller particle diameter showed larger values of wall shear stress. Although the pressure drop increased with an increase in the ice volume fraction and the flow velocity, the effect of particle diameter was different for low values of flow velocity when compared with those at higher velocities. At low velocities, fine particles induced a lower pressure drop compared to coarse particles. Curved geometry of bends affect the flow structure of ice slurry flows. This in turn influences the transition of flow regimes from homogenous to heterogeneous and moving bed states.

Finally, flow characteristics of 5% monopropylene glycol ice slurry flowing through horizontal and vertical U-bends with two diameters were experimentally studied. The ice slurry flow was also visualized in the straight and curved sections of the pipe. The change of particular flow regime from homogenous to heterogeneous and moving-bed layer was observed. The pressure drop and loss coefficient were measured for two pipe diameters (25 and 32 mm) positioned at horizontal and vertical orientations. For all cases, pressure drop increased with an increase in flow rate and ice volume fraction. However, the larger pipe diameter showed a lower pressure drops. The loss coefficients decreased with an increase in the inlet velocity. For the horizontal orientation, the change in the loss coefficient was insignificant for lower ice volume fractions (5% and 10%). Rheology analysis of the flow confirmed the Power law behaviour of the non-Newtonian ice slurry.

This study provides an inclusive understanding of the effects of various factors on the performance of ice slurry flows in coils and bends. To find the optimal operating conditions and mixture characteristics, it is of prime importance to understand then identify the conditions offering the best compromise between high heat transfer and low pressure drop. The obtained information contributes to the better design of ice slurry cooling systems.

7.2 Recommendations for future work

Based on the potential research ideas identified during the completion of this study, a number of recommendations can be listed for future investigations, as follows;

- Non-isothermal multiphase modelling of ice slurry in helical coil heat exchangers can shed light on the effect of heat transfer on the pressure drop and flow pattern of ice slurry. Effect of phase change of ice particles on the intensity of secondary flows, wall shear stress and thermodynamic irreversibility can provide useful information on the cooling efficiency of the ice slurry.

- Effect of chaotic advection on the pressure drop, heat transfer and flow pattern of ice slurries is recommended for future numerical and experimental investigations. Efficacy of the chaotic geometry of a heat exchanger in improving the heat transfer while maintaining the pressure loss at an efficient level, is an interesting design topic that can be done for ice slurry flows.

- Shape of ice particles affects the concentration distribution of ice slurries. As the ice slurry production method influences the shape of particles, future numerical studies can focus on the effect of the change in the shape of particles on the pressure drop and flow regimes of ice slurry flows in pipes.

- Knowing the thermo-hydrodynamic performance of ice slurry as a coolant, a techno-economic analysis of ice slurry-based bulk air cooler for an underground mining environment is suggested as a future extension of the current study. This can be useful in knowing the suitability of ice slurry as a potential mine cooling alternative for ultra-deep mines.

References

[1] Brake, D. *Design of the world's largest bulk air cooler for the Enterprise Mine in Northern Australia*. in *Mine Ventilation: Proceedings of the North American/Ninth US Mine Ventilation Symposium*. 2002.

[2] Brake, D. *The application of refrigeration in mechanised mines*. in Proceedings of the Australasian Institute of Mining and Metallurgy. 2001. Parkville, Victoria.

[3] Marx, W., E. von Glehn, and R. Wilson. *Design of energy efficient mine ventilation and cooling systems*. in 11th US/North American Mine Ventilation Symposium 2006: Proceedings of the 11th US/North American Mine Ventilation Symposium, 5-7 June 2006, Pennsylvania, *USA*. 2006. CRC Press.

[4] McPherson, M.J., *Subsurface ventilation and environmental engineering*. 2012, New Delhi: Springer Science & Business Media.

[5] Wagner, H., *The management of heat flow in deep mines.* Mining Report, 2013. **149**(2): p. 88-100.

[6] Wagner, H., *The development of a novel hydraulic powering system for deep-level mines.* Proc. Leobener Bergmannstag, 1987.

[7] Hartman, H.L., J.M. Mutmansky, R.V. Ramani, and Y. Wang, *Mine ventilation and air conditioning*. 2012. John Wiley & Sons.

[8] Whillier, A. *Predicting cooling requirements for caving and sub-level stoping in hot rock*. in International Conference on Cavin 9 and Sub-Level Stoping. 1981.

[9] Yaglou, C., *Temperature, humidity, and air movement in industries: the effective temperature index.* Journal of Industrial Hygiene, 1927. **9**: p. 297-309.

[10] Belle, B. and M. Biffi. *Cooling pathways for deep Australian longwall coal mines of the future*. International Journal of Mining Science and Technology, 2018. **28**(6): p. 865-875.

[11] Brake, D. and R. Fulker, *The ventilation and refrigeration design for Australia's deepest and hottest underground operation: the Enterprise mine.* Proc MassMin, 2000: p. 611-621.

[12] Gao, Y. and F. Liu. *The study of thermal pollution disposal on the deep coal mine working face*. in 2009 Asia-Pacific Conference on Computational Intelligence and Industrial Applications (PACIIA), IEEE.

[13] Nowakowski, G.A. and R.L. Busby, *Advances in natural gas cooling.* ASHRAE journal, 2001. **43**(4): p. 47.

[14] Van Baalen, G. and M.J. Howes. *Evaluation of future refrigeration for the Enterprise Mine, Mount Isa*. in *9th International Mine Ventilation Congress*. 2009.

[15] Brake, D. *Key engineering considerations in the specification and selection of mine refrigeration plants. in Proceedings of the Australasian Institute of Mining and Metallurgy*. 2001, Parkville, Victoria.

[16] Hooman, M., R. Webber-Youngman, J. du Plessis, and W. Marx, *A decision analysis guideline for underground bulk air heat exchanger design specifications.* Journal of the Southern African Institute of Mining and Metallurgy, 2015. **115**(2): p. 125-129.

[17] O'Connor, T., M. Kizil, and B. Belle. *Required cooling system capacities for extended longwall panels at a Bowen Basin mine*. in The Australian Mine Ventilation Conference. 2013. The Australasian Institute of Mining and Metallurgy.

[18] Ramsden, R., A. Branch, and R. Wilson, *Factors influencing the choice of cooling and refrigeration systems for mines.* Journal of the Mine Ventilation Society of South Africa, 2007. **60**(3): p. 92-98.

[19] van den Berg, L., R. Funnell, and S. Bluhm. *Mine cooling for hot underground mines*. 2013. Australasian Institute of Mining and Metallurgy.

[20] Bluhm, S., R. Moreby, F. von Glehn, and C. Pascoe, *Life-of-mine ventilation and refrigeration planning for Resolution Copper Mine.* Journal of the Southern African Institute of Mining and Metallurgy, 2014. **114**(6): p. 497-503.

[21] Ranque, G., *Experiments on expansion in a vortex with simultaneous exhaust of hot air and cold air.* Journal de Physique et Le Radium, 1933. **4**(7): p. 112-114.

[22] Ameen, A., *Refrigeration and air conditioning*. 2006, New Delhi: PHI Learning Pvt. Ltd.

[23] Xue, Y., M. Arjomandi, and R. Kelso, *The working principle of a vortex tube.* International Journal of Refrigeration, 2013. **36**(6): p. 1730-1740.

[24] Ahlborn, B.K. and J.M. Gordon, *The vortex tube as a classic thermodynamic refrigeration cycle.* Journal of Applied Physics, 2000. **88**(6): p. 3645-3653.

[25] Jinggang, W., G. Xiaoxia, and J. Shanlin. *The application of vortex tube in deep mine cooling*. in International Conference on Energy and Environment Technology. 2009. IEEE.

[26] Butterworth, M. and T. Sheer, *High-pressure water as the driving fluid in an ejector refrigeration system.* Applied thermal engineering, 2007. **27**(11): p. 2145-2152.

[27] Raynerd, P., *Ejectors, selection and use of vacuum equipment.* Institute of Chemical Engineers, North Western Branch Papers, 1987(1): p. 3.1-3.16.

[28] Butterworth, M. and T. Sheer. *Ejector Refrigeration Systems for Chilled Water Using High-Pressure Water as the Motive Fluid*. in 8th International Mine Ventilation Congress. 2005. Brisbane, QLD, Australia.

[29] Gebler, W.F., *A review of mine cooling practices through the ages.* Journal of the Mine Ventilation Society of South Africa, 1980. **33**(11): p. 209-222.

[30] Kidd, J., *Slurry ice production in gold mining.* The South African Mehanical Engineer, 1995. **45**: p. 11-14.

[31] Ophir, A. and A. Koren. *Vacuum freezing vapor compression process (VFVC) for mine cooling*. in Proceedings of the 20th International Congress of Refrigeration, IIF/IIR. 1999.

[32] Mackay, L., S. Bluhm, and J. Van Rensburg. *Refrigeration and cooling concepts for ultra-deep platinum mining*. in The 4th International Platinum Conference, Platinum in transition 'Boom or Bust'. The Southern African Institute of Mining and Metallurgy, 2010.

[33] Webbeer-Youngman, R.C.W., *An integrated approach towards the optimization of ventilation, air cooling and pumping requirements for hot mines*. 2005, North-West University.

[34] Pelzer, R., E. Mathews, and A. Schutte. *Energy efficiency by new control and optimisation of fridge plant systems.* in International Conference on the Industrial and Commercial use of Energy (ICUE), Cape Town. 2010.

[35] Vosloo, J., L. Liebenberg, and D. Velleman, *Case study: Energy savings for a deep-mine water reticulation system.* Applied Energy, 2012. **92**: p. 328-335.

[36] du Plessis, G.E., L. Liebenberg, and E.H. Mathews, *Case study: The effects of a variable flow energy saving strategy on a deep-mine cooling system.* Applied energy, 2013. **102**: p. 700-709.

[37] Du Plessis, G.E., L. Liebenberg, and E.H. Mathews, *The use of variable speed drives for cost-effective energy savings in South African mine cooling systems.* Applied Energy, 2013. **111**: p. 16-27.

[38] Mare, P., J. Marais, and J. van Rensburg. *Improved implementation strategies to sustain energy saving measures on mine cooling systems*. in International Conference on the Industrial and Commercial use of Energy (ICUE). 2015. IEEE.

[39] Ping, Q., Q. Jingshun, T. Jing, J. Zhengjun, and H. Qiaoyun. *The cooling principle of high temperature exchange machinery system with plenty of cold source*. in 2nd International Conference on Digital Manufacturing and Automation *(ICDMA).* 2011. IEEE.

[40] Qi, P., H. Manchao, M. Li, and C. Chen, *Working principle and application of HEMS with lack of a cold source.* Mining Science and Technology (China), 2011. **21**(3): p. 433-438.

[41] Niu, Y., *Research on Thermal Energy Recycling Utilization in High Temperature Mines.* Procedia Engineering, 2015. **121**: p. 389-395.

[42] Manchao, H., C. Xiuling, X. Qiao, Y. Jiahua, Q. Ping, Y. Qing, and C. Xueqian, *Principles and technology for stepwise utilization of resources for mitigating deep mine heat hazards.* Mining Science and Technology (China), 2010. **20**(1): p. 20-27.

[43] Schutte, A., R. Pelzer, and E. Mathews. *Improving cooling system efficiency with pre-cooling*. in International Conference on the Industrial and Commercial use of Energy (ICUE), 2012. IEEE.

[44] Egolf, P.W. and M. Kauffeld, *From physical properties of ice slurries to industrial ice slurry applications.* International Journal of Refrigeration, 2005. **28**(1): p. 4-12.

[45] Kauffeld, M., M.J. Wang, V. Goldstein, and K.E. Kasza, *Ice slurry applications.* International Journal of Refrigeration, 2010. **33**(8): p. 1491-1505.

[46] Grozdek, M., R. Khodabandeh, and P. Lundqvist, *Experimental investigation of ice slurry flow pressure drop in horizontal tubes.* Experimental Thermal and Fluid Science, 2009. **33**(2): p. 357-370.

[47] Ayel, V., O. Lottin, and H. Peerhossaini, *Rheology, flow behaviour and heat transfer of ice slurries: a review of the state of the art.* International Journal of Refrigeration, 2003. **26**(1): p. 95-107.

[48] Kitanovski, A., D. Vuarnoz, D. Ata-Caesar, P.W. Egolf, T.M. Hansen, and C. Doetsch, *The fluid dynamics of ice slurry.* International Journal of Refrigeration, 2005. **28**(1): p. 37-50.

[49] Bellas, I. and S. Tassou, *Present and future applications of ice slurries.* International Journal of Refrigeration, 2005. **28**(1): p. 115-121.

[50] Egolf, P.W., A. Kitanovski, D. Ata-Caesar, E. Stamatiou, M. Kawaji, J.-P. Bedecarrats, and F. Strub, *Thermodynamics and heat transfer of ice slurries.* International Journal of Refrigeration, 2005. **28**(1): p. 51-59.

[51] Davies, T., *Slurry ice as a heat transfer fluid with a large number of application domains.* International Journal of Refrigeration, 2005. **28**(1): p. 108-114.

[52] Melinder, Å., *Thermophysical properties of aqueous solutions used as secondary working fluids*, Phd Thesis. Department of Energy Technology, Royal Institute of Technology, KTH. 2007. Sweden.

[53] Melinder, Å. and E. Granryd, *Using property values of aqueous solutions and ice to estimate ice concentrations and enthalpies of ice slurries.* International journal of refrigeration, 2005. **28**(1): p. 13-19.

[54] Monteiro, A.C. and P.K. Bansal, *Pressure drop characteristics and rheological modeling of ice slurry flow in pipes.* International Journal of Refrigeration, 2010. **33**(8): p. 1523-1532.

[55] Niezgoda-Żelasko, B. and J. Żelasko, *Generalized non-Newtonian flow of ice-slurry.* Chemical Engineering and Processing: Process Intensification, 2007. **46**(10): p. 895-904.

[56] Stokes, J.R., J.H. Telford, and A.-M. Williamson, *The flowability of ice suspensions.* Journal of Rheology, 2005. **49**(1): p. 139-148.

[57] Mika, L., *Rheological behaviour of low fraction ice slurry in pipes and pressure loss in pipe sudden contractions and expansions.* International Journal of Refrigeration, 2012. **35**(6): p. 1697-1708.

[58] Mellari, S., *Experimental investigations of ice slurry flows in horizontal pipe based on monopropylene glycol.* International Journal of Refrigeration, 2016. **65**: p. 27-41.

[59] Trabelsi, S., M. Hafid, S. Poncet, M. Poirier, and M. Lacroix, *Rheology of ethylene- and propylene-glycol ice slurries: Experiments and ANN model.* International Journal of Refrigeration, 2017. **82**: p. 447-460.

[60] Vuarnoz, D., O. Sari, P. Egolf, and H. Liardon. *Ultrasonic velocity profiler UVP-XW for ice-slurry flow characterisation*. in 3rd International symposium on Ultrasonic Doppler method for fluid mechanics and fluid engineering, Lausanne, Switzerland. 2002.

[61] Niezgoda-Żelasko, B. and W. Zalewski, *Momentum transfer of ice slurry flows in tubes, modeling.* International Journal of Refrigeration, 2006. **29**(3): p. 429-436.

[62] Niezgoda-Żelasko, B. and J. Żelasko, *Melting of ice slurry under forced convection conditions in tubes.* Experimental Thermal and Fluid Science, 2008. **32**(8): p. 1597-1608.

[63] Niezgoda-Żelasko, B. and J. Żelasko. *Flow resistance of ice slurry in bends and elbow pipes*. in *Journal of Physics: Conference Series*. 2014. IOP Publishing.

[64] Niezgoda-Żelasko, B. and J. Żelasko, *Heat transfer of ice slurry flowing in rectangular and slit channels.* Czasopismo Techniczne, 2015.

[65] Wang, J., S. Wang, T. Zhang, and F. Battaglia, *Mathematical and experimental investigation on pressure drop of heterogeneous ice slurry flow in horizontal pipes.* International Journal of Heat and Mass Transfer, 2017. **108**: p. 2381-2392.

[66] Mellari, S., M. Boumaza, and P. Egolf, *Physical modeling, numerical simulations and experimental investigations of Non-Newtonian ice slurry flows.* international journal of refrigeration, 2012. **35**(5): p. 1284-1291.

[67] Mika, Ł., *Pressure loss coefficients of ice slurry in horizontally installed flow dividers.* Experimental Thermal and Fluid Science, 2013. **45**: p. 249-258.

[68] Illán, F. and A. Viedma, *Experimental study on pressure drop and heat transfer in pipelines for brine based ice slurry Part II: Dimensional analysis and rheological model.* International Journal of Refrigeration, 2009. **32**(5): p. 1024-1031.

[69] Martinez, L.C. and S.L. Braga. *Experimental determination of transport coefficients for ice slurry in plate heat exchanger*. in 18th International Congress of Mechanical Engineering. 2005. Ouro Preto, Brazil.

[70] Lee, D.W. and A. Sharma, *Melting of ice slurry in a tube-in-tube heat exchanger.* International Journal of Energy Research, 2006. **30**(12): p. 1013-1021.

[71] Grozdek, M., R. Khodabandeh, P. Lundqvist, B. Palm, and Å. Melinder, *Experimental investigation of ice slurry heat transfer in horizontal tube.* International Journal of Refrigeration, 2009. **32**(6): p. 1310-1322.

[72] Illán, F. and A. Viedma, *Prediction of ice slurry performance in a corrugated tube heat exchanger.* International Journal of Refrigeration, 2009. **32**(6): p. 1302-1309.

[73] Shire, G., G.L. Quarini, and T. Evans, *Pressure drop of flowing ice slurries in industrial heat exchangers.* Applied Thermal Engineering, 2009. **29**(8): p. 1500-1506.

[74] Kousksou, T., A. Jamil, T. El Rhafiki, and Y. Zeraouli, *Prediction of the heat transfer coefficient for ice slurry flows in a horizontal pipe.* Energy Conversion and Management, 2010. **51**(6): p. 1311-1318.

[75] Kumano, H., T. Hirata, M. Shirakawa, R. Shouji, and Y. Hagiwara, *Flow characteristics of ice slurry in narrow tubes.* International Journal of Refrigeration, 2010. **33**(8): p. 1513-1522.

[76] Kumano, H., T. Hirata, R. Shouji, and M. Shirakawa, *Experimental study on heat transfer characteristics of ice slurry.* International Journal of Refrigeration, 2010. **33**(8): p. 1540-1549.

[77] Renaud-Boivin, S., M. Poirier, and N. Galanis, *Experimental study of hydraulic and thermal behavior of an ice slurry in a shell and tube heat exchanger.* Experimental Thermal and Fluid Science, 2012. **37**: p. 130-141.

[78] Fernández-Seara, J. and R. Diz, *Thermo-hydraulic behavior of ice slurry in an offset strip-fin plate heat exchanger.* International Journal of Refrigeration, 2014. **41**(0): p. 171-180.

[79] Singh, R. and S.S. Kachhwaha, *Heat transfer and pressure drop analysis of chilled water and ice slurry in a plate heat exchanger.* Journal of Thermal Science and Engineering Applications, 2015. **8**(1): p. 011020-011029.

[80] Niezgoda-Żelasko, B., *Heat transfer of ice slurry flows in tubes.* International journal of refrigeration, 2006. **29**(3): p. 437-450.

[81] Onokoko, L., M. Poirier, N. Galanis, and S. Poncet, *Experimental and numerical investigation of isothermal ice slurry flow.* International Journal of Thermal Sciences, 2018. **126**: p. 82-95.

[82] Bordet, A., S. Poncet, M. Poirier, and N. Galanis, *Advanced numerical modeling of turbulent ice slurry flows in a straight pipe.* International Journal of Thermal Sciences, 2018. **127**: p. 294-311.

[83] Wang, J., S. Wang, T. Zhang, and Y. Liang, *Numerical investigation of ice slurry isothermal flow in various pipes.* International Journal of Refrigeration, 2013. **36**(1): p. 70-80.

[84] Tian, Q., G. He, H. Wang, and D. Cai, *Simulation on transportation safety of ice slurry in ice cooling system of buildings.* Energy and Buildings, 2014. **72**: p. 262-270.

[85] Zhang, P. and X. Shi, *Thermo-fluidic characteristics of ice slurry in horizontal circular pipes.* International Journal of Heat and Mass Transfer, 2015. **89**: p. 950-963.

[86] Long, Y., S. Wang, J. Wang, and T. Zhang, *Numerical and analytical investigations of heat transfer for a finned tube heat exchanger with ice slurry as cooling medium.* Science and Technology for the Built Environment, 2017. **23**(3): p. 478-489.

[87] Wang, J., S. Wang, T. Zhang, and F. Battaglia, *Numerical and analytical investigation of ice slurry isothermal flow through horizontal bends.* International Journal of Refrigeration, 2018. **92**: p. 37-54.

[88] Rawat, K. and A. Pratihar. *Numerical Investigation of Ice Slurry Flow in a Horizontal Pipe*. in *IOP Conference Series: Materials Science and Engineering*. 2018. IOP Publishing.

[89] Liu, S., M. Song, L. Hao, and P. Wang, *Numerical simulation on flow of ice slurry in horizontal straight tube.* Frontiers in Energy, 2017: p. 1-7.

[90] Bergman, T.L., F.P. Incropera, D.P. DeWitt, and A.S. Lavine, *Fundamentals of heat and mass transfer*. 2011, Hoboken, New Jersey: John Wiley & Sons.

[91] Languri, E.M. and H.B. Rokni, *Flow of microencapsulated phase change material slurry through planar spiral coil.* Heat Transfer Engineering, 2018. **39**(11): p. 977-984.

[92] Kurnia, J.C., A.P. Sasmito, S.V. Jangam, and A.S. Mujumdar, *Heat transfer in coiled square tubes for laminar flow of slurry of microencapsulated phase change material.* Heat Transfer Engineering, 2013. **34**(11-12): p. 994-1007.

[93] Zhao, Z., R. Hao, and Y. Shi, *Parametric analysis of enhanced heat transfer for laminar flow of microencapsulated phase change suspension in a circular tube with constant wall temperature.* Heat Transfer Engineering, 2008. **29**(1): p. 97-106.

[94] Bejan, A., *A study of entropy generation in fundamental convective heat transfer.* Journal of heat transfer, 1979. **101**(4): p. 718-725.

[95] Strub, F., J. Castaing-Lasvignottes, J.-P. Bédécarrats, and C. Peuvrel, *Application of the second law analysis to a heat exchanger working with ethanol/water ice slurry.* International Journal of Thermodynamics, 2004. **7**(4): p. 183-188.

[96] Bouzid, N., S. Saouli, and S. Aïboud-Saouli, *Entropy generation in ice slurry pipe flow.* International Journal of Refrigeration, 2008. **31**(8): p. 1453-1457.

[97] Voller, V.R. and C. Prakash, *A fixed grid numerical modelling methodology for convection-diffusion mushy region phase-change problems.* International Journal of Heat and Mass Transfer, 1987. **30**(8): p. 1709-1719.

[98] *ANSYS FLUENT 15.0, Theory Guide*. 2014: Canonsburg, Pennsylvania.

[99] Melinder, Å., *Thermophysical properties of aqueous solutions used as secondary working fluids*. 2007, KTH Royal Institute of Technology: Stockholm, Sweden.

[100] Raznjevic, K., *Handbook of thermodynamic tables and charts*. 1976, Washington DC: Hemisphere Publication Corporation.

[101] Charunyakorn, P., S. Sengupta, and S. Roy, *Forced convection heat transfer in microencapsulated phase change material slurries: flow in circular ducts.* International journal of heat and mass transfer, 1991. **34**(3): p. 819-833.

[102] Skelland, A.H.P., *Non-Newtonian flow and heat transfer*. 1967: Wiley.

[103] Kozicki, W., C. Chou, and C. Tiu, *Non-Newtonian flow in ducts of arbitrary cross-sectional shape.* Chemical Engineering Science, 1966. **21**(8): p. 665-679.

[104] Zhou, Y. and S.N. Shah, *New Friction Factor Correlations of Non-Newtonian Fluid Flow in Coiled Tubing.* SPE Drilling & Completion, 2006. **21**(01): p. 68-76.

[105] Patankar, S.V., V. Pratap, and D. Spalding, *Prediction of laminar flow and heat transfer in helically coiled pipes.* Journal of Fluid Mechanics, 1974. **62**(3): p. 539-551.

[106] Ko, T. and K. Ting, *Entropy generation and thermodynamic optimization of fully developed laminar convection in a helical coil.* International Communications in Heat and Mass Transfer, 2005. **32**(1): p. 214-223.

[107] Bejan, A., *Entropy generation through heat and fluid flow*. 1982, New York: John Wiley & Sons.

[108] Paoletti, S., F. Rispoli, and E. Sciubba. *Calculation of exergetic losses in compact heat exchanger passages*. in ASME AES. 1989.

[109] Haruki, N. and A. Horibe, *Flow and heat transfer characteristics of ice slurries in a helically-coiled pipe.* International Journal of Refrigeration, 2013. **36**(4): p. 1285-1293.

[110] Inaba, H., *New challenge in advanced thermal energy transportation using functionally thermal fluids.* International Journal of Thermal sciences, 2000. **39**(9): p. 991-1003.

[111] Knodel, B., D. France, U. Choi, and M. Wambsganss, *Heat transfer and pressure drop in ice-water slurries.* Applied Thermal Engineering, 2000. **20**(7): p. 671-685.

[112] Liu, Y., E. Zhang, J. Zhao, and P. Chen, *Experiment study on friction loss characteristics of pipes with ice slurry.* Science et technique du froid, 1997: p. 490-494.

[113] Zhao, Z. and Y. Shi, *Experimental investigations of flow resistance and convection heat transfer and prediction of cold heat-storage characteristics for a phase-change emulsion in a coiled circular tube.* Heat transfer engineering, 2005. **26**(6): p. 32-44.

[114] Ko, T. and K. Ting, *Optimal Reynolds number for the fully developed laminar forced convection in a helical coiled tube.* Energy, 2006. **31**(12): p. 2142-2152.

[115] Ko, T.H. and K. Ting, *Entropy generation and optimal analysis for laminar forced convection in curved rectangular ducts: A numerical study.* International Journal of Thermal Sciences, 2006. **45**(2): p. 138-150.

[116] Aneke, M. and M. Wang, *Energy storage technologies and real life applications–A state of the art review.* Applied Energy, 2016. **179**: p. 350-377.

[117] Kauffeld, M., M. Kawaji, and P.W. Egolf, *Handbook on Ice Slurries: Fundamentals and Engineering*. 2005. International Institute of Refrigeration.

[118] Wang, J., T. Zhang, and S. Wang, *Heterogeneous ice slurry flow and concentration distribution in horizontal pipes.* International Journal of Heat and Fluid Flow, 2013. **44**: p. 425-434.

[119] Lun, C., S.B. Savage, D. Jeffrey, and N. Chepurniy, *Kinetic theories for granular flow: inelastic particles in Couette flow and slightly inelastic particles in a general flowfield.* Journal of fluid mechanics, 1984. **140**: p. 223-256.

[120] Syamlal, M. and T.J. O'Brien. *Computer simulation of bubbles in a fluidized bed*. in Fluidization and Fluid Particle Systems: Fundamentals and Applications, Ed. Fan, L.S., AIChE Symposium Series nº270, 1989. **85**: p. 22-31.

[121] Gidaspow, D., R. Bezburuah, and J. Ding, *Hydrodynamics of circulating fluidized beds: kinetic theory approach*. 7th International Conference on Fluidization, Gold Coast, Australia, 1992.

[122] Ding, J. and D. Gidaspow, *A bubbling fluidization model using kinetic theory of granular flow.* AIChE journal, 1990. **36**(4): p. 523-538.

[123] Ekambara, K., R.S. Sanders, K. Nandakumar, and J.H. Masliyah, *Hydrodynamic simulation of horizontal slurry pipeline flow using ANSYS-CFX.* Industrial & Engineering Chemistry Research, 2009. **48**(17): p. 8159-8171.

[124] Gidaspow, D., *Multiphase flow and fluidization: continuum and kinetic theory descriptions*. 1994: Academic press.

[125] Drew, D. and R. Lahey, *In particulate two-phase flow*. ButterworthL Heinemann, Boston, 1993. **509**(0): p. 566.

[126] Tomiyama, A. *Drag, lift and virtual mass forces acting on a single bubble*. in in 3rd Internaional Symposium of Two-Phase Flow Modeling and Experimentation, Pisa, 2004.

[127] Burns, A.D., T. Frank, I. Hamill, and J. M. Shi. *The Favre averaged drag model for turbulent dispersion in Eulerian multi-phase flows*. in 5th international conference on multiphase flow, ICMF. Yokohama, Japan, 2004.

[128] Launder, B.E. and D.B. Spalding, *Mathematical models of turbulence*. 1972: Academic press.

[129] Johnson, P. and R. Jackson, *Frictional–collisional constitutive relations for granular materials, with application to plane shearing.* Journal of Fluid Mechanics, 1990. **176**: p. 67-93.

[130] Stamatiou, E. and M. Kawaji, *Thermal and flow behavior of ice slurries in a vertical rectangular channel. Part I: Local distribution measurements in adiabatic flow.* International Journal of Heat and Mass Transfer, 2005. **48**(17): p. 3527-3543.

[131] Kaushal, D.R., K. Sato, T. Toyota, K. Funatsu, and Y. Tomita, *Effect of particle size distribution on pressure drop and concentration profile in pipeline flow of highly concentrated slurry.* International Journal of Multiphase Flow, 2005. **31**(7): p. 809-823.

[132] Nørgaard, E., T. Sørensen, T. Hansen, and M. Kauffeld, *Performance of components of ice slurry systems: pumps, plate heat exchangers, and fittings.* International Journal of Refrigeration, 2005. **28**(1): p. 83-91.

[133] Belozerov, G.A., Mednikova, N.M., and V.P. Pytchenko, *Investigation of Heat Exchange During Movement in a Horizontal Tube of an Aqueous Propylene-Glycol Ice Slurry*. Chemical and Petroleum Engineering, 2017. **53**, nos. 3-4.

[134] Koffler, M. and M. Kauffeld. *Particle size distribution in ice slurry systems - analysis of dual-view particle images.* in 11th IIR Conference on Phase Change Materials and Slurries for Refrigeration and Air Conditioning. 2016. Karsruhe, Germany.

[135] Bordet, A., Poncet, S., Poirier, M., and N. Galanis, *Flow visualizations and pressure drop measurements of isothermal ice slurry pipe flows*. Experimental Thermal and Fluid Science, 2018. **99**: p. 595-604.

[136] Hirochi, T., Maeda, Y., Yamada, S., Shirakashi, M., Hattori, M., and A. Saito, *Flow Patterns of Ice/Water Slurry in Horizontal Pipes*. Journal of Fluids Engineering, 2004. **26**(3): p. 436-441.

[137] Giguère, R., Fradette, L., Mignon, D., and P.A. Tanguy, *Analysis of slurry flow regimes downstream of a pipe bend*. Chemical Engineering Research and Design, 2009. **87**(7): p. 943-950.

[138] Liu, M., and Y.F. Duan, *Resistance properties of coal–water slurry flowing through local piping fittings*. Experimental Thermal and Fluid Science, 2009. **33**: p. 828-837.

[139] Metzner, A., *Non-Newtonian Fluid Flow. Relationships between Recent Pressure-Drop Correlations.* Industrial & Engineering Chemistry, 1957. **49**(9): p. 1429-1432.